THESIS



This is to certify that the

dissertation entitled

THE EFFECTS OF PLASTIC DEFORMATION ON THE ELECTRICAL RESISTIVITY AND THERMOELECTRIC RATIO OF POTASSIUM FROM 0.07K TO 4.2K

presented by

Mark Lyndon Haerle

has been accepted towards fulfillment
of the requirements for

Ph.D. degree in Physics

William P. Pratt
Major professor

Date March 29, 1983



O-12771

# THE EFFECTS OF PLASTIC DEFORMATION ON THE ELECTRICAL RESISTIVITY AND THERMOELECTRIC RATIO OF POTASSIUM FROM 0.07K TO 4.2K

By

Mark Lyndon Haerle

A DISSERTATION

Submitted to
Michigan State University
in partial fullfillment of the requirements
for the degree of

DOCTOR OF PHILOSOPHY

Department of Physics and Astronomy

1983

ABSTRACT

THE EFFECTS OF PLASTIC DEFORMATION ON THE ELECTRICAL RESISTIVITY AND THERMOELECTRIC RATIO OF POTASSIUM FROM 0.07K TO 4.2K

By

Mark Lyndon Haerle

Samples of pure polycrystalline potassium were plastically deformed at 4.2K and at 60K. One sample of polycrystalline potassium - rubidium alloy was deformed at 60K. Such deformations had a significant effect on both the electrical resistivity and the thermoelectric ratio.

In the resisitivity, deformation enhanced the electron - phonon term from 4.2K to below 1K causing a $DT^5$ term to appear in $\rho$, possibly due to the quenching of phonon drag. Furthermore, a new term was seen ( $\rho_{e\text{-}dis}$), which dominates the temperature dependent resistivity in deformed samples below 1K. This new term was interpreted as being caused by dislocations, and could be fit resonably well by a model in which the electrons scatter inelastically off localized phonon modes associated with the dislocations.

The effects of dislocations on the electron - electron term in the resistivity were obscured by $\rho_{e\text{-}dis}$. Until $\rho_{e\text{-}dis}$ is more fully understood, it will remain difficult to identify any variation in the electron - electron term caused by dislocations.

For the thermoelectric ratio, both the normal and umklapp phonon drag terms were suppressed by the introduction of dislocations. In addition, the magnitude of the diffusion term was increased by both point defects and dislocations, with the systematic addition of dislocations giving agreement with the Gorter - Nordheim relation.

Finally, a resistance minimum near 0.2K was seen for potassium in contact with various plastics. The added term to the resistivity followed a -ln(T) behavior, which is seen in Kondo - effect systems. The thermoelectric ratio for these samples was variable and followed no clear pattern.

ACKNOWLEDGMENTS

I wish to thank both Dr. Pratt and Dr. Schroeder for their supervision and invaluable aid in all aspects of this dissertation. I am particularly grateful for the many late nights both worked while taking data.

I extend a thanks to Dr. Bass for many helpful discussions, to John Zwart who helped take data on several occasions, and to Vern Heinen who helped calibrate GRT2.

Finally, I acknowledge the financial support of the National Science Foundation and Michigan State University.

TABLE OF CONTENTS

LIST OF TABLES

LIST OF FIGURES

# Introduction

This dissertation is an experimental study of the effects of plastic deformation on the electrical transport properties of polycrystalline potassium, from 70mK to 4.2K. The two parameters measured as a function of temperature were the electrical resistivity and the thermoelectric ratio, with the main emphasis on resistivity.

Potassium has long been a material of considerable theoretical and experimental interest. The reasons for this are clear. Potassium is believed to have a nearly spherical Fermi surface which does not touch the Brillouin zone boundary. Thus the nearly free electron model is a good approximation for many calculations, making transport theory comparatively easy to carry out. Furthermore, in contrast to potassium; lithium, sodium, and possibly even rubidium(1) undergo martensitic phase transformations at low temperatures which complicates the interpretation of measurements. Also potassium is less reactive than rubidium or cesium and thus is easier to work with experimentally. Finally, Overhauser(2) believes potassium is a good testing ground for the existence of charge density waves (CDW), which result in broken translational symmetry of the ground state. If found to exist, CDW's would radically change our

basic understanding of transport in metals.

The main motivation for this study was a theory by Kaveh and Wiser(3) which predicted for electron - electron scattering an $AT^2$ term in the resistivity, where T is the absolute temperature. At low temperatures when scattering off phonons can be ignored, the resistivity was predicted to be,

$$\rho = \rho_o + AT^2$$

where the coefficient A was dependent on the relative level of impurities and -dislocations. It was believed that a systematic variation in the number of dislocations would provide a good test of this theory. Plastic deformation at low temperatures is a good way to produce dislocations, so it was proposed that we plastically deform potassium and measure the change in the resistivity.

## CHAPTER 1

### Previous work on Potassium

This chapter is an overview of the previous work on potassium. As in all studies of electrical transport, the fundamental basis of the work are the transport equations,

$$\mathbf{J} = \mathbf{L}_{ee}\, E + \mathbf{L}_{et}\nabla T \tag{1.1}$$

$$\dot{\mathbf{Q}} = \mathbf{L}_{te}\, E + \mathbf{L}_{tt}\nabla T \tag{1.2}$$

where $\mathbf{J}$ is the electric current density, $\dot{\mathbf{Q}}$ is the heat flow current density, and $E$ is the electric field. The $\mathbf{L}$ coefficients are in general tensors, but since potassium has cubic symmetry, they can be replaced with scalars. The two quantities of importance to this study are $\rho$ the electrical resistivity and S the thermopower. We define the electrical resistivity when $\nabla T=0$ by the equation,

$$\mathbf{J} = \sigma\, E = \rho^{-1}\, E \tag{1.3}$$

$$\text{so,}\quad \sigma = \rho^{-1} = \mathbf{L}_{ee} \tag{1.4}$$

Similarly, we can define the thermopower generated by a

temperature gradient when J = 0.

$$S = E(\nabla T)^{-1} = -[\, L_{ee}]^{-1} L_{et} \qquad (1.5)$$

## 1.1 Resistivity

Using Matthiessen's rule, the resistivity of potassium is generally interpreted as a sum of terms,

$$\rho = \rho_o + \rho_{ep}(T) + \rho_{ee}(T) + \rho_{other} \qquad (1.6)$$

where $\rho_o$, the residual resistivity, is a constant independent of temperature. It is due to scattering off various static imperfections in the crystal such as impurities, other point defects, and dislocations.

The second term $\rho_{ep}(T)$ is due to electrons scattering off phonons, and at low enough temperatures (below 1.3K in undeformed potassium) this term becomes negligible. In a pure sample it accounts for 20% - 30% of the total change in the resistivity between 1K and 4.2K.

$\rho_{ee}(T)$ is the resistivity due to electrons scattering off other electrons in the sample. At 1K this term is $\sim 10^4$ times smaller than the residual resistivity in pure potassium. A careful study of this term requires temperatures below 1.2K and at least one part in $10^7$ precision.

The last term, $\rho_{other}$ could easily represent a sum of terms itself. The first of these is $\rho_{e\text{-phason}}$, the

resistivity due to electrons scattering off phasons, the elementary excitation of charge density waves. Although recent evidence(4) suggests there is no need for such a term, its existence in potassium is still under debate.

Another possible temperature dependent resistivity would be $\rho_{e\text{-}dis}$, due to interactions between dislocations and electrons. A dislocation is an extended line defect in a crystal. On deforming potassium, one expects the dislocations added to be mostly edge dislocations. Figure 1.1 shows an edge dislocation at the surface of a crystal, the line of the dislocation is perpendicular to the page. Electrons can interact with dislocations through several possible mechanisms. For example, the dislocations might vibrate about their equilibrium positions and the electrons could scatter inelastically off the dislocations by changing the energy of the vibrations. Resonant scattering of phonons by dislocations has been observed by A.C. Anderson(5). Moreover, Motowidlo et al.(6) have observed the effects of electrons damping the motion of dislocations. Thus the interactions between electrons, phonons, and dislocations are well established. Several models for such interactions exist. Another mechanism proposed by Brown(7) would be the scattering of electrons off localized electron states associated with the dislocation cores. Dislocations may also modify the other terms, such as $\rho_{ep}$ and $\rho_{ee}$.

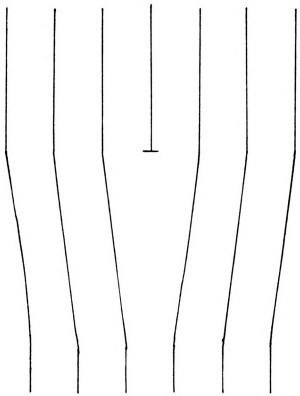

Figure 1.1 An edge dislocation

1.1.1 The residual resistivity

The first term I will discuss is $\rho_o$ a temperature independent resistivity due to scattering off static imperfections in a crystal. It is quite often considered a good measure of the purity of a sample, for the smaller the concentration of impurities the lower will be the residual resistivity.

A theory relating the change in $\rho_o$ due to adding dislocations was proposed by Basinski et al.(8). In this theory one calculates the mean displacement from equilibrium due to the strain field around a dislocation. Then one asks what temperature is needed to give the same mean displacement due to random thermal motion. One then assumes that the increase in $\rho_o$ due to the dislocations is the same as the resistivity due to the electron - phonon interaction at this temperature. One gets,

$$\rho_d = W \times N_d \qquad (1.7)$$

where $\rho_d$ is the increase in $\rho_o$ due to $N_d$ dislocations. This theory predicted for potassium that $W = 4 \times 10^{-19}\ \Omega cm^3$. The above equation was tested indirectly, and the resulting experimental value of W was in good agreement with theory. In other metals, where this theory has been tested directly, the agreement with experiment is quite good. Unfortunately, no direct measurements of dislocation densities in potassium

have been made.

Brown(9) arrived at a similar result using a very different argument. He calculated the resistivity due to resonance S-wave scattering of the electrons. The resonance being created by virtual bound states associated with the dislocation cores. His theory predicted, for potassium, a coefficient of $8 \times 10^{-19}\ \Omega\,cm^3$, off by a factor of two from the experiment. But Brown argued against a correction factor used by Basinski to obtain the experimental results, which if omitted would bring Brown's theory in closer agreement with experiment.

An early study of the effects on $\rho_o$ of annealing a wire of deformed potassium was made by Gurney and Gugan.(10) In this study the residual resistivity of the sample was measured, then the sample was plastically deformed at 4.2K, and again $\rho_o$ was measured. Then the sample was warmed slightly, and cooled to 4.2K where the resistivity was measured. This process, of warming to increasingly higher temperatures and then cooling to 4.2K, was continued until the residual resistivity had recovered to its initial value. Gurney and Gugan claimed to have found five annealing stages as they rewarmed the sample.

The first stage occurred below about 7K and was attributed to annealing out of interstitials, for this stage only about 5% of the total recovery of $\rho_o$ occurred. The next stage, from 7K to 20K, was attributed to long range migration of vacancies and included 40% of the recovery.

The third and fourth stages, 20K to 40K and 40K to 80K, covered a 30% recovery and were attributed to the interaction between impurities and vacancies, with possibly some dislocation relaxation. The final stage, 80K to 150K, was believed due to the annealing out of dislocations and included about 25% of the total recovery of $\rho_o$.

The temperature ranges given are rough guesses based on the breaking points in the complicated annealing curves of $\rho_o$ vs the annealing temperature. There were variations among samples with one not entirely recovering until 200K. Furthermore, many mechanisms used to explain the various recovery stages were largely unsubstantiated. Nonetheless, the study does provide a basis on which the effects of dislocations on the temperature dependent resistivity may be examined.

### 1.1.2 Electron-phonon scattering

The second term I will discuss is due to electron - phonon scattering. These interactions are usually divided into two groups, normal and umklapp. To better understand these interactions let us look at a collision in momentum space. Let **K** be the momentum of an incoming electron, **K'** the momentum of the scattered electron, **q** the momentum of a phonon which interacts with the electron, and **G** a reciprocal lattice vector. Then the change in momentum of the electron will be,

$$\mathbf{K' - K = q + G} \qquad (1.8)$$

Potassium is believed to have a nearly spherical Fermi surface which does not touch the Brillouin zone boundary. This is illustrated in Figure 1.2, which shows phonon annihilations for the two types of electron - phonon processes. For a normal process, G is zero, and the scattering is within a single Brillouin zone. For an umklapp process, G is not zero and we have,

$$\mathbf{K' - G = K + q} \qquad (1.9)$$

The scattering in this case extends outside one Brillouin zone. Clearly for an umklapp process to take place a minimum value of phonon momentum ($q_{min}$) is required.

A theory was worked out for the electrical resistivity by Bloch(11) who assumed an equilibrium phonon distribution, the relaxation time approximation of the Boltzmann transport equation, no umklapp scattering, and the Debye theory for phonons. He predicted that,

$$\rho_{ep}(T) = D'(T/\Theta_d)^5 \; j_5(\Theta/T_d) \qquad (1.10)$$

where D' ia a constant, and $\Theta_d$ is the Debye temperature, and

$$j_x(y) = \int_0^{\Theta_d/T} z\,[(\exp(z)-1)\,(1-\exp(z))]^{-1}dz \qquad (1.11)$$

is the Bloch-Gruneisen function. Since the Debye temperature for potassium is ~100K, and we will be

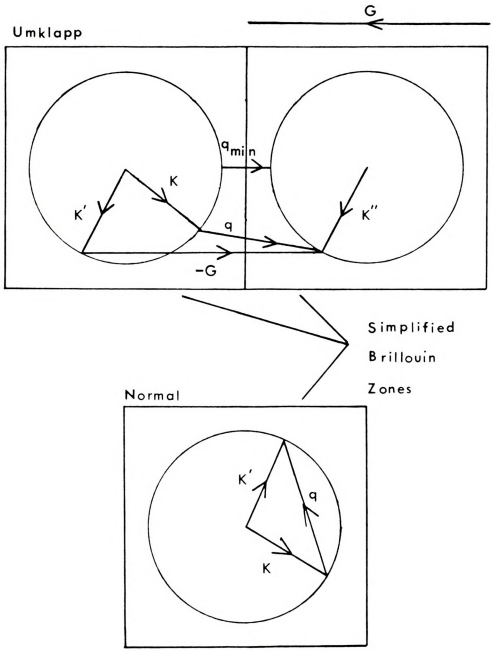


Figure 1.2 Normal and umklapp scattering

concentrating on results below 4.2K, we will be in the low temperature regime. Then $j_5(\Theta_d/T)$ approaches a constant and the resistivity becomes,

$$\rho_{ep}(T) = D\ T^5 \qquad (1.12)$$

Measurements by Gugan(12) (T>1.2K), Ekin and Maxfield(13) (T>1.5K), and van Kempen et al.(14) (T>1.1K) on potassium did not showed this $T^5$ term. Instead their results could be fit to an equation of the form:

$$\rho_{e-p} = B\ T^n\ \exp(-\Theta^*/T) \qquad (1.13)$$
$$\text{with } n\sim 1 \qquad \text{and } \Theta^*\sim 20K$$

The main reason for the failure of this early model was attributed to the presence of phonon drag(12). Basically phonon drag arises when the phonon distribution is disturbed from its of equilibrium value. This happens when the phonons gain momentum from collisions with the electrons and have no scattering mechanism through which equilibrium might be restored. Then the electrons and phonons drift along together, and so the resistivity due to electrons scattering off phonons is reduced. At high temperatures this effect is quenched, because phonon - phonon umklapp scattering equilibrates the phonons with the crystal. At low temperatures in potassium, phonon drag becomes important, and effectively suppresses the $T^5$ term in the electrical resistivity.

The exponential behaviour seen experimentally can be

understood in terms of electron - phonon umklapp scattering, which is scattering between two Brillouin zones. This scattering requires phonons with at least the minimum momentum ($q_{min}$) to jump the gap between the two cells. Phonons obey Bose-Einstein statistics, and at low temperature the density of phonons which can participate in an umklapp process goes as,

$$\exp(-\hbar v\, q_{min}/kT) \qquad (1.14)$$

where v is the velocity of the phonons. This factor dominates the electron - phonon resistivity seen experimentally.

Detailed calculations have been made including the effects of phonon drag and both umklapp and normal scattering. Orlov(15), K. Frobose(16), and Kaveh and Wiser(17) have all derived slightly different equations to describe the resistivity for electron - phonon scattering below 4.2K. All of these theories were brought together in a paper by Kaveh, Leavens, and Wiser(18), who stated an empirical expression,

$$\rho_{ep}(T) = B\, T^{n} \exp[-\theta^{*}/T] \qquad (1.15)$$

where the value of n was related to that of $\theta^{*}$. They noted that increasing n by one, would reduce $\theta^{*}$ by about 2.8K. On adjusting the value of n and $\theta^{*}$, the earlier predictions (15-17) for electron - phonon scattering were reproduced.

There are mechanisms other than phonon - phonon umklapp

scattering which can pull the phonons into equilibrium. For example a high concentration of impurities or dislocations (R. Taylor 1978) could interact with the phonons providing a way for the phonons to lose the momentum given to them by the electrons, resulting in an equilibrium distribution.

Detailed theories using this mechanism have been worked out for potassium by R. Taylor et al.(19) and Danino et al.(20) predicting the effects of dislocations on the electron - phonon scattering term. These theories give the same dislocation densities for which at least 90% of phonon drag is quenched, $N_d \sim 4 \times 10^{11}$ /cm$^2$. These theories are compared with experimental results in Figure 1.3. $\rho^a_{ep}$ is the electron - phonon term of an annealed sample, where the phonon drag would be maximal. The solid lines are from the theory of Danino et al. The dot-dash curve is from Taylor et al. (The curve representing the theory of Taylor et al. was obtained by taking the ratio of two plots from their paper. The difficulty of obtaining accurate values from the plots gives an uncertainty to the line of $\pm$ 0.1.) In the high $N_d$ limit, both theories give about the same result. For a sample with no dislocations, both theories would predict a horizontal straight line of value 1.0. The data of Gugan(21) for sample K5d has the same general form as the theories, but the fit is not very good over the whole temperature range. Moreover, the data plotted include the effects of electron - electron scattering, whereas the theories do not. Correcting the data by subtracting the

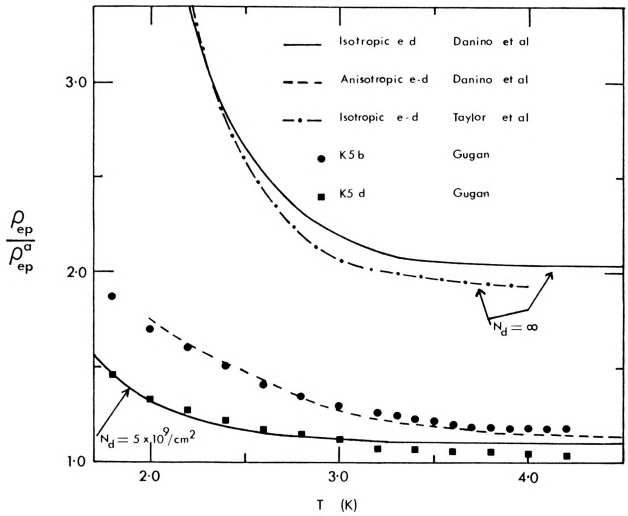


Figure 1.3 Comparison with theory for the elecrton - phonon term

electron - electron term would increase the ratio significantly only below 2.5K on this graph, and at 2K it would add ~0.5 to the ratio.

Both theories require dislocation densities of ~5 x $10^9/cm^2$ to ~5 x $10^{10}/cm^2$ in order to fit the data. Such a high level of dislocations is debatable. These theories require at least an order of magnitude more dislocations than indicated by the expression $\rho_d = N_d \times 4 \times 10^{-19} \Omega\, cm^3$ obtained by Basinski(22), which would predict 0.6 x $10^9/cm^2$ for sample K5d and 3 x $10^9/cm^2$ for sample K5b. However, both theories used Klemens formula to approximate phonon - dislocation scattering, and Taylor has pointed out that this formula does not include core scattering, so the actual scattering strength will be much higher, reducing the dislocation densities required to fit the data near 4K.

Another mechanism by which dislocations may modify the electron - phonon scattering term was suggested by Hans-Lennard Enquist(23) and later by Danino, Kaveh, and Wiser(24). In these papers it is argued that the normal electron - phonon scattering term ($DT^5$) is enhanced by the anisotropy of electron - dislocation scattering. Enquist predicted the result in two limits. The first is where the phonon drag is quenched by dislocations.

$$\rho \sim \rho_o + [\, 1 + 6\, Q \,]^2\, D\, T^5 \qquad (1.16)$$

where Q is a measure of the anisotropy of the scattering and

D is the coefficient from Bloch's low temperature formula for normal electron - phonon scattering (see Equation 1.12). The second is where one has the full effects of phonon drag,

$$\rho \sim \rho_o + [15/4]\ Q^2\ D\ T^5 \qquad (1.17)$$

with the same values for Q and D. These two equations show that dislocations enhance the coefficient of the $T^5$ term. The dashed line shown in Figure 1.3 is a fit of the theory by Danino, Kaveh, and Wiser to the data of Gugan. This fit includes the contribution of electron - electron scattering in that an $AT^2$ term was added to both $\rho_{ep}$ and $\rho_{ep}^a$. It gives better agreement with the data than the first mechanism discussed

### 1.1.3 Electron-electron scattering

The third term is due to electron - electron scattering, which becomes important below about 1.5K as $\rho_{ep}$ becomes small. Both the form and size of this term has been controversial. A theory was worked out for potassium by Lawrence and Wilkins(25) for a screened coulomb interaction. The theory was later refined by MacDonald et al.(26), who included both screened coulomb scattering and phonon - exchange scattering. MacDonald et al. found that the screened coulomb interaction gave a much smaller contribution than the earlier work of Lawrence and Wilkins had suggested, and instead that the dominant term was due to

phonon - exchange scattering. Both theories predicted an $AT^2$ term with $A=0.17p\,\Omega\,cm/K^2$.

The experimental results of van Kempen et al.(27) and Levy et al.(28) supported the existence of a $T^2$ term, but the coefficient A was seen to be sample dependent. Also their analysis was complicated by a significant contribution due to $\rho_{ep}$ since the lowest temperature they could obtain was 1.1K. The work by Rowlands(29) showed, for temperatures as low as 0.5K, a term of the form $AT^n$, where the best fits were obtained for $n\sim1.5$ with a variable A. The most definitive work to date on undeformed potassium by Lee et al.(30), from 4.2K to 70mK, showed a term $AT^2$ where A was relatively constant among samples.

In order to explain the variation in the observed values of A, several suggestions were made: size effects(31), the presence of dislocations modifying the electron - electron scattering(3), and electron - phason scattering(41).

The study of Lee et al. suggested that size effects were not important for samples larger than 1mm in diameter. Very recent unpublished work by the same group(32) has since shown that a notable size dependence can be seen for samples less than ~1mm in diameter. Thus part of the variation in A can be attributed to a size effect since the samples of previous groups were less than 1mm in diameter.

However, a sample of van Kempen et al.(33), upon rapid cooling to liquid nitrogen temperature, showed a sizable

increase in both $\rho_o$ and A. After the sample was annealed at room temperature and then slowly cooled, both decreased to the lower values previously obtained. Annealing at room temperature should remove dislocations from the sample. Danino, Kaveh, and Wiser(34) attributed the observed increase in A as being due to dislocations caused by strain induced in the sample during the rapid cooling. They contended that the data of this sample supported their theory; that is, dislocations modify electron - electron scattering. But Gugan(35) has claimed that the high level of dislocations needed by Kaveh and Wiser was not necessarily present in the sample. At slow cooling rates impurities may freeze out in clumps, and have little effect on the resistivity, so the large increase in $\rho_o$ might be due to there being a larger fraction of impurities in solution rather than a large number of dislocations

Before discussing the theory of Kaveh and Wiser, we first need to define the concept of normal and umklapp scattering for electron - electron interactions. Following an argument similar to that used for the electron - phonon case, we let $\mathbf{K}_1$ and $\mathbf{K}_2$ be the initial states of the electrons, and $\mathbf{K}_3$ and $\mathbf{K}_4$ the final states. Then for an umklapp process,

$$\mathbf{K}_1 + \mathbf{K}_2 = \mathbf{K}_3 + \mathbf{K}_4 + \mathbf{G} \qquad (1.18)$$

where $\mathbf{G}$ is a reciprocal lattice vector. For the normal process the electrons must remain in a single Brillouin

zone, so G is zero.

From Ziman(36) we know that the approximate solution to Boltzmann's equation for normal electron - electron scattering contains an integral with a factor of the form,

$$\{[(t(\mathbf{K}_1)\mathbf{K}_1+t(\mathbf{K}_2)\mathbf{K}_2- t(\mathbf{K}_3)\mathbf{K}_3-t(\mathbf{K}_4)\mathbf{K}_4] \cdot \mathbf{U}\}^2$$

$$\times \delta(\mathbf{K}_1+\mathbf{K}_2-\mathbf{K}_3-\mathbf{K}_4) \qquad (1.19)$$

where $\mathbf{K}_1$, $\mathbf{K}_2$ are the initial states and $\mathbf{K}_3$, $\mathbf{K}_4$ are the final states. $t(\mathbf{K})$ is the relaxation time, and $\mathbf{U}$ is a unit vector in the direction of the electric field. Clearly when $t(\mathbf{K})$ is a constant the integral will vanish, so to first order a normal process with an isotropic relaxation time does not contribute to the resistivity.

In the second order approximation, umklapp scattering can take place, and the delta function is replaced with,

$$\delta(\mathbf{K}_1+\mathbf{K}_2-\mathbf{K}_3-\mathbf{K}_4+ \mathbf{G}) \qquad (1.20)$$

Then umklapp scattering gives a finite, but small value for A, even if $t(\mathbf{K})$ is isotropic. But if $t(\mathbf{K})$ were anisotropic, the above integral for the normal process would not, in general, vanish. Since the resulting term is of first order, one would expect it to be quite large. Kaveh and Wiser(37) estimated the coefficient A to be 8 times larger in the anisotropic $t(\mathbf{K})$ (normal) limit than it is in the isotropic $t(\mathbf{K})$ (umklapp) limit. Thus for even small levels of anisotropy, the normal process may be significant compared to the umklapp process.

Kaveh and Wiser(38) in their theory argue that the magnitude of the electron - electron scattering term depends on the relative contribution to $\rho_o$ of isotropic and anisotropic scatterers. They define $\rho_{oi}$ as the component of the residual resistivity due to isotropic scattering and $\rho_{oa}$ as that due to anisotropic scattering, where

$$\rho_o = \rho_{oi} + \rho_{oa} \qquad (1.21)$$

By isotropic Kaveh and Wiser mean the scattering time {t(K)} of the electrons is constant over the fermi surface. They claim A is a function of $\rho_{oi}/\ \rho_{oa}$.

To understand how this dependence of A on the dominant scattering mechanism occurs, let us take a look at the significant scattering mechanisms present near 1K. Electrons are scattered predominantly by defects since electron - phonon and electron - electron scattering make negligible contibutions to the residual resistivity. The important defects are impurities and dislocations.

The residual resistivity added by dislocations is assumed to be predominately anisotropic, whereas impurity scattering is almost totally isotropic. The amount of anisotropy in t(K) depends on the dominant scattering mechanism. For impurity scattering where one only has isotropic scattering, clearly t(K) will be a constant and a particular value $A=A_o$ will result. Similarly, when the scattering is dominated by anisotropic scattering (due to dislocations, for example), another limiting value

$A=A_o+A_n$ will result. The relationship Kaveh and Wiser(38) predict is,

$$A = A_o + A_1( 1 + \rho_{oi}/ \rho_{oa})^{-2} \qquad (1.22)$$

where $A_o$ is the value predicted for dislocation free potassium, and $A_1$ is an adjustable constant. Figure 1.4 shows the result of the Kaveh and Wiser theory with the data of some research groups.

The major difficulty with this theory was that it required at least two orders of magnitude more dislocations in strain free samples than were believed could easily exist. Furthermore, there was no way to definitively separate $\rho_{oi}$ from $\rho_{oa}$, so each data set plotted had one adjustable parameter, making it easier to fit the theory.

It was clear that a study of samples that were systematically deformed and annealed was needed. At about the same time the group at MSU started working on this project, a group in the Netherlands, headed by van Kempen(39) also began work. They finished their study first, but the limited temperature range, down to only ~0.9K made their analysis of the data questionable, since the electron - phonon term appears to be quite large in these deformed samples in this temperature range. Furthermore, we were able to obtain at least 50 times higher precision. Comparison of their results with ours will be made in the experimental results chapter.

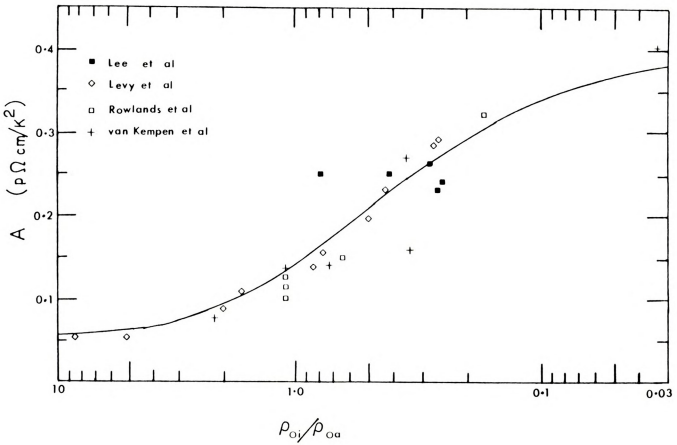


Figure 1.4 Comparison with theory for the effects of dislocations on A.

### 1.1.4 Electron - phason scattering

An alternate theory first derived by Boriack and Overhauser(40) and later corrected by Bishop and Overhauser(41) was used to explain the $AT^{1.5}$ term in the resistivity of potassium, observed by Rowlands et al.(29). This theory contends that there are periodic oscillations (charge density waves - CDW) in the electronic density, which are incommensurate with the crystal lattice. If these CDW's were to exist in a metal, then the properties of the metal would be greatly changed, for instance the fermi surface would no longer be spherical, but instead a complex interconnected one.

The existence of CDW's is a matter of considerable controversy. CDW theory can explain many observations on potassium which conventional theory has not explained(2). But other measurements on potassium are at variance with CDW theory(2). Since the scatter in the data of Rowlands et al. does not preclude a simple $AT^2$ behavior, it is not absolutely necessary to invoke CDW theory to explain the observed resistivity data for undeformed potassium. In addition, the recently observed size effect by our group(32) can explain why the 0.8-mm-diameter samples of Rowlands et al. appear to have a $T^{1.5}$ behavior. So far, the CDW theory has not addressed the observed size effect.

Bishop and Overhauser(41) have claimed that CDW's

should enhance electron - electron scattering. This enhancement depends on the relative orientation of the 'Q' domains (regions over which long range correlation of the CDW's exist) and the electic field. Since the orientation of the 'Q' domains is sample dependent, the electron - electron scattering should also be sample dependent. The details of this theory have not been worked out.

### 1.1.5 Electron - dislocation scattering

This section is a discussion of the other ways electrons and dislocations can interact. For some of these mechanisms no analytic theory has been worked out.

The first theory to be discussed was proposed by Brown(42), who suggested dislocations could have virtual bound states for electrons with energies slightly above the fermi surface. He estimated these energy levels for potassium to be at about $10^{-4}$ eV. These energy levels would be localized near the cores of the dislocations. Gantmakher and Kulesko(43) derived an equation for elastic scattering off such states,

$$\rho_{e\text{-}dis} = a\,[\,1 + b\,\exp(E/kT)\,]^{-1} \qquad (1.23)$$

where a, b, and E are constants, and b is related to the spin degeneracy of the localized energy levels at energy E above the fermi energy.

Other calculations have been performed for interactions

with localized energy levels in the crystal. Fulde and Peschel(44) calculated the resistivity due to electrons scattering inelastically off localized energy levels produced by a crystalline electric field. This theory may be applicable to scattering off local electron states caused by dislocations such as the virtual bound states predicted by Brown. Theory predicts that,

$$\sigma(T) = \sigma_o \left[ 1 - \frac{G^2 \; D/T}{\sinh(D/T)} \right] \qquad (1.24)$$

and if one applies Matthiessen's rule in the derivation one gets,

$$\sigma(T) = \sigma_o \left[ 1 + \frac{G^2}{1+(2/3)[\sinh^2(D/2T)]} \right]^{-1} \qquad (1.25)$$

where G and D are constants, and $\sigma_o$ is the residual conductivity. D is the energy level splitting for the assumed doublet.

As mentioned earlier, another mechanism is inelastic scattering off local phonon modes associated with the dislocation. A. Anderson and Ohara(45)(46) have made measurements of thermal conductivity on superconducting metals, which showed resonant phonon absorption at certain energies. This work supports the existence of dynamic dislocations at low temperatures. These local modes can be pictured by considering a dislocation which is pinned at both ends. There is a restoring force pulling the dislocation back to a straight line. The oscillations of

the dislocation around this equilibrium line form the local modes. The lowest energy state is one that has the longest wavelength. The pinning sources can be other dislocations or impurities and other point defects. Clearly the frequencies of the local modes will depend on the distance between these pinning sources. Hence adding more dislocations and impurities should increase the fundamental frequencies of the system. Also there will be a distribution of lengths, due to the random placement of the dislocations and impurities.

The inelastic interaction of these local modes in the phonon spectrum with the electrons was calculated by Gantmakher and Kulesko(47) who approximated the local modes by a single frequency oscillator. They found,

$$\rho_{e\text{-}dis} = (C/4T) \sinh^{-2}(\hbar w/kT) \qquad (1.26)$$

where C is a constant and w is the ground state frequency of the oscillator.

The above are the only cases where the resulting electrical resistivity for a dislocation scattering mechanism has been calculated. A few of the other possible scattering mechanisms include: the tunneling of dislocations, and the scattering of electrons off localized electron energy levels produced by the interaction between dislocations.

## 1.2 Thermoelectric power

In this section previous work on the thermopower of potassium will be discussed. When there is a temperature drop across a sample, there will be a thermoelectric voltage. The thermopower is this voltage divided by the temperature drop. One can view the thermopower as being the sum of two terms. The first term is diffusion thermopower and the second, phonon drag thermopower. Phonon drag thermopower arises as phonons (heat) flow from the hot to the cold end of the sample. As phonons flow they interact with and transfer momentum to the electrons. This causes the electrons to flow along with the phonons until enough electrons have moved to form an electric field which stops any additional net motion of the electrons.

### 1.2.1 Diffusion thermopower

Diffusion thermopower is generally written using the Mott(48) expression as,

$$S_{diff} = \frac{-\pi^2 k^2 T}{3e} \left. \frac{\partial \ln \sigma(E)}{\partial E} \right|_{E=E_f} \qquad (1.27)$$

(where $E_f$ = the fermi energy, $\sigma$ = conductivity) Expanding the above equation, Guénault and MacDonald(49) obtained,

$$S_{diff} = \frac{-\pi^2 k^2 T}{3\, e\, E_f}\left(\frac{\partial \ln[n(E)\, v^2(E)]}{\partial \ln E} + \frac{\partial \ln t(E)}{\partial \ln E}\right)\Bigg|_{E=E_f} \qquad (1.28)$$

where t(E) is the relaxation time, n(E) is the density of states, and v(E) is the average electron velocity at energy E. When impurity scattering dominates one expects for potassium that the quantity in the parenthesis will be independent of temperature. Thus one expects the diffusion thermopower in potassium to linearly increase with temperature.

The measurements carried out on potassium by Guénault and MacDonald(49)(50) have shown this linear term to exist, but the coefficient varied from sample to sample. This variation in the coefficient has been attributed to a small shift in the concentration of impurities which can easily change the dominant scattering mechanism. Guénault and MacDonald argued that slight variations in the preparation of the sample could easily change the impurity content. More recently, Gugan(51) has pointed out that the rate of cooling of a sample may affect the number of impurities which come out of solution (with the majority of impurities clumping together for slow cooling and thus giving a small contribution to the residual resistivity or the thermopower).

The effect of having more than one scattering process in a sample can be viewed as follows: If Matthiessen's rule applies, one can express the resistivity as a sum with each term due to a separate process,

$$\rho = \rho_i + \rho_d \tag{1.29}$$

where we will take $\rho_i$ as the initial impurity scattering and $\rho_d$ as that from adding a new type of impurity or dislocation. Using Mott's formula,

$$S = \frac{\pi^2 k^2 T}{3 e} \frac{\partial \ln \rho(E)}{\partial E} \Bigg|_{E_f} \tag{1.30}$$

one gets the Gorter - Nordheim relation.

$$S = S_i - \frac{\rho_i}{\rho} ( S_i - S_d) \tag{1.31}$$

For fixed $S_i$ and $S_d$, a plot of S vs $1/\rho$ should yield a straight line. Such a plot is called a Gorter - Nordheim plot. This relation was observed by Guénault and MacDonald(52) for rubidium impurities in potassium.

For diffusion thermopower one might expect the temperature independent dislocation scattering to act in much the same way as impurity scattering, so one would expect to obtain a straight line on a Gorter - Nordheim plot when $\rho$ is increased by the addition of dislocations.

An additional term may be present besides the usual diffusion term. Fulde and Peschel(53) calculated the thermopower due to inelastic scattering off crystal field split states, and their equation may apply for the virtual bound states predicted by Brown. They get,

$$S = S_1 + S_2 \tag{1.32}$$

where,

$$S_1 = -b^2 \pi T/(3 e E_f) \tag{1.33}$$

and,

$$S_2 = - a D \tanh\{(D/2T)[1+(D/2\pi T) \mathrm{Im}(\Upsilon(iD/2\pi T)]\} \tag{1.34}$$

where $\Upsilon(z)$ is the trigamma function, D is the level splitting energy, and both a and b are constants.

### 1.2.2 Phonon drag thermopower

Phonon drag thermopower becomes important at slightly higher temperatures in potassium. It is usually divided into two parts, one due to normal electron - phonon processes and the other due to umklapp processes. The theory in both cases tends to be rather complicated; fortunately we will be working in the low temperature limit.

The normal processes involve scattering of electrons within a single Brillouin zone. In the low temperature limit this contribution to S goes roughly as the lattice specific heat, which has a $T^3$ temperature dependence.

$$S_g^n = B T^3 \tag{1.35}$$

The umklapp process is more complicated. To scatter from one Brillouin zone to another, a minimum phonon wave vector ($q_{min}$) is needed. The number of these phonons available goes as,

$$N(q) = \frac{\exp(-\hbar v q_{min}/kT)}{1-\exp(-\hbar v q_{min}/kT)} \sim \exp(-\hbar v q_{min}/kT) \quad (1.36)$$

This exponential decay is clearly the predominant factor in umklapp scattering. An approximation was worked out by Guénault and MacDonald(54), who obtained for low T,

$$S_{ph}^{u} = \left[\frac{1/t_e}{1/t_e+1/t_i}\right](.200)\left[\frac{k}{e}\right]\left[\frac{\theta^*}{\theta_d}\right]\left[\frac{\theta^*}{T} + 3 + 6\frac{T}{\theta^*}\right]\exp(-\theta^*/T) \quad (1.37)$$

Where $t_e$= phonon - electron relaxation time, $t_i$= phonon - impurity relaxation time, $\theta_d$ = Debye temperature, and $\theta^*$= a constant.

More detailed theories have been worked out by Ziman(55) and Bailyn(56), but so far, fitting to the data has been done using only the simplest forms for the umklapp scattering process. Guénault and MacDonald fit their data to a simple equation of the form,

$$S = S_o T + BT^3 + C\exp(-\theta^*/T) \quad (1.38)$$

which gave fairly good agreement with their data where $\theta^* \sim 21K$. For pure potassium, they found, as expected, that $S_o$ and B were negative while C was positive.

### 1.2.3 Thermoelectric ratio

The actual measurements taken for this thesis were of the thermoelectric ratio. Very little theory has been

worked out for this quantity, but fortunately it can be related to the thermopower using a simple expression to be derived in this section.

As we saw earlier,

$$J = L_{ee} E + L_{et} \nabla T \tag{1.39}$$

$$\dot{Q} = L_{te} E + L_{tt} \nabla T \tag{1.40}$$

G, the thermoelectric ratio, is defined as $J/\dot{Q}$ at zero electric field, so $G=L_{et}/L_{tt}$. S is defined as $S=-L_{et}/L_{ee}$. Relating the two,

$$G= L_{et}/L_{tt}=L_{et}L_{ee}/(L_{tt}L_{ee}) \tag{1.41}$$

$$= -S\ L_{ee}/L_{tt} = S\ w\ /\rho \tag{1.42}$$

$w\ (=1/L_{tt})$ is the thermal resistivity. The Lorenz ratio is defined as,

$$L= \rho/(wT) \tag{1.43}$$

so,

$$G= S/(LT) \tag{1.44}$$

Thus the theory for thermopower may be related to the thermoelectric ratio. Ideally L would be a constant, and at low temperatures when impurity scattering dominates this is indeed the case. Using our earlier equation for pure potassium,

$$\rho = \rho_o + AT^2 + B\,T\,\exp(-\theta^*/T), \tag{1.45}$$

and the expression from Newrock and Maxfield(57) for the thermal resistivity in potassium,

$$w = E/T + F\,T^2, \tag{1.46}$$

one can calculate,

$$L = \frac{\rho_o + AT^2 + B\,T\,\exp(-\theta^*/T)}{E + F\,T^3} \tag{1.47}$$

Clearly L approaches a constant value $L_o$ at low temperatures.

$$L_o = \rho_o / E \tag{1.48}$$

This limiting value for L has been calculated assuming elastic scattering(36).

$$L_o = \frac{\pi^2\,k^2}{3\,e^2} \sim 2.445 \times 10^{-8}\ V^2/K^2 \tag{1.49}$$

We have measured L in pure undeformed potassium. At 1K, $L/L_o \sim 0.97$ with the ratio becoming closer to 1 at lower temperatures.

Therefore, at low temperatures where the umklapp scattering is frozen out, G will have the following form.

$$G = G_o + b\,T^2 \tag{1.50}$$

where $G_o$ is the diffusion term and $bT^2$ is the normal phonon drag term. A departure from this form would indicate the presence of some other scattering mechanism which has not

been taken into account in the above theory.

# CHAPTER 2

## Experimental techniques

This chapter will cover the techniques and equipment used to study potassium. It will also discuss the uncertainties in those measurements.

The main purpose of this study was to examine the effects of plastic deformation on electron - electron scattering. This placed a high demand on the system used for taking data. First it was essential that one go below 1K to eliminate the effects of electron - phonon scattering. Also, very high precision was needed, since $\rho_{ee}/\ \rho_o \sim 10^{-4}$, near 1K.

All of these requirements were met in this experiment. The measurements were taken in a dilution refrigerator which was locally built by W.P. Pratt,Jr.. This refrigerator was useable from 4.2K to as low as 60mK. The cryostat was equipped with a commercial Superconducting Quantum Interference Device (SQUID model RMPC, from S.H.E. Corporation(58)), which was used in measuring both the

resistivity and the thermoelectric ratio. This SQUID was capable of detecting currents less than $10^{-9}$ A and thus provided the high sensitivity needed.

## 2.1 Sample can

Since potassium reacts with air, and dislocations anneal out at temperatures above 160K, a self-contained sample can was needed, which would permit both measuring the electrical characteristics of the samples, as well as permitting plastic deformation of the sample. Figure 2.1 shows a drawing of the sample can which was designed to permit deformation of the potassium sample while mounted on the dilution refrigerator. The sample can and dilution refrigerator were both mounted inside a main vacuum can, which was surrounded by liquid He. Some features of this sample can were as follows. First note that the sample was mounted horizontally in the sample area (K) between two plates, the lower of which (I) was movable. An expanded view of the sample area is shown inverted in Figure 2.2. The sample was a 0.9mm diameter potassium wire which was connected to permit 4-probe resistance measurements, and also to permit measurement of the thermoelectric ratio. The electrical connections to the samples were made by cold welding the potassium to one silver (V) and three copper probes. The G heater was a 4k$\Omega$ wire-wound resistor mounted on a copper current probe.

Table 2.1 Sample can parts

| Label | description |
|---|---|
| A | stainless steel bellows |
| B | brass cap |
| C | He gas line |
| D | stainless steel push rod |
| E | movable copper squeeze plate |
| F | copper squeeze plate |
| G | brass flange |
| H | copper press plate guide |
| I | movable copper plate |
| J | stainless steel support rod |
| K | potassium sample area |
| L | brass top flange |
| M | brass can |
| N | copper rod for attaching to mixing chamber |
| O | connection to mixing chamber |
| P | stainless steel support for thermal feed through |
| Q | copper thermal conductor |
| R | electrical feed through |
| S | motion detection spring |
| T | copper switch plate |
| U | copper clamp to hold spring in place |
| V | silver wire |
| W | teflon isolator |
| X | indium 'O' ring seals |

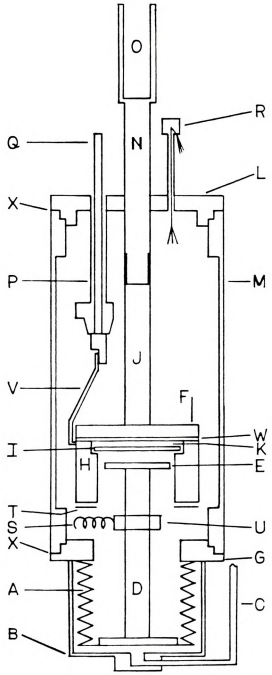


Figure 2.1 Sample can

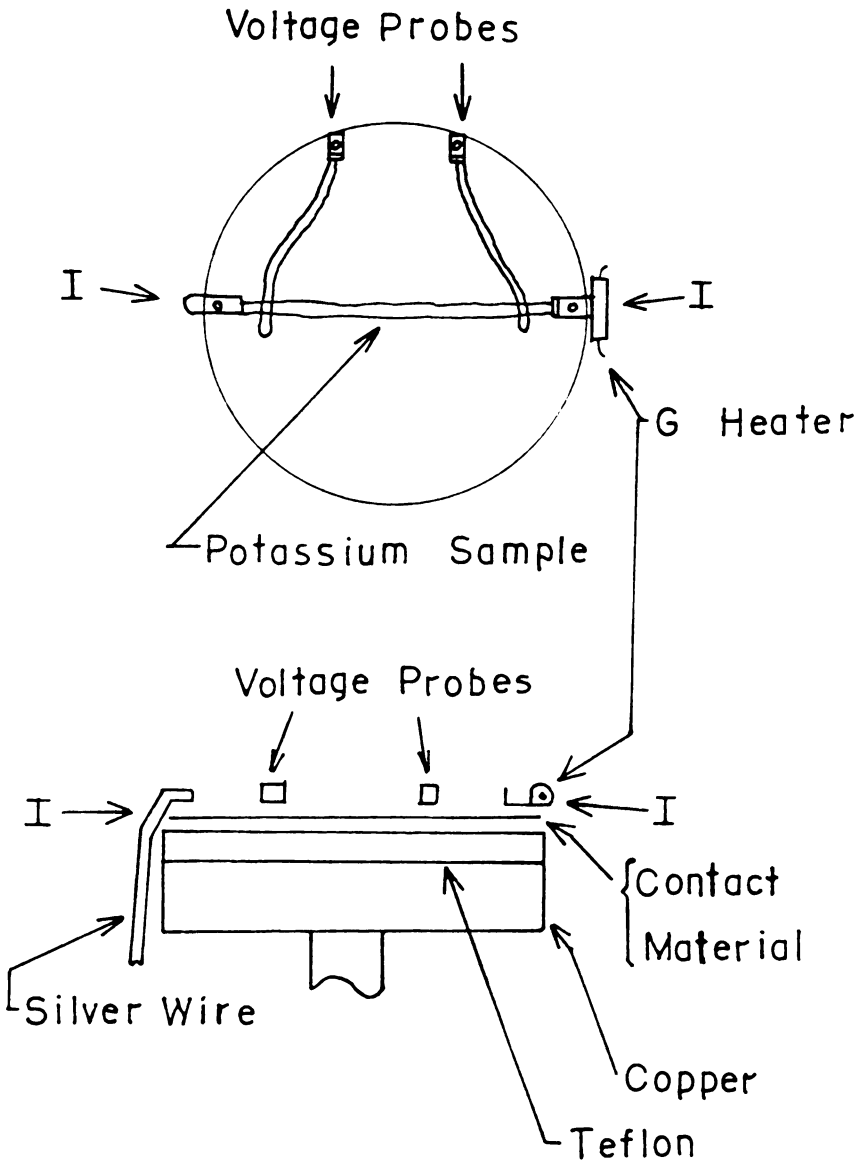


Figure 2.2 Sample area

Temperature measurements were critical to the outcome of this study. The thermometer (GRT2) used to measure the temperature of the samples was mounted outside the sample can, by clamping it to the copper thermal feedthrough (Q). It was important that GRT2 be at the same temperature as the sample, so the thermal path between the sample and GRT2 was designed to be of low thermal resistance and the sample was to be well thermally isolated from the sample can. Thermal isolation of the sample was provided by the stainless steel support (J) holding the upper squeeze plate (F), and also by the stainless steel support (P) holding the thermal feedthrough (Q).

## 2.2 Plastic deformation of the sample

When the sample was to be deformed, the bellows (A) at the bottom of the can was contracted by admitting He gas, thus forcing upward the bottom squeeze plate (E). This squeezing could be done at any temperature from 4.2K to room temperature. The bellows was purchased from the Metal Bellows Corporation(59). It could handle a maximum pressure of 45 psi and had an effective area of 2.1 square inches, so the maximum force the bellows could generate was 95 pounds. Gas was introduced between the bellows (A) and the brass cap (B) through a capillary (C) connected to an external pressurization system. When the bellows moved up, it turned on a switch by grounding the copper switch plate (T) through

the spring (S) attached to the plunger (D). The copper switch plate was connected to a wire which ran out of the sample can through an electrical feed through (R). Using this switch, the initial motion of the bellows could be detected. Thus one could be sure the pressurizing line was not plugged.

The plumbing for the He pressurization system connected to the bellows is shown in Figure 2.3. Normally when operating the bellows, valve #1 was closed and He was slowly added using valves #2 and #3. This two - line system was built for two reasons. If a solid air plug should form when pressurizing at 4.2K, the bellows could still be evacuated using the second line since any such plug would take place in the first line above the liquid He level, which would be above the place where the two lines joined to form one line. Secondly, the pressure was measured using gauge #1, which was connected to a line which had no gas flowing down it, and thus it would give an accurate measure of the pressure down to where the two lines were joined at the top of the main vacuum can. The ballast tanks were 14 cubic inches in volume and were added just before run Kh9. Their purpose was to damp out Taconis oscillations which had occurred in run Khl. These oscillations made accurate measurement of the bellows pressure virtually impossible.

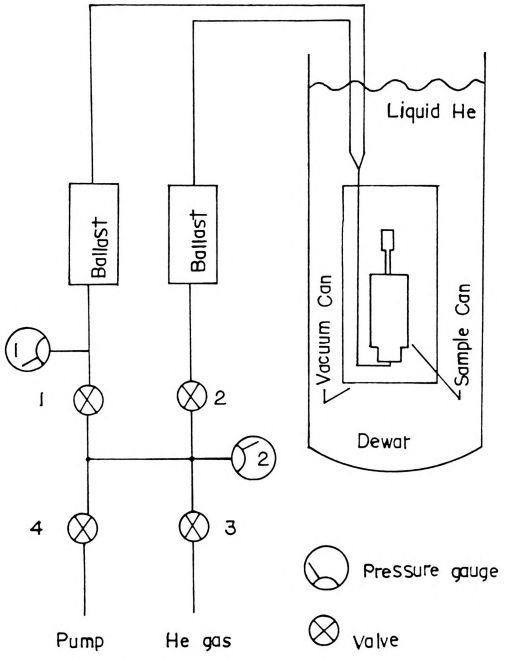


Figure 2.3 The He pressurization system for the bellows

## 2.3 Removing He gas from the sample can

The glove box in which the potassium samples were made was filled with He gas, and thus when the sample can was sealed in the glove box it contained He. The heat convection and conduction through this gas was large enough to make it impossible to accurately measure the sample temperature. This He gas had to be removed. Several methods were used to remove the He. In the first two, the He was adsorbed either on loose 13X molecular sieve pellets(60) or cylinders made by compacting zinc shavings and sieve pellets. The major difficulties with these two methods were outgassing from the adsorbing materials which corroded the sample, and the heat load these materials placed on the sample can at the lowest temperatures, since these materials cooled slowly. The final and most successful method used was to pump the majority of the He gas out at room temperature, and use a sintered silver disk, made from 700A silver powder, to adsorb any residual gas at low temperatures.

When sieve was used it was necessary to outgas it. This was done by placing the sieve in a sealable glass flask, which was heated to 200$^{o}$C and pumped with a diffusion pump for ~2 days. This was important since any water or oxygen released from the sieve would react with the potassium sample. The sieve, while still under a vaccuum,

was then placed in the glove box without exposing it to air. Next it was exposed to the high purity He atmosphere for at least one day prior to making a sample to allow for any additional outgassing. Prior to mounting the sample, the sieve was placed in a stainless steel cage which was screwed to the top flange of the sample can.

When cooling the refrigerator and the sample can to 4.2K, it was found that the sieve cooled very slowly. It was hoped that if one made zinc-sieve pellets, that the zinc would help in cooling the sieve. These zinc-sieve pellets were made by grinding the molecular sieve to a coarse grit, and mixing it in a ratio of 2 parts ground sieve to 3 parts #50 mesh zinc. This mixture was then placed in a press and compressed with several tons of force to 1/2" diameter by ~3/4" long cylinders. These cylinders were then outgassed in the same way as the plain molecular sieve, with the only exception being that at the end of the bake out, hydrogen gas was added to sinter the zinc. The cylinders were then mounted in a copper holder which provided good thermal contact with the sample can.

Even the pellets with their improved thermal contact, cooled slowly and caused difficulty in attaining the lowest temperatures. Consequently, neither the molecular sieve nor the zinc-sieve pellets were used after sample Kh2.

After sample Kh2, the He gas was always pumped out of the sample can before transfering liquid nitrogen. To facilitate this, special indium filled brass tubes were

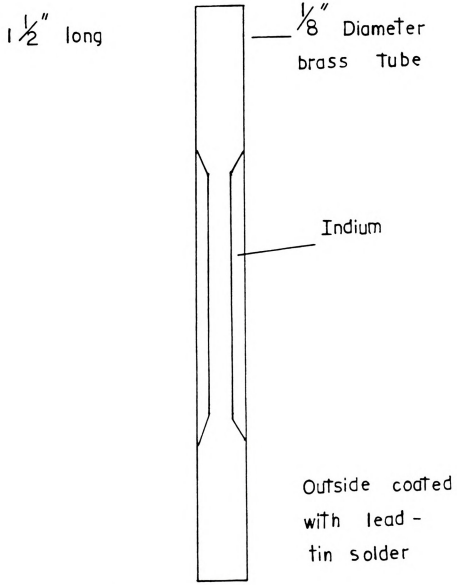


Figure 2.4 Indium filled brass tube

prepared (see Figure 2.4). The purpose of these tubes was to permit pumping out the He gas in the sample can, and then to seal the sample can by crimping the tubes shut. When crimped, the indium inside the tubes would cold weld to itself providing a leak tight seal even at liquid He temperatures. In making these tubes, first the outsides of brass tubes were coated with 50/50 lead/tin solder, to allow easy soldering later. The tubes were heated to ~200°C and filled with indium. "Stay Clean" Flux(61) was found to give the best bond between the brass and the indium. A wire was run down the tubes to ensure that no air bubbles formed. After the tubes were filled with indium, they were allowed to cool, washed under running water, and placed in a beaker filled with bicarbonate of soda for several hours to completely neutralize any trace of the highly corrosive flux. Finally the inside of the tubes were drilled, first ~3/8" deep at each end with a #30 drill and then completely through with a #53 drill bit.

The indium filled tubes once finished were soldered in place. The first one, used to remove He from the sample can, was soldered with Rose's alloy between a copper tube coming out of the sample can and a valve assembly. This low temperature solder was used because it ensured that the indium would not melt and plug the brass tube. These solder joints and the valve assembly were then thoroughly tested by checking first that gas would flow through the system, second that the joints were leak tight, and third that the

valve after sealing was He leak tight. The second tube was soldered on the input line (C) to the bellows(A), just outside the sample can. At the end of the run when the sample was to be removed from the refrigerator, this tube was crimped shut. Thus the bellows remained under a vacuum and the sample can could be disconnected from the pressurizing system without contracting the bellows and further deforming the sample.

## 2.4 Sample preparation

Before placing the sample can in the glove box, sheets of sample contact material were prepared. These were the materials in direct contact with the potassium. Table 2.2 lists what was used for each sample. The sheets were cleaned with high purity ethyl alcohol. Next the copper electrical contacts were cleaned by carefully filing them until they were shiny. The upper layer of contact material was then placed between the teflon isolator plate and the copper contacts. Figure 2.2 shows the sample area which was normally inverted, as shown, when the sample was being prepared. Then the copper contacts were screwed on the teflon disk with 000-120 screws thus holding the contact material in place. The thick teflon disk in turn was screwed onto the copper base plate. Another piece of this contact material was then taped to the guide collar holding the movable copper squeeze plate (I) in place. The sample

Table 2.2 Materials in direct contact with samples

| Sample | material |
|---|---|
| Kh1 | teflon |
| Kh2 | "Handiwrap" (a clear plastic) |
| Kh3 | "Handiwrap" |
| Kh4 | parafilm |
| Kh6 | nothing (this sample was free hanging) |
| Kh7 | polyethylene |
| Kh8 | teflon |
| Kh9 | teflon |
| KRbh | teflon |

area and tools which were to come in contact with potassium were then cleaned with ethyl alcohol to remove any grease or other contaminants. The sample can and tools were then placed in the glove box.

The glove box was made by Vacuum Atmospheres Company(62). It contained a high purity He atmosphere which had a nominal oxygen contamination of less than 0.4 ppm. The water vapor content was not directly measured but exposed potassium remained shiny for hours. Thus in the 30-60 minutes it took to make a sample, no noticable surface deterioration could be seen. To allow the sample can to outgas and to allow the purification system time to remove any residual contamination brought in with the can, all needed materials were placed in the glove box well in advance of making the sample (see Table 2.3 ).

The pure potassium samples were made of 99.95% potassium obtained from Callery Chemical Company, a division of Mine Safety Appliances Company(63). Table 2.4 shows the chemical composition of a similar batch of potassium. The potassium came in glass ampoules sealed under argon gas. The ampoules were opened in the glove box and the potassium melted and transfered to stainless steel presses (see Figure 2.5). Two separate ampoules of potassium were used, both were from the same manufacturers batch. One was used for samples Kh1 to Kh6a+b. The second one was used in samples Kh6b+d to Kh9. The potassium from the two ampoules was directly compared in run Kh6, where a,b represents the

Table 2.3 Time table of making samples

| Sample | time sample can was in glove box before making samples | time from making sample to transfer of liquid nitrogen |
|---|---|---|
| Kh1 | over night | 2 days |
| Kh2 | few hours | 3 days |
| Kh3 | few hours | 7 hours |
| Kh4 | 3 days | 12 hours |
| Kh6 | 2 days | 5 hours |
| Kh7 | 10 hours | 14 hours |
| Kh8 | 13 hours | 6 hours |
| Kh9 | 60 hours | 9 hours |
| KRbh | 17 hours | 7 hours |

Table 2.4 Chemical analysis of potassium

| Element | PPM | Element | PPM | Element | PPM |
|---|---|---|---|---|---|
| Fe | <5 | Cr | <5 | Sr | <1 |
| B | <10 | Si | 25 | Ba | <3 |
| Co | <5 | Ti | <5 | Ca | 8 |
| Mn | 1 | Ni | <5 | Na | 15 |
| Al | <2 | Mo | <3 | Pb | <5 |
| Mg | 2 | V | <1 | Zr | <10 |
| Sn | <5 | Be | <1 | | |
| Cu | <1 | Ag | <1 | | |

This information is from the Callery Chemical Company.

< means less than this level of impurities could not be detected.

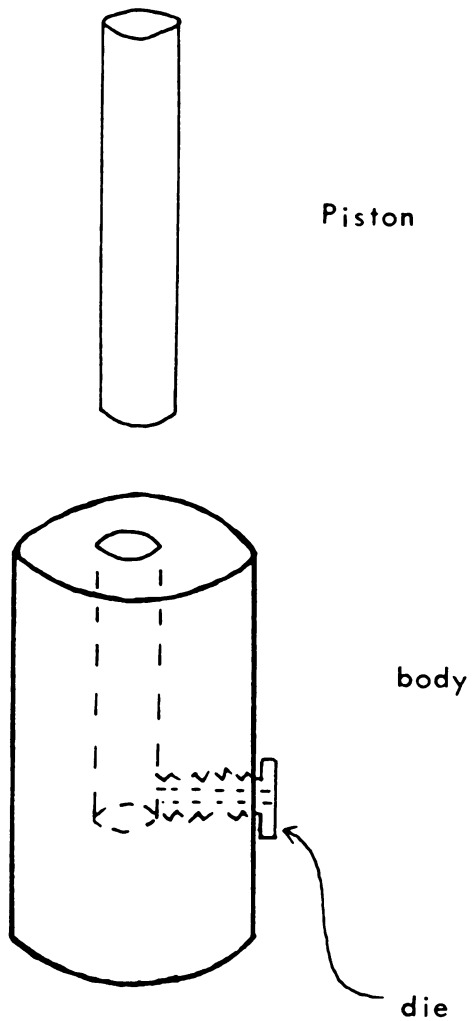


Figure 2.5 Stainless steel press

first ampoule and b,d the second.

The KRbh sample was obtained by first making a 1.3at%Rb mixture using Rb from Callery Chemical Company and then adding some of this mixture to pure potassium, to form a K(0.077at%Rb) alloy. The first potassium ampoule and a third potassium ampoule were used. This 0.077at% mixture was used in sample KRbh.

A 0.9-mm-diameter die was then screwed into the press and a sample extruded. The samples were ~2 inches long and were cold welded between the copper and silver current contacts, see Figure 2.2. Next, two potential probes of potassium were extruded and cold welded first to the sample ~2cm apart and then to the copper voltage contacts. Additional potassium was added to the copper and silver contacts to make sure the cold weld surfaces were entirely coated with potassium. These cold welds were very reliable, and it proved nearly impossible to completely remove the potassium from the contacts short of disolving the potassium in alcohol or oxidizing the potassium and filing the contacts clean.

A sheet of the contact material was placed over the sample and then the potassium potential probes were flattened to ~.1mm. This allowed the total force generated by the bellows to be applied directly to the sample area. Finally, the guide collar (H) was mounted on the copper squeeze plate (F) with screws and the sample can sealed using an indium 'O' ring.

The sample can was then removed from the glove box and mounted in the dilution refrigerator. The room temperature resistance of the sample was measured by passing a known current through the sample and measuring the resulting voltage across the sample with a Keithley 180 nanovoltmeter. The bellows pressurization line was connected and leak tested. Then the bellows movement was tested by pressurizing the bellows until the switch showed that the bellows had moved. Finally, the bellows was evacuated, and left in this state until the first deformation of the sample.

In the case where the He gas in the sample can was to be pumped out, a cryopump ( Figure 2.6 ) was placed in a liquid He storage dewar and connected to the sample can using the gas handling system. This system was then pumped out and leak tested. It was then flushed with He gas and pumped out using the cryopump for ~40 minuties. Then the valve on the sample can was opened and the sample can pumped to about 300 microns pressure. At that point the indium tube was squeezed shut, providing a leak tight seal between the sample area and the valve. The cryopump system was then removed, and the valve was unsoldered from the indium tube and removed from the sample can.

Next the refrigerator was closed and leak tested in the usual manner, with liquid nitrogen being transfered that day, thus limiting the time the sample stayed at room temperature (see Table 2.3). This reduced the amount of

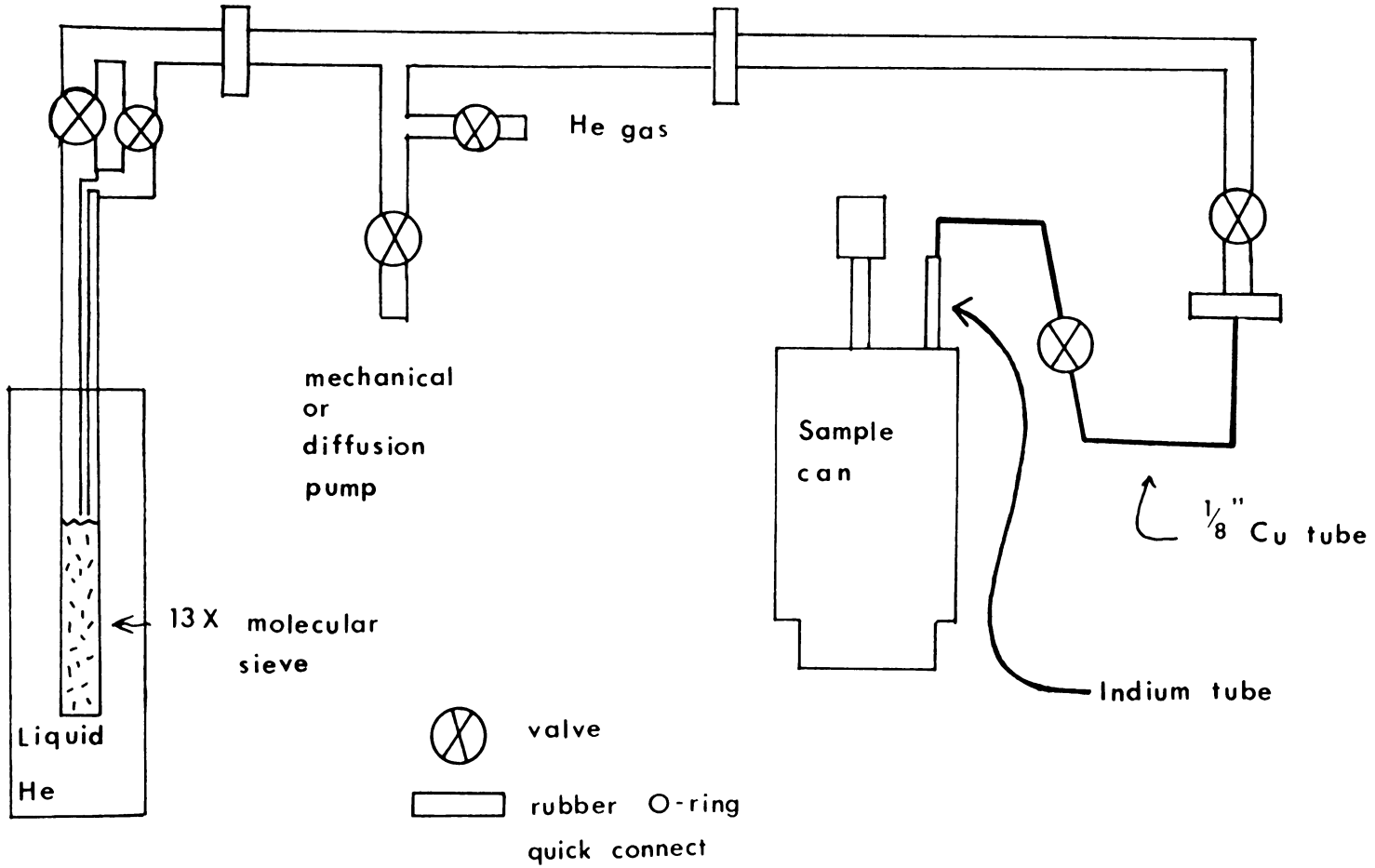


Figure 2.6 He gas handling system for pumping out the sample can

oxide or hydroxide which could form due to outgassing.

## 2.5 Measurements

This section is intended to explain how the various parameters of the samples were measured.

The first parameter is A/L, the cross sectional area of the sample divided by its length. This was obtained by measuring the room temperature resistance of the sample using a constant current source and a Keithley digital nanovolt meter.

$$A/L = \rho(300K)/\ R(300K) \qquad (2.1)$$

$\rho(300K)$ was taken to be $7.19 \times 10^{-6}\Omega cm$, the value measured by Gugan(64). To obtain the resistivity of the sample when T was not 300K, a linear temperature dependence was assumed for $\rho$, which for the few degree correction needed was a good approximation. The A/L values are listed in Table 2.5. The room temperature resistance was also measured after the sample had been deformed. When a sample was only deformed once during a run, the final value for A/L was used for all but the first undeformed measurement. In Kh2 the A/L was unchanged. A/L should remain constant during deformation, since the deformation will not alter A and it is not expected to change L. The handling of Kh8 will be discussed in the next chapter.

Once the sample was cooled to 4.2K or lower, the

Table 2.5 Sample parameters

| sample | A/L | $\rho_o$ | $\rho_{4.2}$ | Pressure of deformation | Temp. of anneal or deformation |
|---|---|---|---|---|---|
| | ($10^{-3}$ cm) | (n$\Omega$cm) | (n$\Omega$cm) | (inches Hg) | |
| Khla | 1.98 | 4.19 | 4.56 | | |
| Khlb | | 6.30 | 6.75 | 95+ | 4.2K |
| Kklc | | 4.76 | 5.17 | | 60K |
| Khld | 1.91 | 4.12 | 4.48 | | 155K |
| Kh2a | 1.61 | 1.87 | 2.19 | | |
| Kh2b | | 2.04 | 2.38 | 23.6 | 60K |
| Kh2c | | 2.28 | 2.62 | 54.1 | 60K |
| Kh2d | | 2.55 | 2.89 | 94.8 | 60K |
| Kh2e | 1.62 | 1.95 | 2.27 | | 160K |
| Kh3 | 1.48 | 1.04 | 1.30 | | |
| Kh4 | 1.96 | 1.05 | 1.30 | | |
| Kh6a | 1.14 | | 1.30 | | |
| Kh6b | 1.60 | | 1.38 | | |
| Kh6c | 1.12 | | 1.44 | | |
| Kh6d | 1.54 | | 1.36 | | |
| Kh7 | 1.38 | 1.24 | 1.51 | | |
| Kh8a | 1.54 | 1.32 | 1.62 | | |
| Kh8b | | 1.38 | 1.68 | 7.1 | 60K |
| Kh8c | | 1.46 | 1.75 | 14.1 | 60K |
| Kh8d | | 1.53 | 1.82 | 21.1 | 60K |
| Kh8e | | 1.81 | 2.11 | 50.1 | 60K |
| Kh8f | 1.40 | 2.05 | 2.36 | 84.3 | 60K |
| Kh9a | 1.99 | 1.09 | 1.35 | | |
| Kh9b | | 2.21 | 2.53 | 95 | 4.2K |
| Kh9c | | 2.20 | 2.51 | | 7.5K |
| Kh9d | | 1.86 | 2.16 | | 20K |
| Kh9e | | 1.49 | 1.77 | | 60K |
| Kh9f | | 1.39 | 1.66 | | 80K |
| Kh9g | | 1.16 | 1.42 | | 120K |
| Kh9h | 1.90 | 1.09 | 1.35 | | 165K |
| KRbha | 3.06 | 10.75 | 11.07 | | |
| KRbhb | | 11.52 | 11.86 | 95 | 60K |
| KRbhc | | 10.78 | 11.10 | | 160K |

+ Due to the Taconis oscillations during Khl the pressure is probably much larger than this.

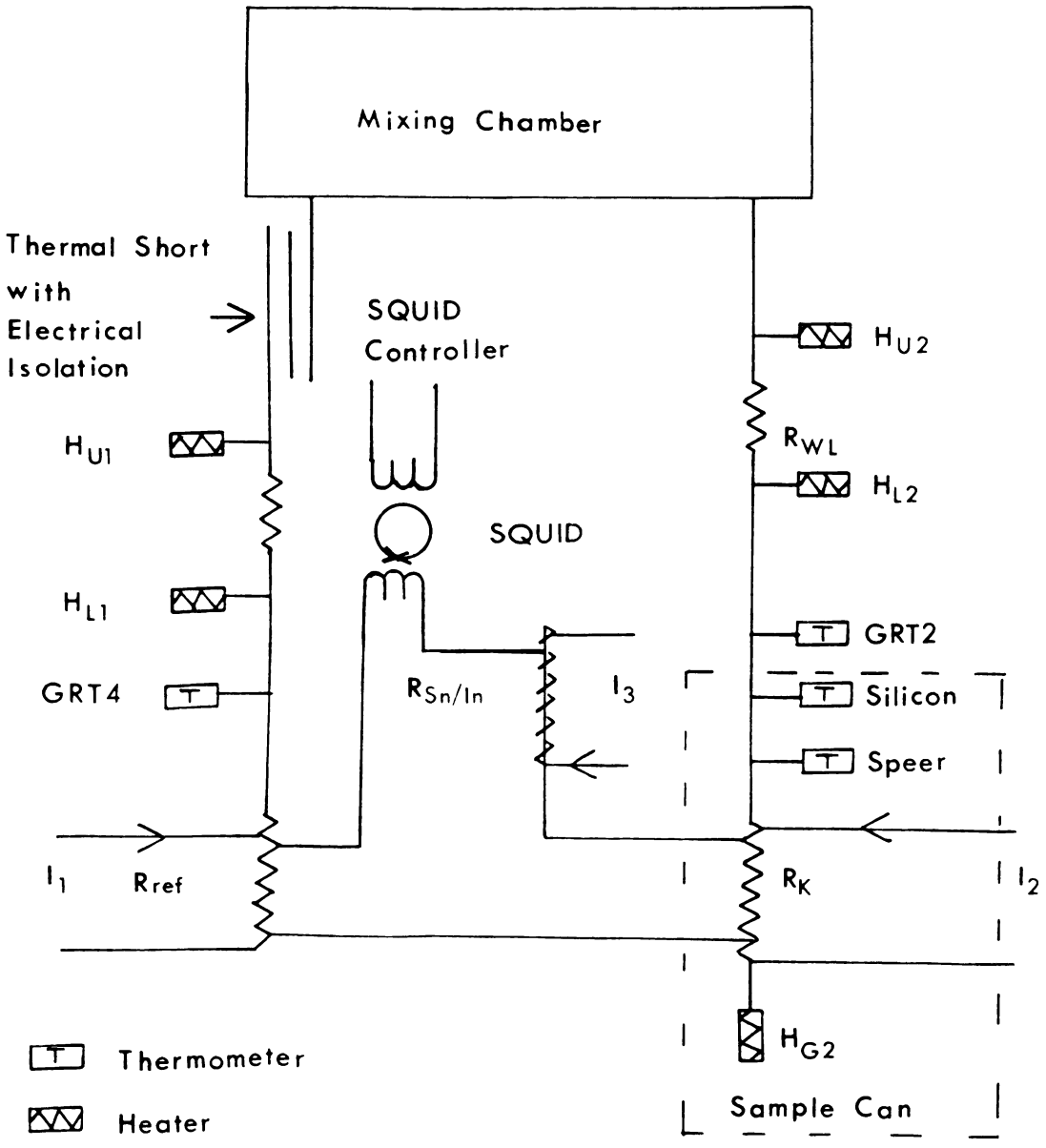


Figure 2.7 The low temperature circuit

circuit shown in Figure 2.7 was used. This low temperature circuit consisted of the SQUID (Superconducting QUantum Interference Device) null detector and 3 resistors wired in series. These three resistors were 1) $R_k$ which was the potassium sample to be measured, 2) $R_{ref}$ which was a copper-silver alloy resistor designed to have a resistance with low temperature and current dependence, and 3) $R_{Sn/In}$ a resistor made of a tin-indium alloy chosen to go superconducting near 3.8K. The wires connecting these resistors were made of Niomax CN, a multi-filament Nb-Ti superconducting wire with Cu-Ni cladding made by Imperial Metal Industries(65). To keep the noise introduced by stray magnetic fields low, the tin-indium resistor and most of the wiring except that near the sample were shielded in superconducting lead tubing. The wires leading to the sample were all carefully tied or varnished down to reduced magnetically induced currents and heating due to vibration.

The wires exited the can through the electrical feedthrough (R, see Figure 2.1). This feedthrough was made by running the Niomax wire through a clean 1/8" diameter stainless steel tube which was then inverted in a cup of Stycast 1266 epoxy(66).

$R_{ref}$ was made of an oxygen annealed Cu 0.02 at% Ag alloy. This alloy was drawn down to .034" diameter wire, which was made into a 4-probe resistor by welding to it 0.030" - diameter oxygen - annealed high purity copper wires about 1.3cm apart. By slowly stretching and twisting the

resistor, a 4.2K resistance of $1.5 \times 10^{-6} \Omega$ was obtained. The temperature dependence of the final resistor is shown in Figure 2.8. The resistance minimum was probably due to iron that diffused into the resistor while spot welding on the voltage probes.

The ratio of the resistances for any two of the resistors in the above circuit could be measured. This was done using a commercial current comparator modified by D. Edmunds et al.(67). This device generated two currents whose ratio was stable to better than 0.1ppm precision. When comparing resistances, one current ($I_m$) passed through what was called the master side resistor ($R_m$), and the second current ($I_s$) passed through the slave side resistor ($R_s$). The resistances $R_m$ and $R_s$ represent here any pair wise combination of $R_k$, $R_{ref}$, $R_{Sn/In}$. The master side current $I_m$ could be ramped slowly to a predetermined value. The current $I_s$ was C x $I_m$ where C was the switch setting of the current comparator. C was adjusted until the SQUID output signal indicated a null condition at its input. Thermal EMFs generated in the low temperature circuit were eliminated by the following procedure. Let $V_s$ be a stray voltage in the circuit due to a thermal EMF. Then for the currents going in one direction the SQUID measured,

$$V^+ = I_s R_s - I_m R_m + V_s \qquad (2.2)$$

and for the reversed currents, one had

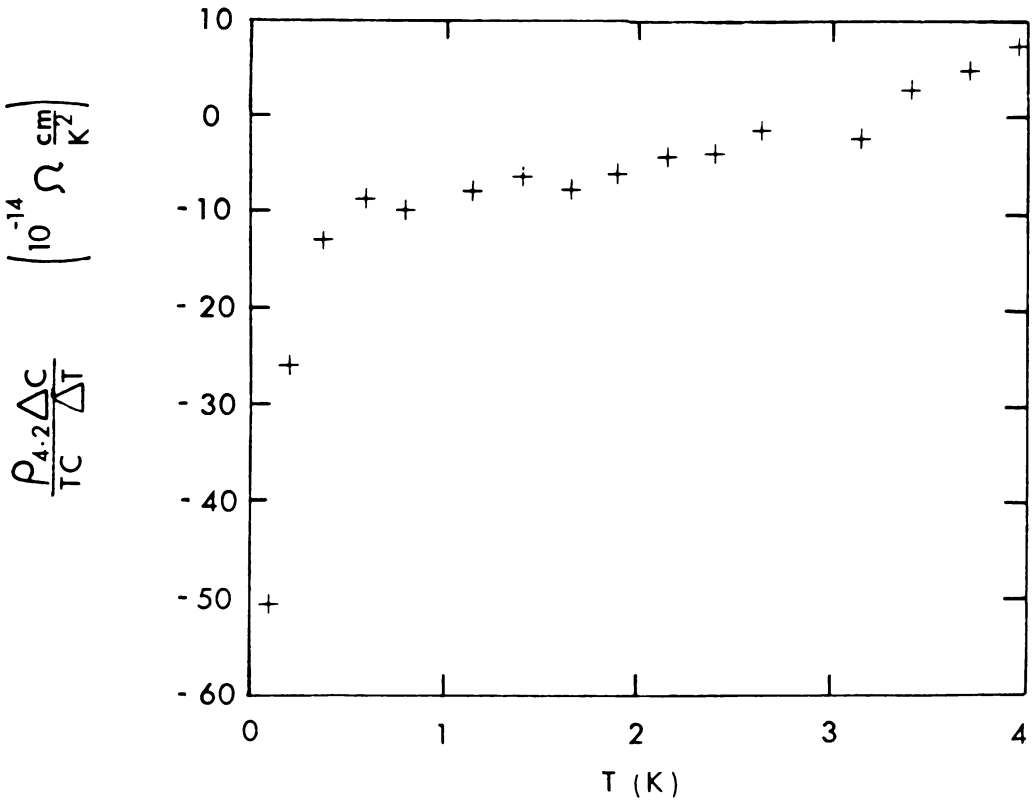


Figure 2.8 Temperature dependence of the copper reference resistor

$$V^- = -I_s R_s + I_m R_m + V_s \qquad (2.3)$$

C was adjusted until $V^+ = V^-$ was obtained. Then

$$I_s R_s - I_m R_m = -I_s R_s + I_m R_m \qquad (2.4)$$

$$2 I_s R_s = 2 I_m R_m \qquad (2.5)$$

so we get

$$C = I_s / I_m = R_m / R_s \qquad (2.6)$$

independent of $V_s$.

On the initial cooling to 4.2K the resistance of the sample and the copper-silver reference was measured using the tin-indium resistor. This double checked the copper silver reference and allowed $\rho_{4.2}$, the resistivity of the potassium sample at 4.2K, to be calculated using the A/L obtained earlier.

$$\rho_{4.2} = R_{4.2} \times \rho(300k) / R(300K) \qquad (2.7)$$

On subsequent deformations or annealings of the sample, just the ratio between $R_{ref}$ and the sample was measured, with this information being used to calculate $\rho_{4.2}$. To cool the system below 4.2K, the 1K pot was pumped. At this point, the tin-indium resistor, which was thermally connected to the 1K pot, was cooled below its superconducting transition temperature.

$\rho_o$ of the sample was measured directly by first stopping the circulation of the dilution refrigerator, after

the temperature of the sample can was less than 1K. Then the 1K pot was warmed up to 4.2K, at which point the tin-indium resistor became normal. Usually the sample warmed little during this process and stayed below 1K. Then the ratio between the tin-indium standard and the potassium or the copper resistor could be measured.

As the reader has already seen, one could measure the ratio between any two resistances in the low temperature circuit (Figure 2.7). This section explains how this ratio was used to obtain a temperature dependent resistivity for the potassium sample. Normally other research groups keep one resistor at 4.2K and just measure the ratio between it and the sample, while varying the temperature of the sample. The disadvantage of that method is that the Johnson noise generated by a resistor at 4.2K can be greater than the noise in the sample at 70mK. To minimize this, one would like to cool the reference to the same temperature as the sample, but then one has the problem of separating its temperature dependence from that of the sample. To avoid this problem, we regulated the temperature of the reference (T') keeping it slightly cooler than the sample. Then some heat was added to $H_{U2}$ and the ratio C measured at temperature T. Next the heat was switched to $H_{L2}$ so that a temperature difference $\Delta T$ was produced across $R_{w1}$, and $C+\Delta C$ was measured at temperature $T+\Delta T$. The current through the sample was usually 50mA, but checks were made to be sure there was no current dependence by using 25mA

occasionally. We then calculated the quantity:

$$\frac{\Delta C}{C_{ave}\Delta T} = \left[\frac{2}{(C + C + \Delta C)}\right] \quad \left[\frac{(C + \Delta C - C)}{(T + \Delta T - T)}\right] \qquad (2.8)$$

but $C = R_k / R_{ref}(T')$

$$\frac{\Delta C}{C_{ave}\Delta T} = \left[\frac{2\, R_{ref}(T')}{(R_k(T+\Delta T) + R_k(T))}\right] \left[\frac{(R_k(T+\Delta T)-R_k(T))}{(\Delta T\, R_{ref}(T'))}\right]$$

$$= \frac{(\Delta R_k(T))}{R_k(T+\Delta T/2)\Delta T} = \frac{1}{\rho(T)}\frac{d\rho(T)}{dT} = \frac{d\ln\rho}{dT} \qquad (2.9)$$

This quantity was normalized by multipling through by $\rho_o$ in the plots of the data.

This technique permits measuring the logarthmic derivatives of resistance to high precision by reducing the thermal noise of the reference. Another advantage is it permits double checking the thermometry, as will be discussed in section 2.7.

Another quantity measured was G, the thermoelectric ratio. This was measured since it was easily obtained, and the only additional equipment required was a heater at the end of the sample as shown in Figure 2.2. G is the ratio of electric current to heat flow at zero voltage drop across the sample. It was measured by sending heat ($\dot{Q}$) through a sample and then a current ($I_g$) to counteract the resulting thermal voltage, as indicated by the nulling condition at the SQUID input.

$$G = \left.\frac{I_g}{\dot{Q}}\right|_{E=0} = \frac{I_g}{I_h \times I_h \times R_h} \qquad (2.10)$$

where $I_h$ is the heater current and $R_h$ is the heater resistance.

## 2.6 Heat Flow in the Sample Can

The primary low temperature thermometer used in these experiments was a GR-200A-30 germanium resistance thermometer from Lake Shore Cryotronics(68). We called this thermometer GRT2. It was without a doubt the most important thermometer, since it was used to measure the temperature of the sample. It was mounted in a copper holder, and this holder was placed in a copper block which clamped it to the copper thermal feedthrough rod (Q, see Figure 2.1) This provided a strong mechanical support and a good thermal connection between the thermometer and the sample.

It was important that GRT2 be at the same temperature as the sample. This meant that the heat flow along the path from the sample to GRT2 had to be very small or a temperature gradient would have developed. Thus the heat flow in the sample can needed careful consideration. The flow of heat from the sample to the mixing chamber went as follows. The sample was cold welded to the silver wire (V) inside the can, providing good electrical and thermal contact. Two internal thermometers were connected to and supported by this silver wire. This wire was then spot

welded to an 1/8 inch diameter copper bar (Q) which took the heat outside the sample can. This copper bar was welded to another silver wire which took the heat to a silver tab which was pressed hard against the silver weak thermal link assembly (see Figure 2.9) with a brass screw. This assembly contained the U2 and L2 heaters and a thermal resistor ($56.45\mu\Omega$). The other side of this assembly was screwed to two silver tabs welded to the copper mixing chamber of the refrigerator. The largest thermal resistance and thus the largest temperature drop was due to the $56\mu\Omega$ resistor.

Let me now discuss the various parts of this thermal path. The silver wire was made of 99.9999% silver which was rolled to ~1 mm square and then oxygen annealed for 3 days at 900°C to give a very high thermal conductivity. This wire was bent as little as possible while shaping and welding in place. Thus few dislocations should have been added, keeping the thermal conductivity high.

The copper rod was made of OFHC copper which was machined to 1/8 inch diameter. This rod was oxygen annealed for 3 days at 950°C to remove dislocations and oxidize magnetic impurities. The electrical resistance of a similar rod was measured at 4.2K to be $\sim 0.07\mu\Omega$, a very small resistance compared to the weak link. This copper rod was part of the thermal feedthrough which conducted the heat outside the sample can. It was supported by a teflon spacer, for electrical isolation, in a copper block and sealed in place using Stycast 2850 GT epoxy(69). The Stycast

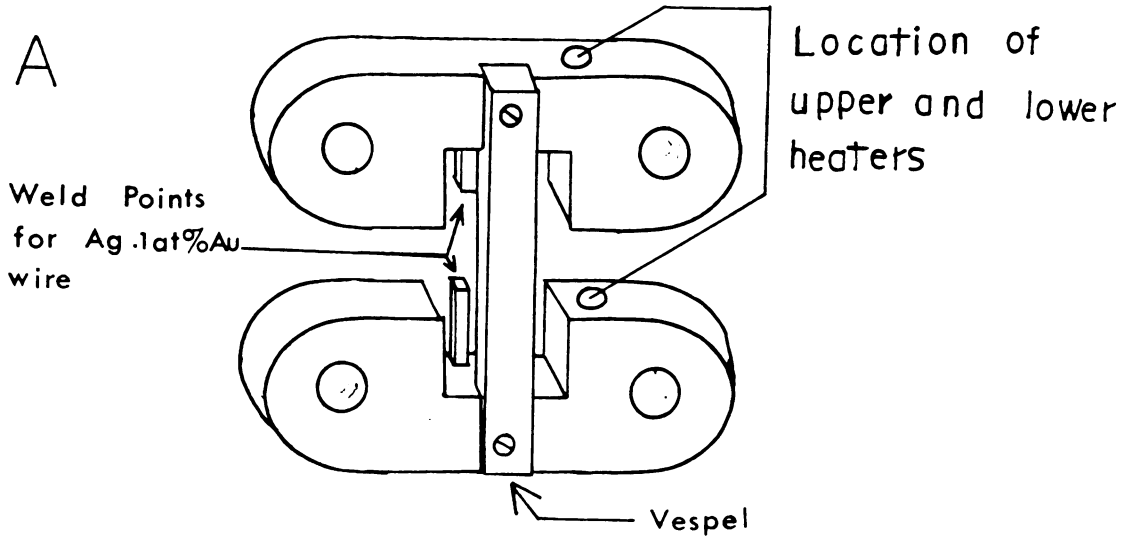



Figure 2.9 A) Weak thermal link assembly
B) thermal connection tab

provided a helium leak tight seal between the two copper parts. The copper block had been hard soldered to a 1/4 inch diameter thin wall stainless steel tube (P) 1.25 inches long, which was soldered to the top flange (L) of the sample can. This stainless steel tube provided thermal isolation for the feedthrough, as well as mechanical support.

The last part to be discussed is the weak thermal link assembly and the silver tabs (Figure 2.9). The electrical resistance between the tabs and the silver blocks was measured to be ~0.3$\mu\Omega$. The tabs and the two silver blocks were made of 99.9999% pure silver. The silver blocks were separated by a square Vespel rod(70), which had a very high thermal resistance. Between the two silver blocks was spot welded a thermal resistor made of Ag 0.1at%Au wire, with a resistance of ~56$\mu\Omega$. The two blocks each had a 4k$\Omega$ Dale resistor(71) as a heater.

On looking at the design, one can see that there are two other paths for heat from the sample to take. One is through the stainless steel tube (P, see Figure 2.1) supporting the copper thermal feedthrough (Q) and the other is through the stainless steel tube (J) supporting the copper squeeze plate (F). Table 2.6 shows the relative sizes of these heat leaks compared to the heat flowing through the weak thermal link at various temperatures used during the experiment. It should be noted that these ratios are upper limits since no account has been taken of the various contact thermal resistances in the alternate heat

Table 2.6 Alternate heat flow paths

| Temperature | | 4K | 1.0K | 0.4K | 0.1K |
|---|---|---|---|---|---|
| thermal feedthrough | r = | 2.6% | 2.8% | 1.9% | 1.6% |
| stainless steel support | r = | 2.2% | 2.4% | 1.6% | 1.5% |

r is the ratio of heat flow through the indicated path to heat flowing through the weak thermal link.

flow paths. Since the thermal resistance of the path between the potassium sample and the weak thermal link was small, and very little heat flowed down this path, there was practically no temperature difference between the sample and GRT2. The estimated temperature error cased by this was less than 0.2mK for the worst case.

Since GRT2 was mounted outside the sample can, thermal radiation and conduction of heat through the residual $He^3$ gas from the surrounding walls at 4.2K could cause significant heating of this thermometer. To eliminate this problem, a copper shield was placed around GRT2 and the sample can, and this shield was thermally connected to the mixing chamber. After transfer of liquid helium, the $He^3$ exchange gas in the vacuum can of the dilution refrigerator was extracted until a He leak detector showed less than $10^{-7}$ cc/sec of $He^3$ coming out of the system.

## 2.7 Thermometry

There were three thermometers outside the sample can and two thermometers inside the sample can. The first thermometer inside the sample can was a silicon diode from Lake Shore Cryotronics, Inc.. This thermometer, used between 4.2K and room temperature, was thermally connected to the cold end of the sample. In use, the voltage across the diode was measured with $10^{-5}$ A reversed biased current. Its temperature characteristics are shown in Figure 2.10.

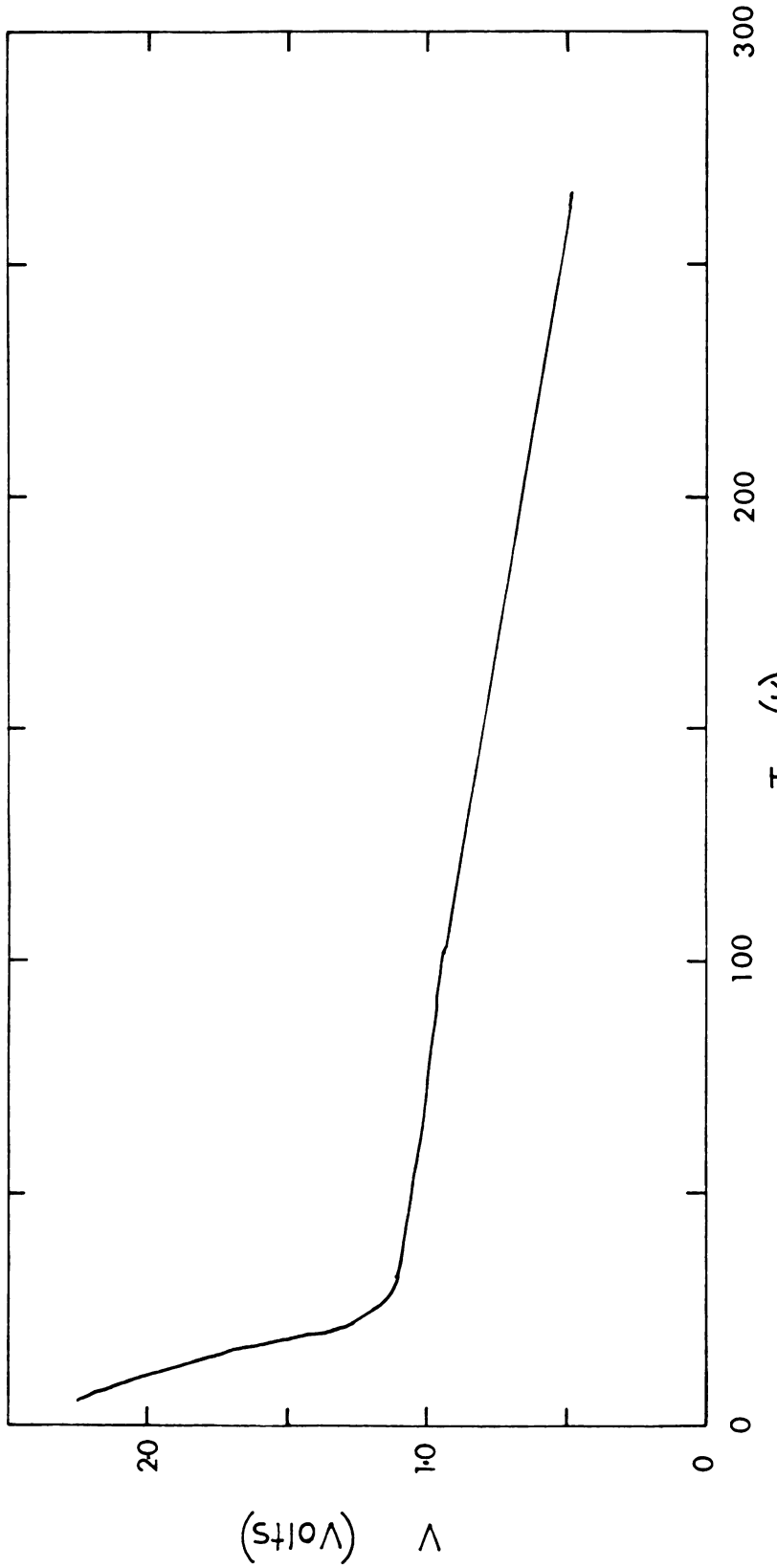


Figure 1.10 The voltage of the silicon diode vs temperature

Below ~30K it had a sensitivity of ~50mV/K, and above 30K about 2.8mV/K. It was calibrated from 4.2K to 80K against a germanium resistance thermometer, and from 80K to 300K against a platinum resistance thermometer. This diode thermometer was used solely for measuring the temperature at which the sample was deformed or annealed.

The other thermometer inside the sample can was a Speer(72) 100 $\Omega$ carbon resistor, which was calibrated against a germanium resistance thermometer (GRT2). The Speer's calibration was good to ~5mK at 90 mK and to ~20mK at 1.0K. No long term drifts due to thermal cycling were observed on comparing it to GRT2. This thermometer was also thermally connected to the potassium sample by a silver wire and was used to make sure that there were no large temperature differences between the sample inside the can and GRT2 outside.

With the exception of the silicon diode, the resistances of the thermometers were measured using two digital conductance bridges from S.H.E. Corporation. An uncalibrated Speer carbon resistor was mounted on the mixing chamber, and it was used when regulation of the mixing chamber temperature was required. The calibration of GRT4 (see Figure 2.7) was made by carefully comparing it to GRT2. This calibration was not important for most work since GRT4 was only used to maintain the reference at a constant temperature. The only exception is that samples Kh6b&d were measured using GRT4.

Next the calibration of GRT2 will be discussed. The first step, taken by J.L. Imes(73) and G.L. Neiheisel(74), was to calibrate a Cryocal CR50 thermometer using the $He^3$ vapor pressure scale and a susceptibility thermometer.

GRT2 was directly compared to the CR50 thermometer from 0.065K to 4.2K. The data from this comparison was fit with the equation,

$$\ln R = \sum_{i=0}^{9} A_i \, (\ln T)^i \qquad (2.11)$$

This first fit has been used for all measurements from 4.2K to 1.3K. However, there were indications that the calibration below 1.3K was not accurate enough for this study. Thus GRT2 was recalibrated below 1.3K.

The first step in the recalibration of GRT2 involved the use of a set of Superconducting Fixed Point Devices, SRM 767 and SRM 768 from the National Bureau of Standards(75). These devices gave an absolute value of temperature at 6 points, from 0.099K to 1.17K. Interpolation between the six points was performed using a susceptibility thermometer made of an irregularly shaped single crystal of CMN where 90% of the Ce was replaced by La. This second set of data, from 0.059K to 1.24K, was then fit with the above equation, and the resulting coefficients used for calculating the temperature below 0.5K.

The second step in the recalibration of GRT2 employed a

large powdered sample of cerrous magnesium nitrate and four of the fixed points between 0.519K and 3.414K. This last set of measurements was used to provide the 0.5K to 1.3K recalibration of GRT2.

The accuracy of these calibrations was then tested using the Wiedemann-Franz (W-F) law. This was done by mounting GRT2 at the end of a resistor made from a Ag 0.1at.%Au Alloy (which had previously been measured and shown to follow the W-F law by Edmunds et al.(76)) and attaching the other end to the mixing chamber, which was kept at a fixed temperature. Then heat was alternately switched from one side of the resistor to the other. The average temperature ($T_{ave}$) and the change in temperature ($\Delta T$) were calculated using GRT2 and the above fits. Then the Lorenz ratio was calculated from the equation:

$$L = \frac{R \dot{Q}}{T_{ave} \Delta T} \qquad (2.12)$$

$R \sim 79.8 \mu\Omega$. Figure 2.11 shows the results in terms of percent deviation from the W-F law. Thus the calibrations gave the product $T\Delta T$ to within an average value of 0.47% with a standard deviation of 1.2%. The maximum deviation from the Wiedemann-Franz law was 2.6%.

Finally, to ensure that there were no obvious problems while taking the data, the W-F law was used to double check the thermometry for every run. Figure 2.12 shows the results where the value of $R_{wf}$, the weak thermal link

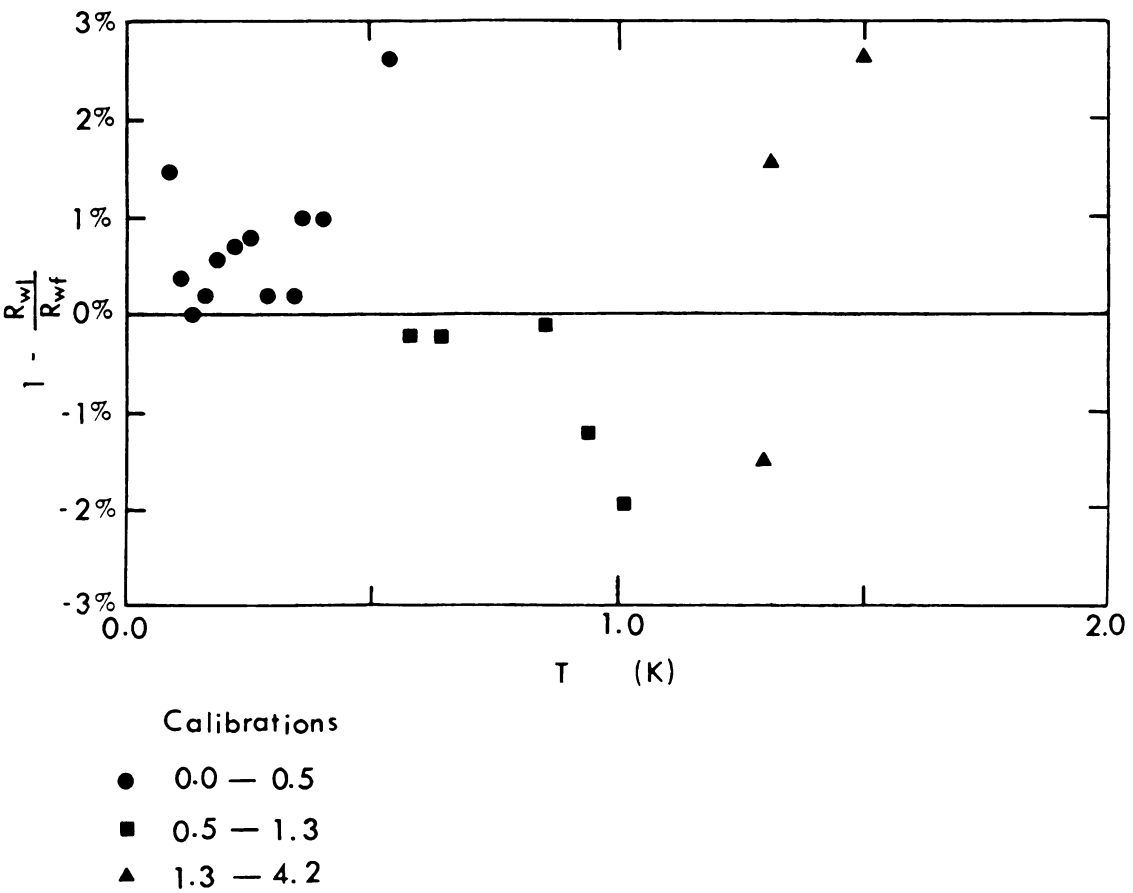


Figure 2.11 W - F law check of T T calculated using the GRT2 calibration

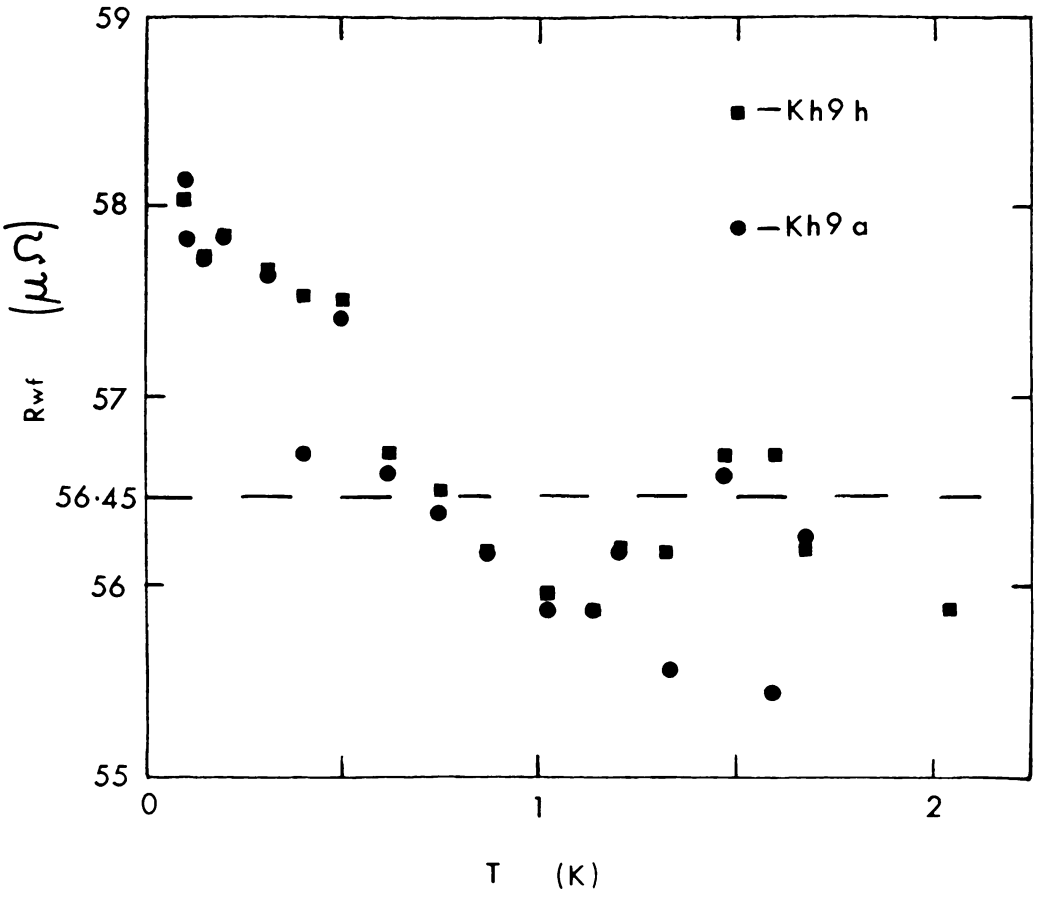


Figure 2.12 $R_{wf}$ vs T

resistance (see Figure 2.9), has been calculated using the W-F law,

$$R_{wf} = \frac{L_o}{\dot{Q}\, T_{ave} \Delta T} \qquad \dot{Q}=R_{L2}\, I^2 \tag{2.13}$$

This is compared with the measured value of the resistor of $56.45 \mu\Omega$. One should note that there is an uncertainty of ~1% in the values of $R_{wf}$ plotted, since the resistance of heater L2 is only known to 1%. The values for $R_{wf}$ have a range of 3%-higher to 2% lower than the measured value of this resistor. The main systematic problem in measuring the temperature of the sample is from the calibration of GRT2.

## 2.8 Uncertainties

The major uncertainty in G was random error due to thermal fluctuations and thermal drifts in the system. I estimate this to produce 2% uncertainty in G, based on temperature measurements made while taking data. The next largest error was in measuring the power to the heater, which for the very lowest measurements (~80mK and lower) was as high as 2%, and was due to the digital round off of the DVM used. Also at the lowest temperatures, Johnson noise limited our null detector resolution to ~1% in G. The other sources of error were mostly systematic and very small in comparison with the random uncertainties. The value of the heater resistance was measured to within 0.1%. The uncertainty of the resistance used to measure the current

through the heater was 0.05%. The current $I_g$ was produced by the current comparator (C. C.) system and was measured to be within 0.16% of the value set. A current setting of 0.1 x50mA was used while measuring G, see Table 2.7. The drift in the zero current of the current comparator was much less than the absolute uncertainty in the current.

Table 2.7 Current comparator error in absolute current

| C.C. Setting | $\left(\frac{\text{Current output}}{\text{C. C. Setting}}\right) - 1$ |
|---|---|
| 0.1 x 50mA | +0.16% |
| 0.2 x 50mA | +0.18% |
| 0.5 x 50mA | +0.22% |
| 1.0 x 50mA | +0.20% |

The random errors in measuring $\rho_o$ and $\rho_{4.2}$ were as follows. First $R_{4.2}$ and $R_o$ were measured to ~2% against $R_{Sn/In}$, the limiting factor being the temperature dependence of $R_{Sn/In}$ near 4.2K. To a lesser degree the measurement of $R_{4.2}$ was also affected by the slight changes in the temperature of the He bath due to changes in atmospheric pressure. Additional systematic error arose from the measurement of A/L. The room temperature resistance of the samples was always measured to better than 1%, but on deforming the samples the A/L sometimes shifted. This was a correctable problem for all but Kh8, where we had to interpolate to obtain the values for A/L. This problem is discussed in the next chapter.

The precision of C has been shown to be better than 0.1 ppm(76). To reduce the uncertainty in $\Delta C$, an averaging

technique was used, which permitted interpolation to less than 0.01 ppm in C. In some cases, however, the averaging technique was not used for small $\Delta C$ and a much larger uncertainty resulted. In the calculation of the quantity

$$\frac{1}{C_{ave}}\frac{\Delta C}{\Delta T} \qquad (2.14)$$

the largest uncertainty (outside of the uncertainty in $\Delta C$) was usually due to the systematic error in $\Delta T$, which was estimated using the W-F law in the last section, to be less than 2.6%. So the uncertainty in this quantity is usually less than ~3%.

Finally, the uncertainty in measuring the heat produced by the upper and lower heaters used for the in-situ W-F law checks is 1%, the uncertainty in the resistance of the $4k\Omega$ Dale resistors.

# CHAPTER 3

## Experimental results

In this chapter the experimental results will be presented and interpreted in light of the many theories discussed in chapter 1. Two pure samples of potassium Kh1 and Kh9 were deformed at 4.2K and then annealed in a series of increasingly higher temperatures. The samples, Kh2 and Kh8, were subject to a series of plastic deformations at 60K. One potassium - rubidium alloy was deformed at 60K and then annealed at 160K. The remainder of the samples were not deformed and were used as a study of the effects on the resistivity of contact with various materials.

For the samples deformed at 4.2K, it was hoped to see the relative effects of both point defects and dislocations. By annealing these samples at 60K, where most point defects are unstable, one could then see the effects of just dislocations. For samples deformed at 60K, one expects mostly dislocations to be introduced.

For samples Kh2 and Kh8 the dependence of dislocation

scattering on the concentration of dislocations was sought.

## 3.1 Resistivity

It is of some interest to compare our results for undeformed samples with the earlier experimental work on potassium. This comparison will be made in two temperature regions; first above 1.1K to show we get the same electron - phonon term and second, below 1.2K to compare the electron - electron term.

Figure 3.1 shows this comparison of samples Kh8a and Kh9a at high temperatures with the previous work of Lee et al.(77), van Kempen et al.(78), and Rowlands et al.(79). Below about 1.5K the temperature dependence seen is due primarily to the electron - electron term in $\rho$. Above 1.8K the electron - phonon umklapp process predominates, and the data follow the expected $\rho \sim \exp(-\theta^*/T)$ dependence. Our data above 1.8K agree very well with the previous work, so the samples in this study have the same electron - phonon term as measured by other groups.

Figure 3.2 shows a comparison below 1.5K with the 0.9mm samples of Lee et al.(80). In this figure an $AT^2$ behavior for $\rho$ would produce a horizontal straight line if A is independent of T. Note that samples Kh8a and Kh9a have, on average, lower values of A than the samples of Lee et al.. Also the departure from the A = constant expectation is more marked for Kh8a and Kh9a. Recent work at MSU has shown that

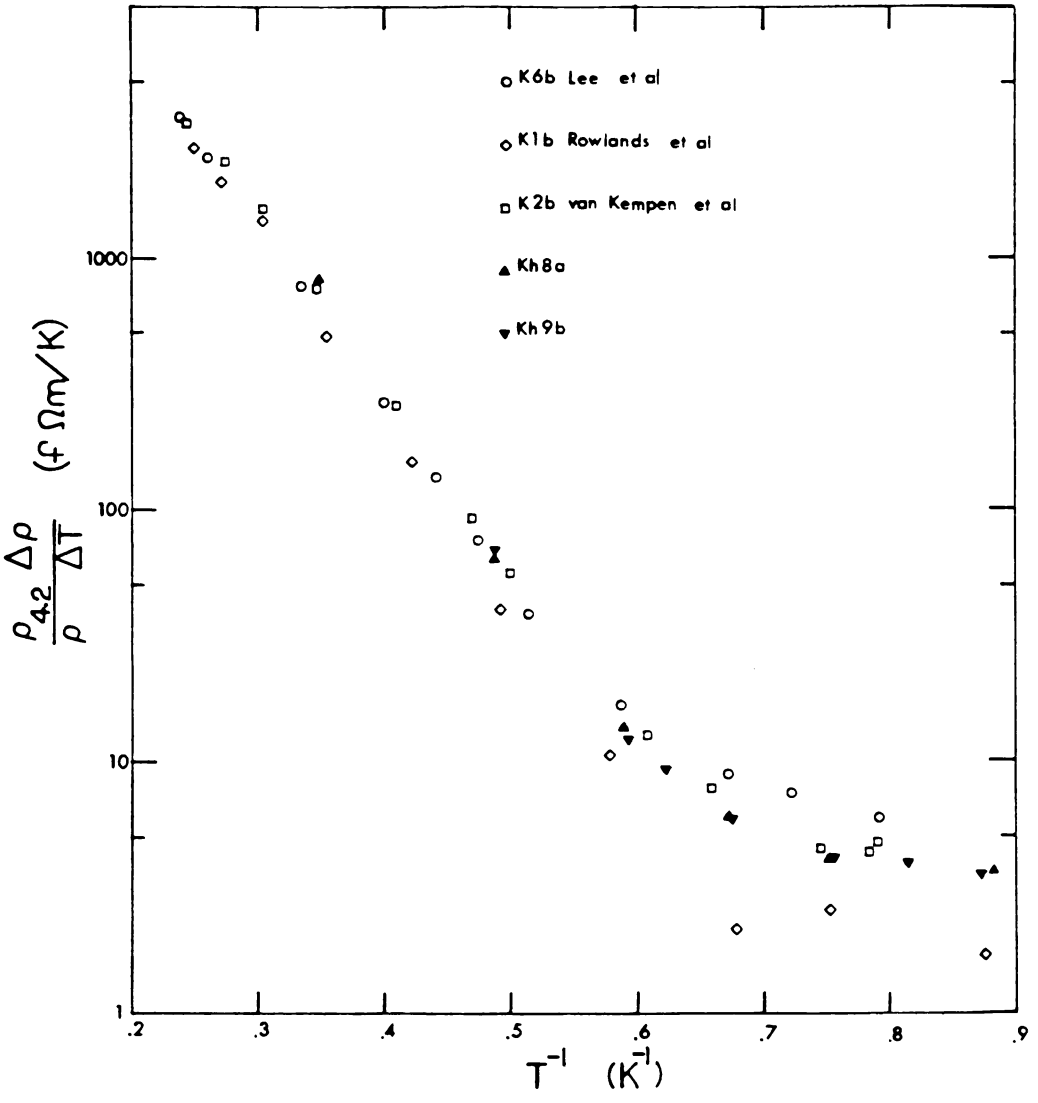


Figure 3.1 High temperature comparison with previous groups.

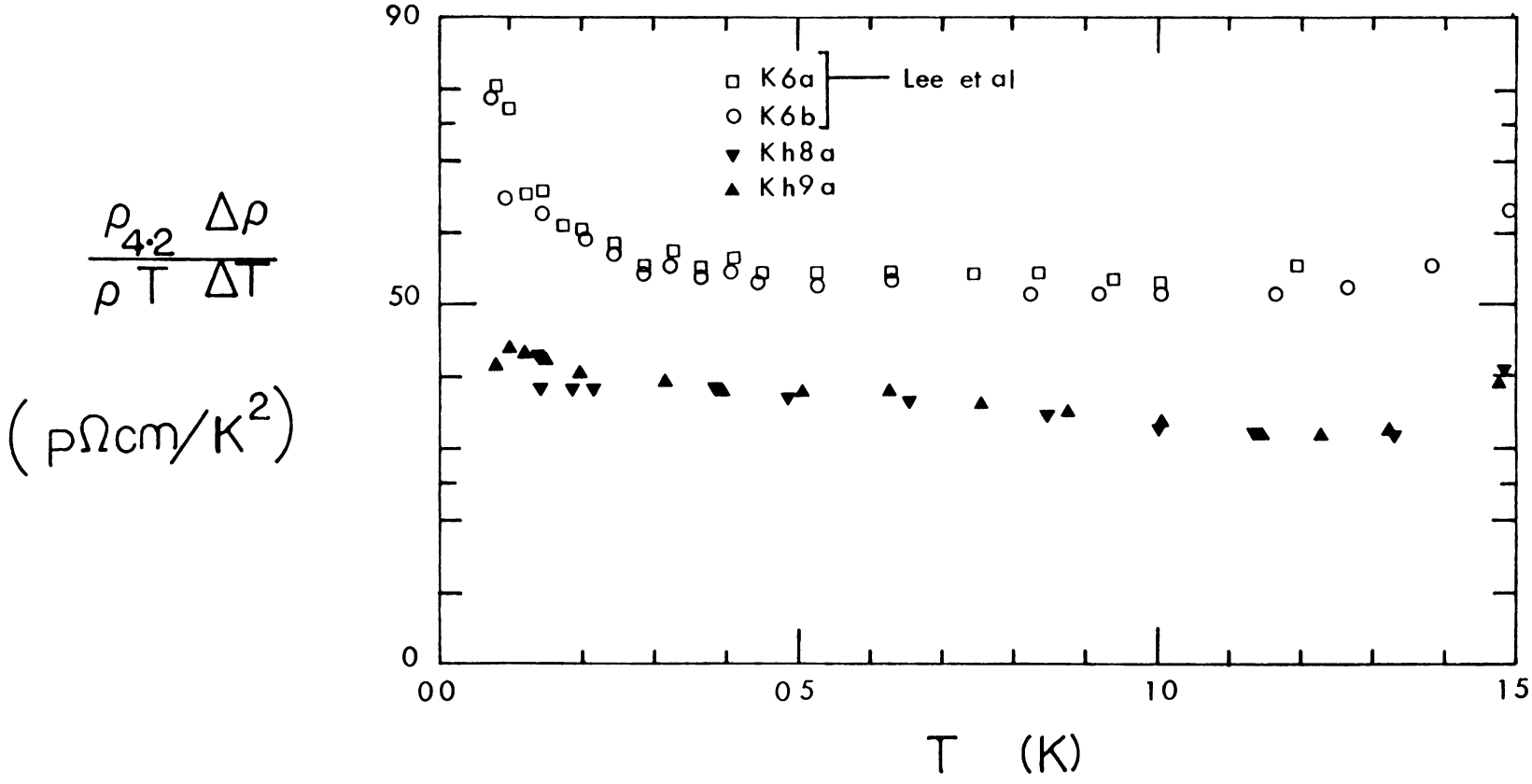


Figure 3.2 Low temperature comparison with previous results

this lowering of A and the temperature variation of A become more pronounced for samples which are thinner than 0.9mm(32). Since the diameter of the extruded samples are determined by the size of the exit hole on the press and since we do not have a direct way of measuring the diameter of the samples, it is possible that Kh8a and Kh9a had slightly smaller diameters than the 0.9mm sample of Lee et al.

### 3.1.1 The residual resistivity

It is of some interest to observe the effects of deformation and annealing on the residual resistivity and to compare these results with the earlier work of Gugan(81). Table 3.1 lists the recovery of the residual resistivity for samples Kh1 and Kh9.

Both samples showed complete recovery by 165K, in agreement with Gugan, who found the last stage of annealing to take place below 150K for most samples. For annealing above 80K, Gugan found ~25% recovery in good agreement with our results. However, we find ~30% recovery from 7.5K to 20K, and 42% from 20K to 80K, whereas Gugan found 40% and 30% respectivly. Thus for our sample slightly more annealing occurred at higher temperatures. Also less annealing is seen in the 4.2K to 7.5K stage, which may be due to a slight heating of our sample during the deformation, near 4.2K. Our samples showed the same general

Table 3.1 Recovery of annealed samples

| Sample | recovery of $\rho_o$ | Temperature of anneal | |
|---|---|---|---|
| Kh1a | ---- | ---- | |
| Kh1b | 0% | 4.2K | (deformation) |
| Kh1c | 78% | 60K | |
| Kh1d | 100% | 155K | |
| | | | |
| Kh9a | ---- | ---- | |
| Kh9b | 0% | 4.2K | (deformation) |
| Kh9c | 1% | 7.5K | |
| Kh9d | 31% | 20K | |
| Kh9e | 64% | 60K | |
| Kh9f | 73% | 80K | |
| Kh9g | 94% | 120K | |
| Kh9h | 100% | 165K | |

features for recovery of the residual resistivity as Gugan.

Now we will look at the dependence of the residual resistivity on the force used to deform the samples at 60K. Figure 3.3 shows a plot of the residual resistivity vs the pressure applied to the bellows. In this plot corrections have been made to the pressure to remove the force needed to move the bellows.

As mentioned before, the A/L for sample Kh8 shifted during the experiment, most likly due to an unexpected change in L during deformation. No such shift took place in Kh2. Since Kh2 showed a roughly linear increase of $\rho_o$ with pressure, it was decided to correct the A/L of Kh8 by requiring $\rho_o$ to be proportional to the pressure. The straight line drawn through the Kh8 data represents this requirement. We know that this line is correct for both end points, since A/L was measured directly for them. The difficulty comes for the points in between, with the maximum correction to $\rho_o$ being 12% for Kh8e if the initial A/L were correct. It is likely that the estimates of A/L are always more accurate than this worst case.

### 3.1.2 The electron - phonon resistivity

As the reader has already seen, we reproduced the high temperature data seen by other research groups for undeformed samples. The next question is how well our deformed sample data compare to the theories on $\rho_{e-p}$ in the

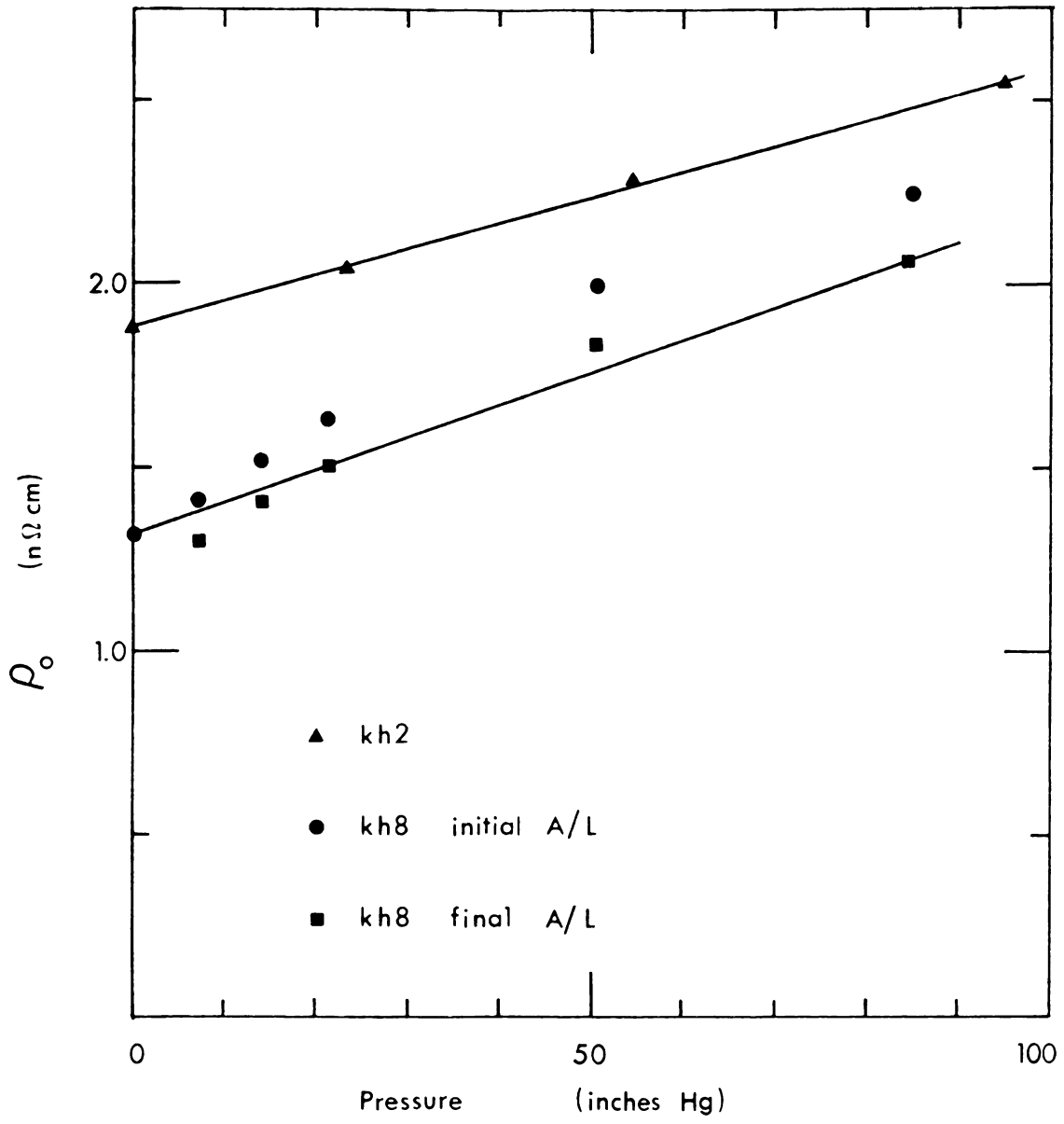


Figure 3.3 The residual resistivity vs the pressure of deformation

limit of a high concentration of dislocations for T>1.7K.

Figure 3.4 is a plot of our data compared to the theory of Danino, Kaveh and Wiser(82). The solid curves represent their theory for the indicated dislocation densities, $N_d$. For this plot $\rho^a_{e-p}$ was calculated by fitting our undeformed pure samples (Kh3, Kh9a, and Kh9h) to an equation of the form,

$$\rho^a(T) = AT^2 + BT \exp(-\theta^*/T) = AT^2 + \rho^a_{ep} \qquad (3.1)$$

where 2<T<4.2K, and the superscript "a" refers to the undeformed samples. The parameters obtained were:

$A = 1.30 \pm .007 \times 10^{-13}\ \Omega\,cm/K^2$

$B = .773 \pm .038 \times 10^{-9}\ \Omega\,cm/K$

$\theta = 20.3 \pm .2\ K$

The resistivity $\rho_{ep}$ was calculated by subtracting the $AT^2$ term from the experimental $\rho(T)$, using the coefficient listed above. The assumption that A does not change appreciably under deformation will be justified later. Sample KRbh is not shown, since it was measured against a different reference resistor, the resistance of which has not been measured as a function of temperature.

One can see from the graph, that the experimental ratio of $\rho_{e-p}/\rho^a_{e-p}$ increases at low temperatures, and is in rough agreement with theory near 2.0K for $N_d \sim 5 \times 10^{10}/cm^2$. However, near 4K the data and the theory are not in agreement for this value of $N_d$. In addition, using Basinski's result(83), one would predict from the change in

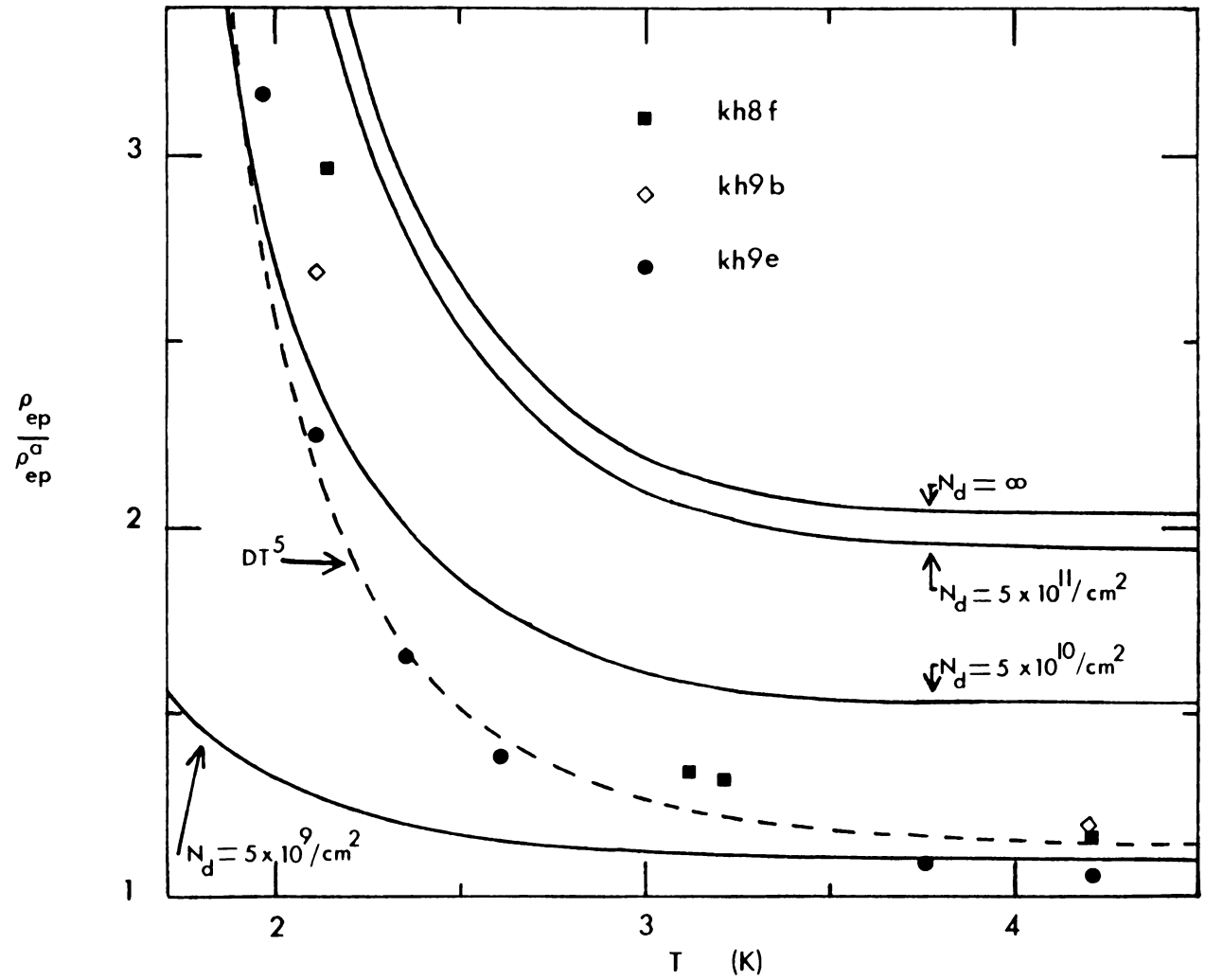


Figure 3.4 The effects of deformation on the electron - phonon term.

$\rho_o$ for sample Kh9e that $N_d \sim 8 \times 10^8/cm^2$ which is almost a factor of 100 smaller than the above number. Thus the theory does correctly predict that the ratio will increase as the temperature is lowered, but the theory does not give the correct overall temperature dependence or a reasonable value for $N_d$.

The more recent theory by Enquist(84) and also by Danino, Kaveh, and Wiser(85) would appear to give a more correct form for our data. This theory was discussed in section 1.1.2. The dash curve shown in Figure 3.4 is the result of fitting this theory ($DT^5$) to sample Kh9e. For this fit only the parameter D was varied. This theory follows the form of the data reasonably well over the entire temperature range. The coefficient obtained ($D=30\ f\Omega cm/K^5$) was less than the maximum theoretical value predicted by Ekin and Maxfield(88) ($D=35.4\ f\Omega cm/K^5$) for the case of full quenching of phonon drag. Moreover, the value obtained for D was larger than that obtained from the low temperature fits discussed in the next section. This is not suprising, since only a crude estimate of A was used for the data of Figure 3.4.

### 3.1.3 The low temperature data

Figure 3.5, Figure 3.6, and Figure 3.7 show the results for Kh8, Kh9, and KRbh respectively. The main feature of the graphs is the very large low temperature

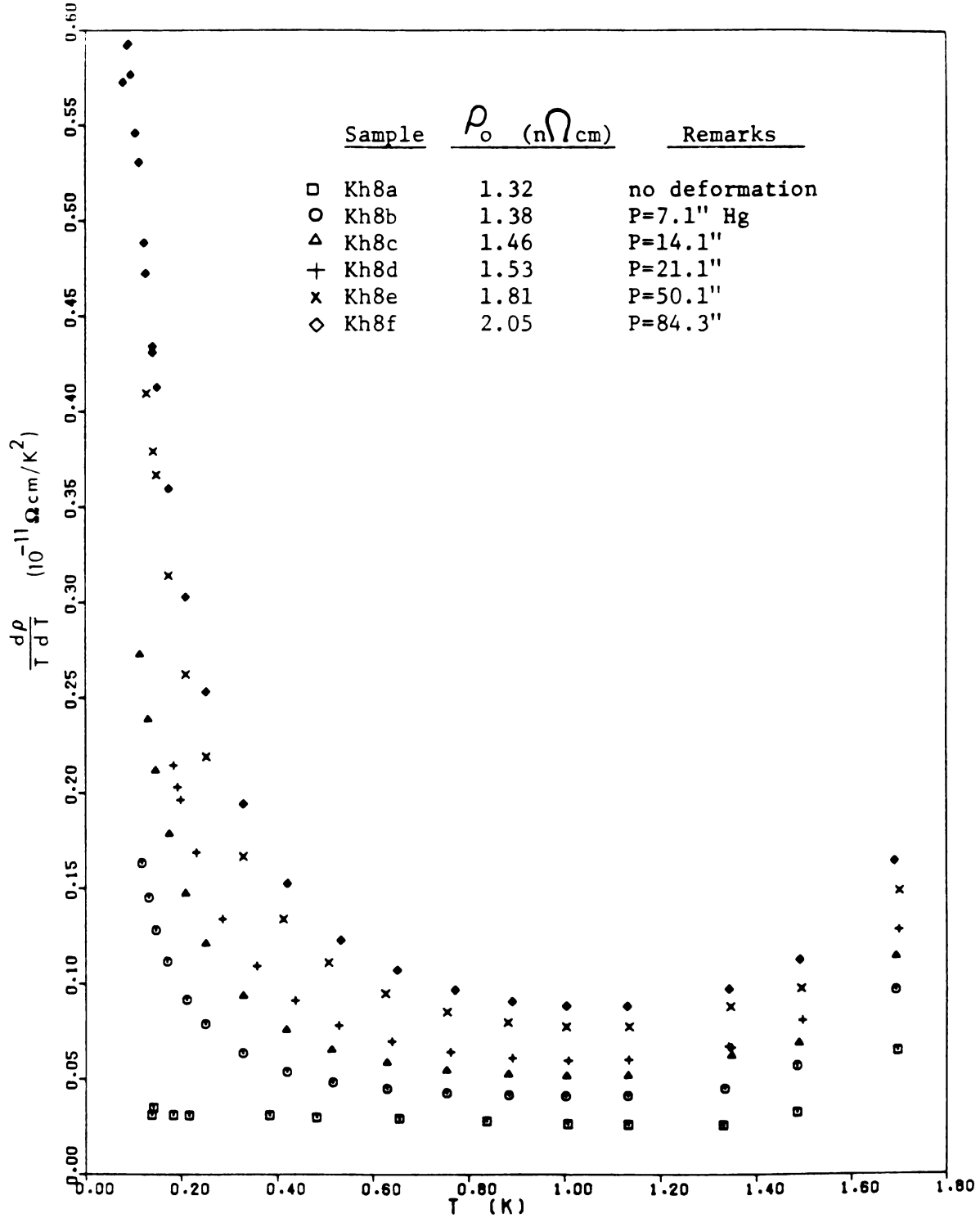


Figure 3.5 (1/T)(d$\rho$/dT) vs T for Kh8

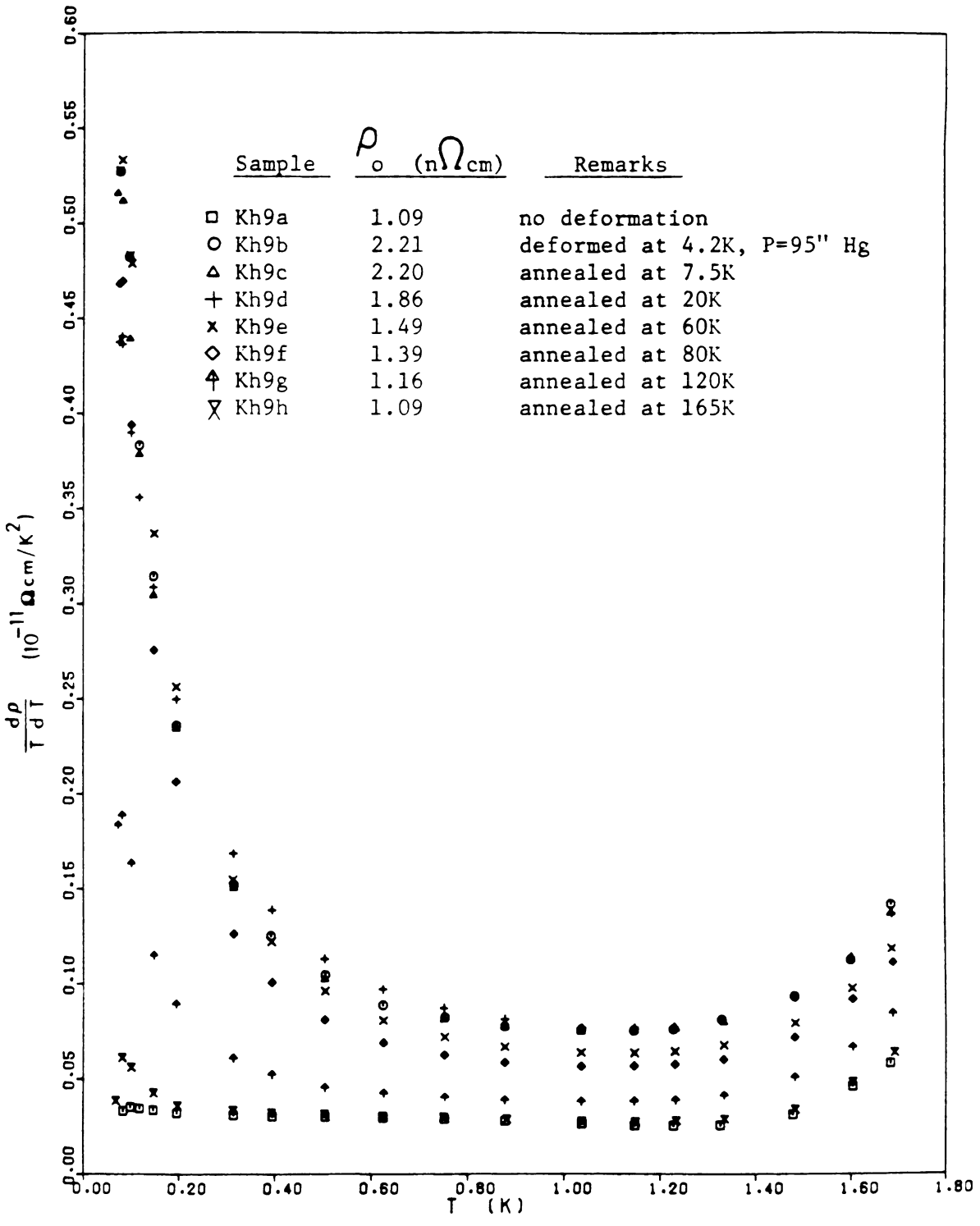


Figure 3.6 (1/T)(d$\rho$/dT) vs T for Kh9

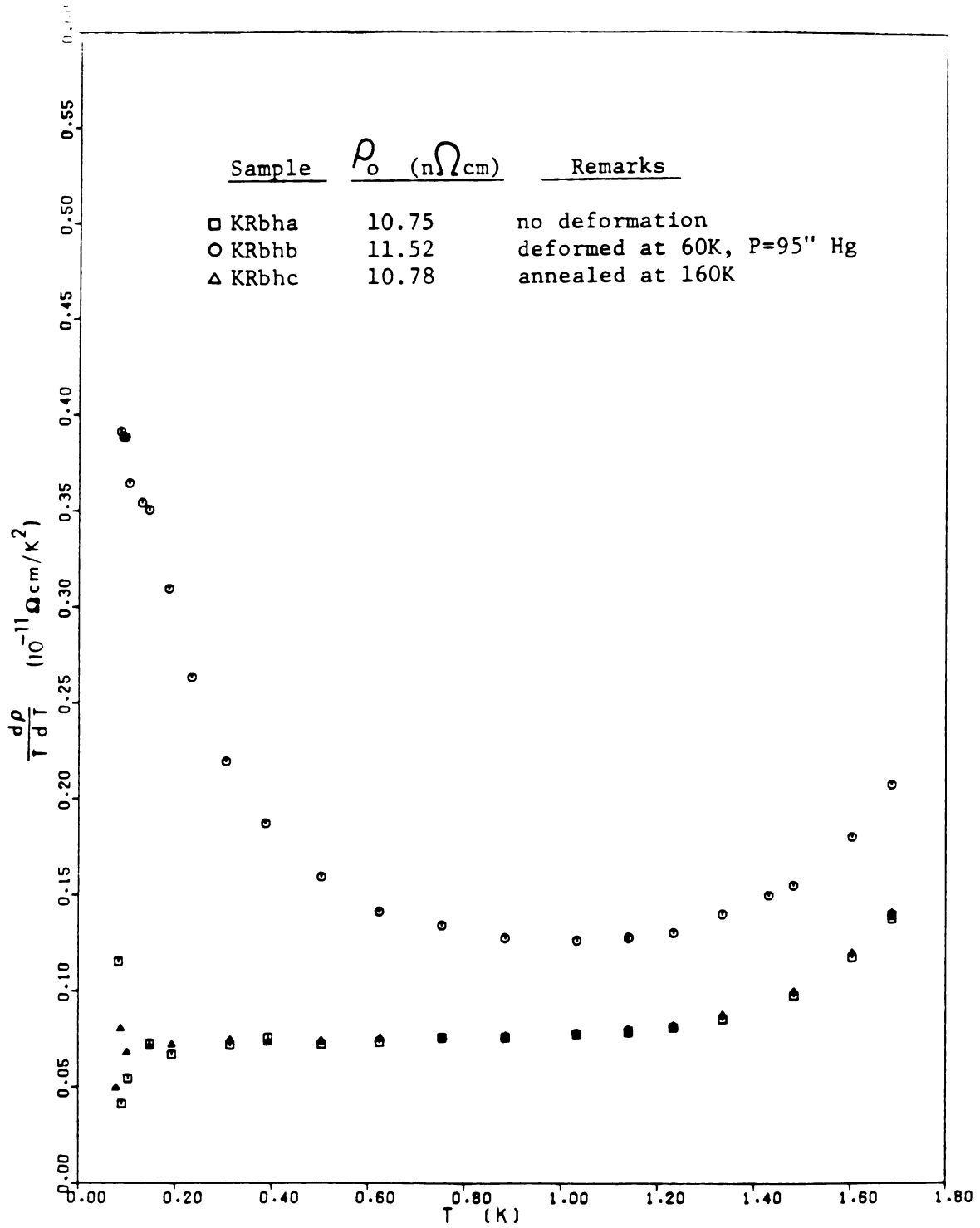


Figure 3.7 $(1/T)(d\rho/dT)$ vs T for KRbh

divergence after deformation. Since these divergences are not seen for these samples in the undeformed state, we may associate them with some new scatterer introduced through plastic deformation. Another point of interest, seen in Kh9 and KRbh is that after annealing the samples near 160K, one recovers almost completely the temperature dependence prior to deformation. This recovery coincides with the obseved recovery of $\rho_o$ (discussed in Section 3.1.1). Hence, it is concluded that dislocations are the major contribution to the divergence.

Looking at Kh8, one can see that as one increases the number of dislocations, the size of the divergence increases. Although it is somewhat harder to see, the slopes also increase for T> 1.2K, which is expected since, as discussed in section 3.1.2, $\rho_{ep}$ increases under deformation.

If one were to have electron - electron, electron - phonon, and electron - dislocation scattering, the resistivity would be of the form,

$$\rho = \rho_o + A\,T^2 + \rho_{e\text{-}p} + \rho_{e\text{-}dis} \qquad (3.2)$$

$$d\rho/dT = 2\,A\,T + \rho'_{e\text{-}p} + \rho'_{e\text{-}dis} \qquad (3.3)$$

In the limit where $\rho'_{e\text{-}p}$ and $\rho'_{e\text{-}dis}$ were negligible the data would follow a horizontal straight line, on these graphs. All these figures show such a region, but the actual size of the electron - electron term can not be easily deduced from the height of this plateau, since the

low temperature tail of $\rho'_{e\text{-}p}$ and high temperature tail of $\rho'_{e\text{-}dis}$ are present in this region. However, the height of the plateau does give a maximum value for the size of the electron - electron term. Let A' be this maximum value of A, as listed in Table 3.2. Sample Kh9 shows that annealing at temperatures upto 20K, has little effect on the height of the plateau. Thus the annealing out of point defects below 20K does not influence A' appreciably.

Next, our results will be compared to those of the Netherlands group. When van Vucht et al.(86) analysed their data, they were not aware of the low temperature $\rho_{e\text{-}dis}$ term, since they could not measure below 0.9K. Because of the plateau, it is understandable why this group chose to interpret their data as having $AT^2$ behavior near 1K. Thus the values they quoted for A should be compared to A'.

Figure 3.8 is a comparison of A' of Kh8, Kh9, and KRbh with the data of van Vucht et al. This graph shows the change in A' ($\Delta$A') vs the change in the residual resistivity ($\Delta\rho_o$). Plotting the data this way removes differences between the samples due to different initial impurity levels and different initial sample sizes in their undeformed states.

Sample K7 (measurements 7 to 9) was deformed at 4.2K with several levels of deformation. One sees a somewhat non - linear increase of $\Delta$A' with $\Delta\rho_o$. Comparing this to sample Kh8, which was deformed with progressivily higher

Table 3.2 Effective A for the samples

| Sample | $\rho_o$ ($n\Omega$ cm) | A' ($10^{-13}\ \Omega$ cm/K$^2$) |
|---|---|---|
| Kh1a | 4.19 | 3.00 |
| Kh1b | 6.30 | 6.96 |
| Kh1c | 4.76 | 5.75 |
| Kh1d | 4.12 | 3.06 |
| Kh2a | 1.87 | 2.25 |
| Kh2b | 2.04 | 3.23 |
| Kh2c | 2.28 | 4.09 |
| Kh2d | 2.55 | 4.81 |
| Kh2e | 1.95 | 2.24 |
| Kh8a | 1.32 | 1.52 |
| Kh8b | 1.38 | 2.07 |
| Kh8c | 1.46 | 2.60 |
| Kh8d | 1.53 | 3.01 |
| Kh8e | 1.81 | 3.92 |
| Kh8f | 2.05 | 4.42 |
| Kh9a | 1.09 | 1.45 |
| Kh9b | 2.21 | 3.79 |
| Kh9c | 2.20 | 3.76 |
| Kh9d | 1.86 | 3.85 |
| Kh9e | 1.49 | 3.19 |
| Kh9f | 1.39 | 2.89 |
| Kh9g | 1.56 | 1.93 |
| Kh9h | 1.09 | 1.51 |
| KRbha | 10.75 | 3.65 |
| KRbhb | 11.52 | 6.38 |
| KRbhc | 10.78 | 3.72 |

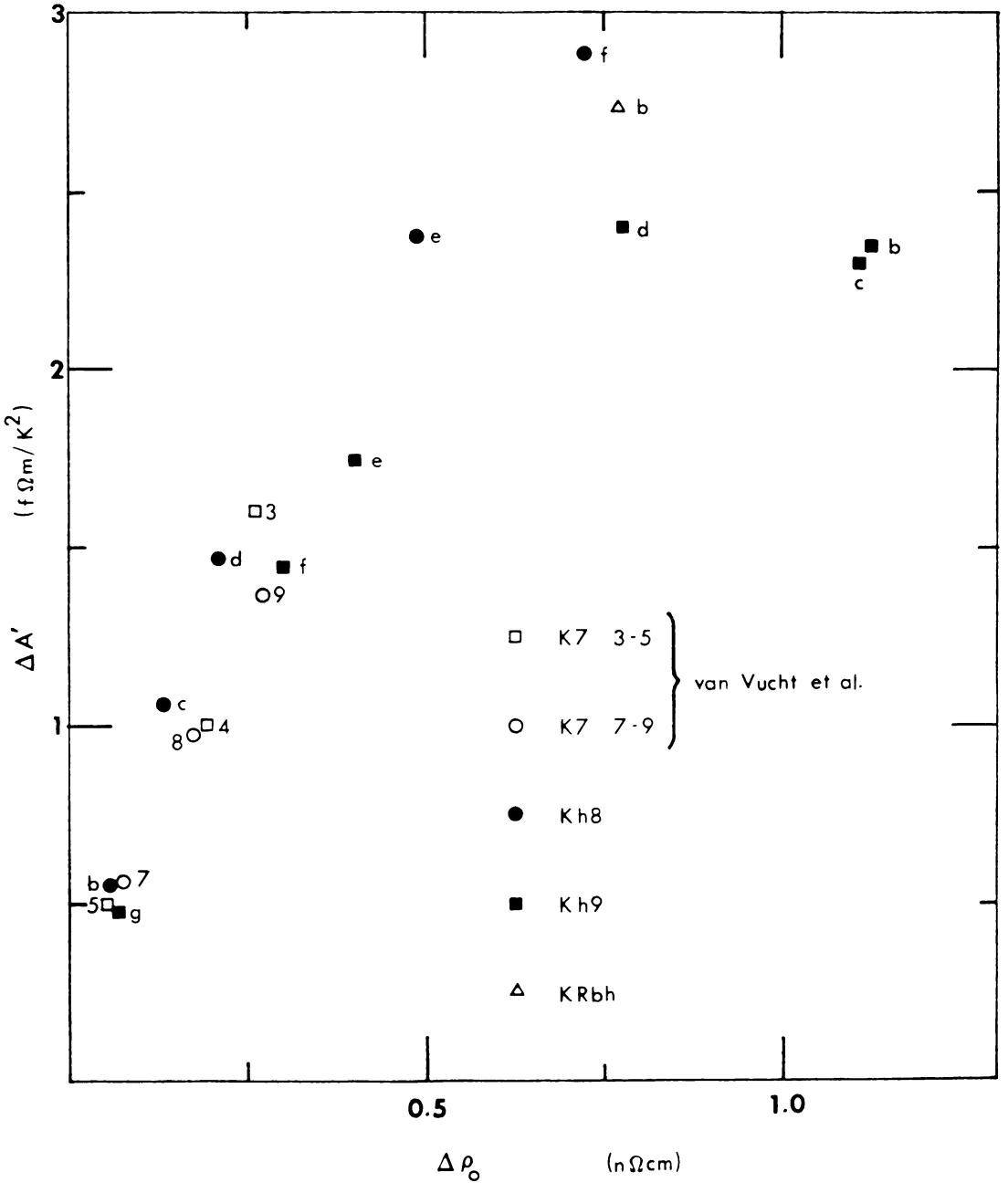


Figure 3.8 $\Delta$A' vs the change in the residual resistivity.

pressures at 60K, one sees that $\Delta A'$ also increases with $\Delta \rho_o$, in a non - linear fashion. The relatively small differences between the two curves are most likely due to the different temperatures at which the samples were deformed. The smaller overall slope of these van Vucht et al. data is consistent with the fact noted earlier that the defects which anneal out below 20K have little effect on A'. Since these defects would still contribute to $\Delta \rho_o$, one would expect a smaller dependence of $\Delta A'$ upon $\Delta \rho_o$.

Next, sample K7 (measurements 3 to 5) will be compared with sample Kh9. Both samples were deformed at 4.2K and annealed at several higher temperatures. K7,3 and Kh9b are the unannealed samples. The samples K7,4 and Kh9d were annealed at 18K and 20K respectively, and samples K7,5 and Kh9f at 78K and 80K respectively. The data of van Vucht et al. showed a gradual recovery of A' with increased annealing temperature, whereas, Kh9 showed little recovery until it was annealed above 20K. After 20K, Kh9 does show the same gradual recovery as K7. One may conclude that the behavior of the deformed (0.9-mm-diameter) samples in this study is rather similar to those of van Vucht et al., even though their 3-mm-diameter samples were twisted instead of squashed. Finally, one should note, that KRbhb had about the same increase in the residual resistivity as Kh8f, and showed about the same increase in A'.

Next let us compare A' with the theory of Kaveh and Wiser. Samples Kh8 and KRbh were deformed at 60K. In both

samples, there was a similar increase in the residual resistivity and A'. These increases in A' are much larger than would be predicted by Kaveh and Wiser (see Figure 1.4, page 23). Moreover, Kaveh and Wiser claimed that A was a function of $\rho_{oi}/\rho_{od}$. Sample KRbh should be in the impurity dominated limit, since the undeformed sample had $\rho_o \sim 10.75 n\Omega cm$ which was many times larger than the residual resistivity of a pure sample ($1.32 n\Omega cm$ for the pure undeformed Kh8a). Thus, while adding $0.73 n\Omega cm$ of dislocations to a pure sample like Kh8 should have a large effect on A, one would expect to see little change for sample KRbh. Since the change in A' is the same for both samples, one must conclude that some mechanism other that that proposed by Kaveh and Wiser causes most of the change in A'.

One must remember that A' is most likely an over estimate of the correct value of A. To make a realistic comparison with the theory of Kaveh and Wiser, the $\rho_{e\text{-}dis}$ and the $\rho_{e\text{-}ph}$ terms must be examined.

Figure 3.9, Figure 3.10, and Figure 3.11 show plots of the resistivity data for Kh8, Kh9, and KRbh, which emphasize the behavior of $\rho_{e\text{-}dis}$. All three graphs show similar behavior: a peak in the data for the deformed samples near 0.2K. On these graphs the electron - electron term would appear as a straight line (2AT) going through the origin. Again one sees in samples Kh9 and KRbh that annealing near 160K brings back the initial temperature dependence of the

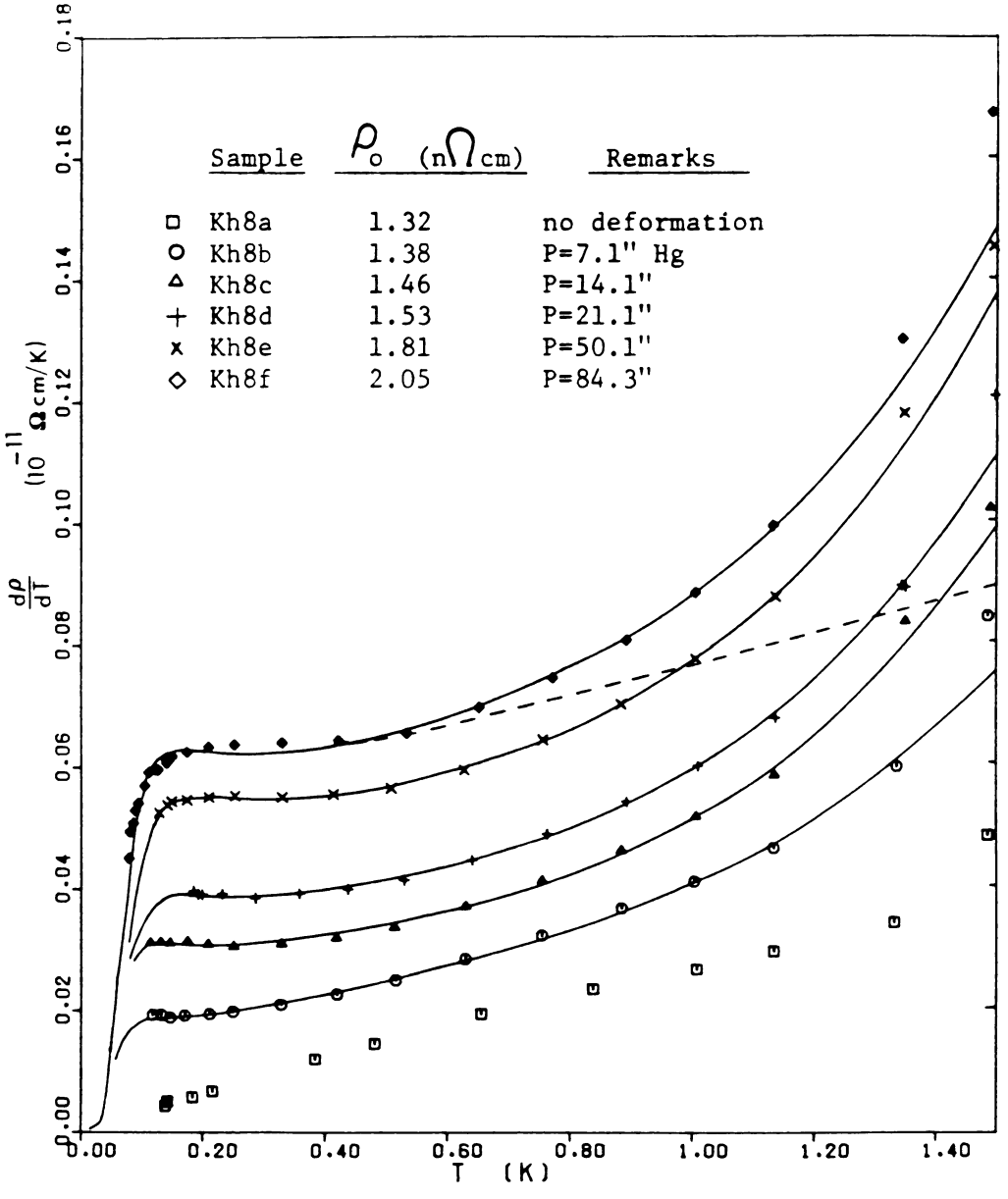


Figure 3.9 $d\rho/dT$ vs T for Kh8

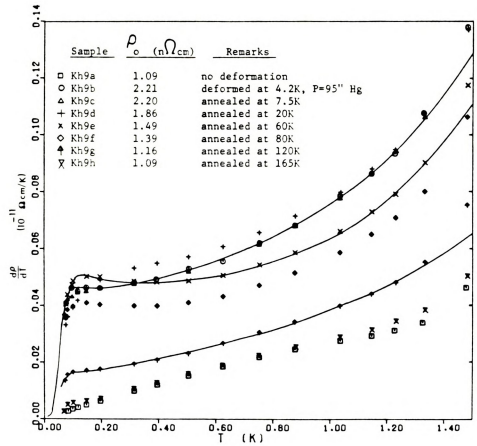


Figure 3.10 $d\rho/dT$ vs T for Kh9

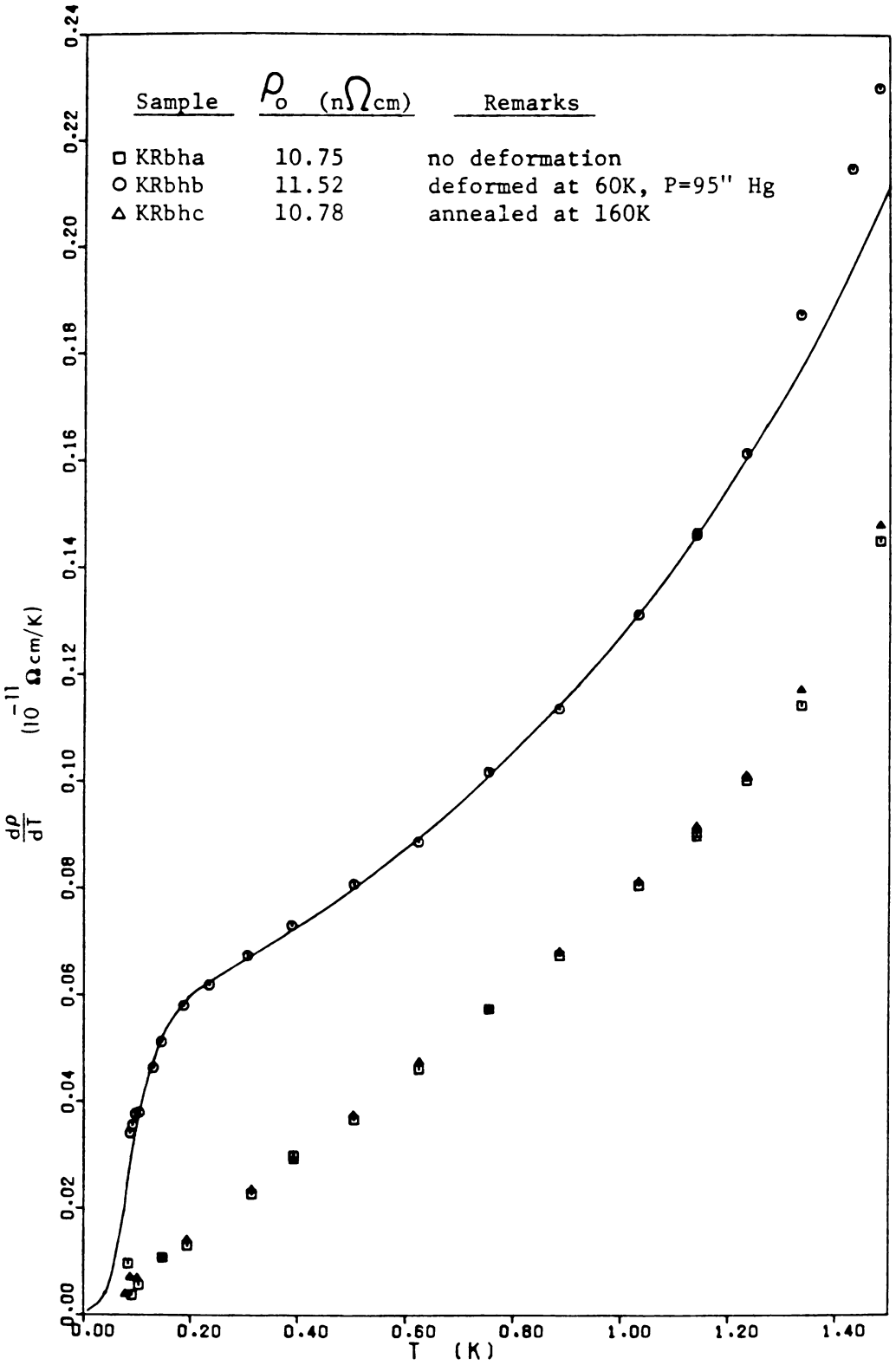


Figure 3.11 $d\rho/dT$ vs T for KRbh

undeformed samples.

Sample Kh8 shows a gradual increase of $d\rho/dT$, as one increases $\rho_o$. The form of $\rho_{e\text{-}dis}$ changed markedly when sample Kh9 was annealed at 20K and 60K, but for later annealings the main effect was to reduce the size of $d\rho/dT$, not its shape. Thus it seems unlikely that this peak is caused by point defects such as vacancies or interstitials but rather it is mostly due to dislocations, with the form being affected somewhat by the presence of point defects.

To further understand the form of $\rho_{e\text{-}dis}$, an equation of the following form was fitted to the data for T<1.3K.

$$\rho = \rho_o + AT^2 + \rho_{e\text{-}dis} + DT^5 \qquad (3.4)$$

where $DT^5$ represents the effects of quenching of phonon drag by the defects and $\rho_{e\text{-}dis}$ represents the different equations listed in Chapter 1, which might decribe the resistivity due to scattering off dislocations. The umklapp electron - phonon term has been neglected in this equation since below 1.3K it is not expected to make a major contribution.

The Equation 1.26 from Gantmakher and Kulesko for electrons scattering off localized phonon modes gave the best fit to the low temperature data, and these fits are shown as solid curves in Figure 3.9, Figure 3.10, and Figure 3.11. The discrepancy between the curves and the data at ~1.5K is due to the onset of the umklapp electron - phonon term, which was not included in the fits. These fits

showed the presence of the $T^5$ term in deformed samples. Furthermore, for these fits, the value of A varied little when compared to A' ( Table 3.3 lists the coefficients obtained).

Figure 3.12 compares the best fits for the two equations of Gantmakher and Kulesko (Equation 1.26 and 1.23) to the data of sample Kh8f. No set of parameters for the localized electron model (Equation 1.23) gave a better fit to the data. The normal electron - phonon term ($DT^5$) was forced to zero in this fit, which is inconsistent with the T>2K analysis. To compansate for D=0, the program then chose a value of A greater than A'. It is possible that some combination of different energy levels might produce a better fit.

The agreement of the vibrating dislocation model with the data is nonetheless surprising. Gantmakher and Kulesko assumed a single energy of vibration, but one would expect a distribution of dislocation lengths and thus a distribution of energies. The closeness of these fits may be fortuitous.

The energies ($E=\hbar w$) obtained from the fits follow an interesting pattern. Sample Kh8 shows a steady increase in E as one adds more dislocations. This is consistent with having shorter dislocation lengths due to the dislocations pinning each other. One would expect point defects also to pin the dislocations and thus increase E. But, when sample Kh9 was annealed at 20K (Kh9d), presumably removing point defects, E increased. Perhaps the defects that anneal out

Table 3.3 Parameters from fits to the resistivity data

| Sample | $\rho_o$ ($n\Omega$ cm) | A ($p\Omega$ cm/K$^2$) | E=$\hbar\omega$ (K) | C/4 ($10^{-13}\Omega$cm) | D ($10^{-13}\Omega$cm/K$^5$) |
|---|---|---|---|---|---|
| Kh8a | 1.32 | | | | |
| Kh8b | 1.38 | .107 ± .007 | .250 ± .105 | .085 ± .066 | .118 ± .016 |
| Kh8c | 1.46 | .087 ± .006 | .278 ± .049 | .187 ± .062 | .195 ± .017 |
| Kh8d | 1.53 | .093 ± .012 | .353 ± .129 | .378 ± .250 | .208 ± .017 |
| Kh8e | 1.81 | .105 ± .003 | .395 ± .008 | .677 ± .028 | .248 ± .010 |
| Kh8f | 2.05 | .134 ± .007 | .340 ± .006 | .571 ± .024 | .233 ± .023 |
| Kh9a | 1.09 | | | | |
| Kh9b | 2.21 | .150 ± .005 | .268 ± .011 | .259 ± .021 | .186 ± .013 |
| Kh9c | 2.20 | .154 ± .004 | .275 ± .006 | .265 ± .012 | .185 ± .010 |
| Kh9d | 1.86 | .192 ± .014 | .353 ± .014 | .442 ± .045 | .095 ± .030 |
| Kh9e | 1.49 | .060 ± .004 | .307 ± .005 | .389 ± .014 | .206 ± .009 |
| Kh9f | 1.39 | .070 ± .004 | .274 ± .008 | .249 ± .015 | .186 ± .009 |
| Kh9g | 1.16 | .114 ± .003 | .256 ± .025 | .076 ± .014 | .077 ± .007 |
| KRbha | 10.7 | .366 ± .002 | ---------- | ---------- | .082 ± .096 |
| KRbhb | 11.52 | .393 ± .010 | .486 ± .014 | .874 ± .059 | .221 ± .023 |
| KRbhc | 10.78 | .370 ± .001 | ---------- | ---------- | .082 ± .096 |

$\rho_o$ was not obtained from this fit, and is listed for comparison purposes on this table. The constant C is the coefficient of Equation 1.26.

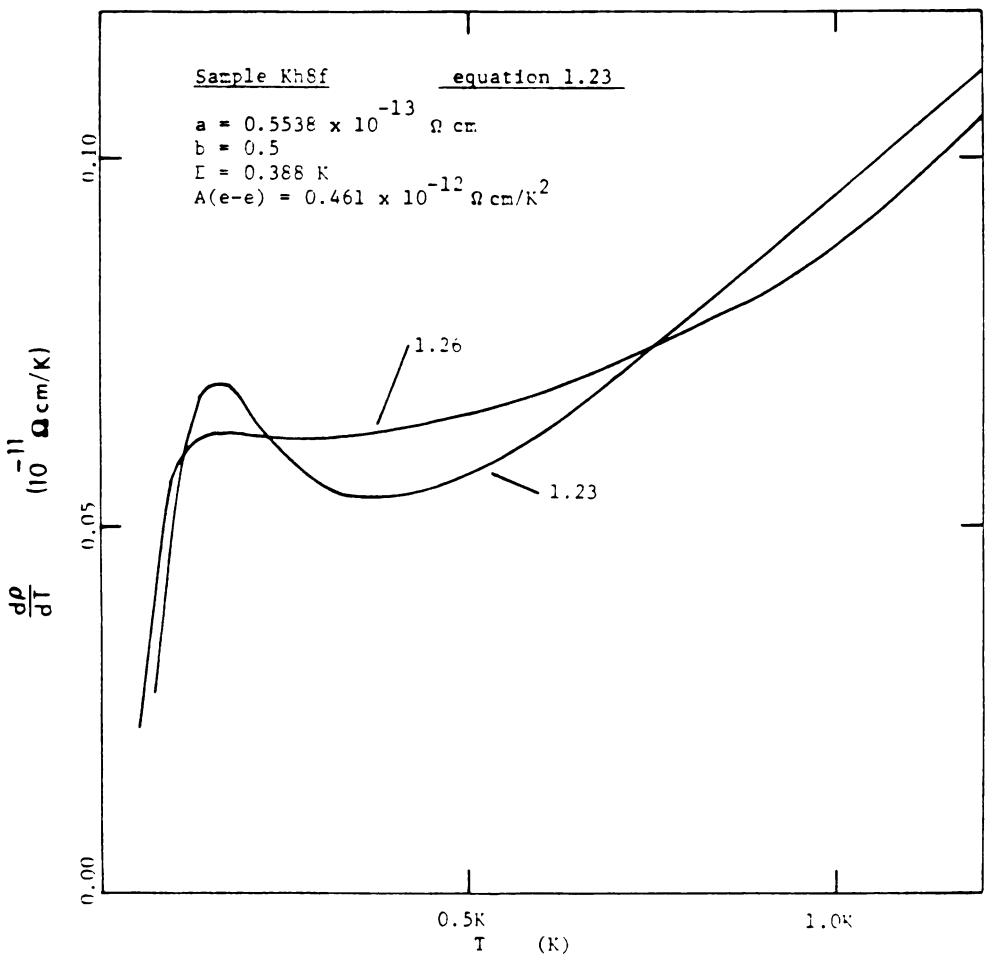


Figure 3.12 Comparison of the best fits of equations 1.26 and 1.23 to the data of Kh8f

at 20K form small dislocation loops which might increase E.

The values for A obtained from the above fits (listed in Table 3.3) can be compared to the theory of Kaveh and Wiser. Figure 3.13 shows a comparison with samples Kh8 and KRbh. One must remember that $\rho_{oi}$ is unknown, and its common value for each sample was obtained by finding the best fit to the curve. If one ignores Kh8a (undeformed sample) and Kh8b (slightly deformed sample) the data of Kh8 would give a reasonable fit to the theory. It is difficult to estimate accurately the value of A in an undeformed sample, since it does not follow exactly a $T^2$ behavior due to the previously mentioned size effect(32). In the well deformed samples, one would expect the mean free path of the electrons to to be sufficiently decreased that the size effect would be no longer significant.

The theory of Kaveh and Wiser does have difficulties with sample KRbh. The A values shown in Figure 3.13, are the values from the above fits, with a contribution to A due to vibrating impurities ($0.091p\Omega cm/K^2$) subtracted out(87). If one chooses to assign only $2.04n\,\Omega\,cm$ of the residual resistivity as being due to the impurities, a reasonable fit to the curve in obtained. However, it is very unlikely that the impurity contribution to $\rho_o$ will be this low, since the effects of adding rubidium to potassium has been observed in many laboratories to produce a much higher contribution to the residual resistivity. A more reasonable estimate of the impurity contribution to the residual resistivity, as shown

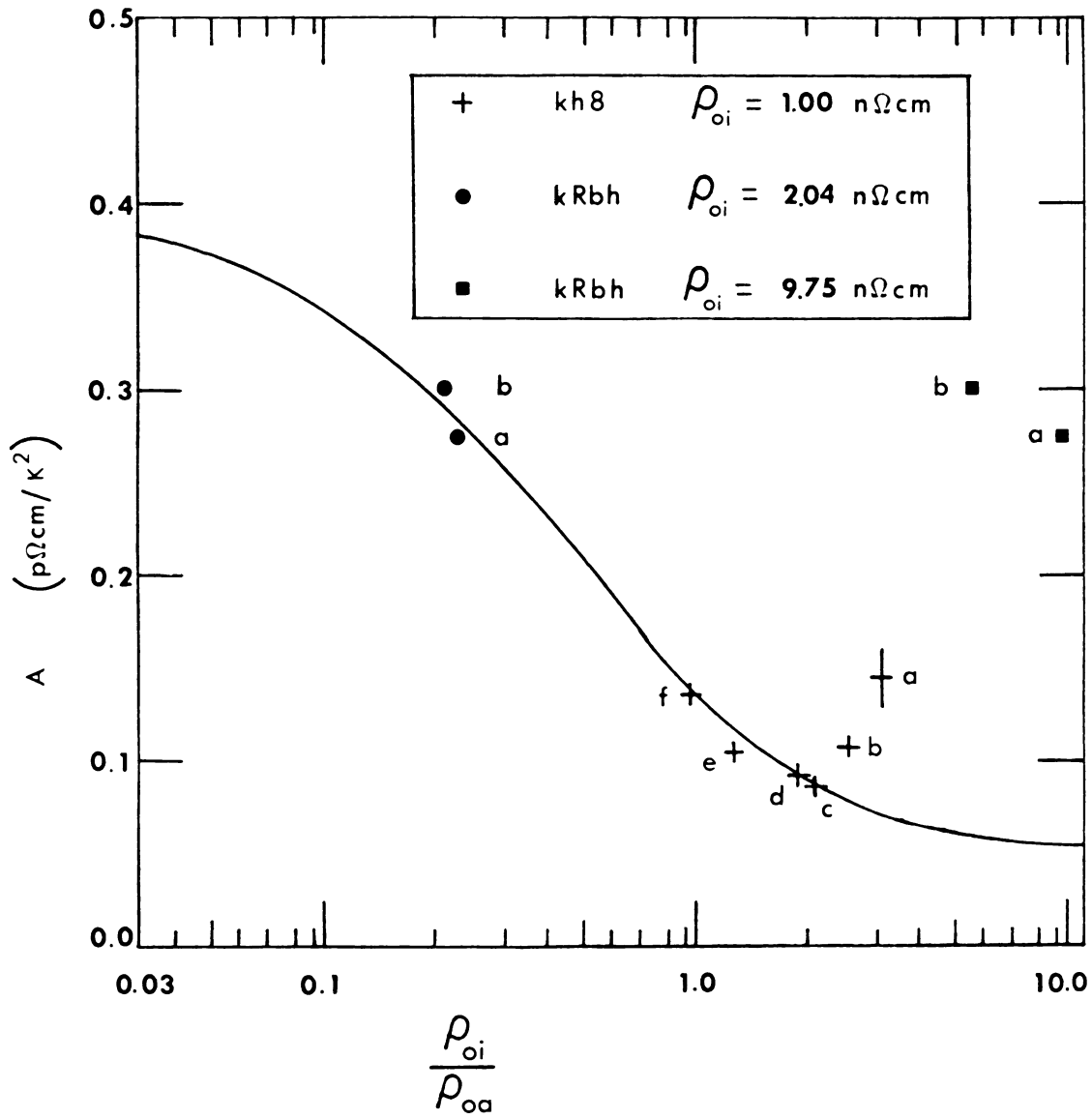


Figure 3.13 Comparison of A with Kaveh and Wiser's theory.

in the figure, causes the data to deviate significantly from the theory. If Kaveh and Wiser were to choose a higher value for $A_o$ of $0.27 p\Omega cm/K^2$ (see Equation 1.22), then the theoretical curve would be shifted up; and the data of KRbh would agree better with this theory. This choice of a larger value of $A_o$ seems reasonable since we have observed in thick, pure samples $A=0.24 \pm 0.02\ p\Omega cm/K^2$(4). Since the size effect makes uncertain the proper value of A in the pure samples, it is not clear whether a conflict exists between the theory and the data of Kh8.

A direct comparison of the results of Kh9 cannot be made with the theory of Kaveh and Wiser, since both $\rho_{oi}$ and $\rho_{oa}$ vary as one anneals out the various defects. Nonetheless, a qualitative comparison is possible. Starting with Kh9b, one sees that annealing out point defects at 20K increases A, as listed in Table 3.3. This is what Kaveh and Wiser would predict, because the ratio $\rho_{oi}/\rho_{oa}$ is decreasing, so A should increase (see Equation 1.22). On annealing at 60K, A drops substantially. One should still be annealing out point defects, so Kaveh and Wiser would predict that A would increase. Furthermore, on annealing at 120K, the value of A increases. Since $\rho_{oa}$ is decreasing at these temperatures, Kaveh and Wiser would predict A should decrease, in contrast to the result seen.

All of the above comparisons assume that the Gantmakher and Kulesko formula, for electrons scattering off the local phonon modes of dislocations, correctly describes the low

temperature resistivity data. This may be an incorrect assumption.

### 3.1.4 The intermediate temperature range

Finally, one should note that the fits do show an increase of the $DT^5$ term, as one increases the number of dislocations. This is consistent with the quenching of phonon drag. The dash line in Figure 3.9 is the fit to Kh8f with the $T^5$ term subtracted out. The $DT^5$ term gives a large contribution to $d\rho/dT$ near 1.5K. On examining the coefficients from Table 3.3, one sees that D increases for Kh8 as one adds more dislocations. The maximum value obtained of $0.233 \times 10^{-13}\Omega cm/K^5$ is much less than the theoretical value one would expect when phonon drag is completely quenched. Ekin and Maxfield(88) predicted for queched drag that $D=0.354 \times 10^{-13}\Omega\ cm/K^5$, so the numbers obtained for D are consistent with only partial quenching of phonon drag. Sample KRbha shows a normal electron - phonon term even before deformation. One would expect this, since the added point defects would provide a way for the phonons to lose their momentum. For sample Kh9, little reduction of the $DT^5$ term is seen (aside from Kh9d, which has a large uncertainty for D) until one anneals at 120K (Kh9g). Thus the largest effect on the $DT^5$ term is due to dislocations. This is reasonable, since the normal electron - phonon term is predicted to be enhanced both by the anisotropy of the

dislocations and by their shortening of the phonon mean free path (see page 16).

## 3.2 Thermoelectric ratio results

From Chapter 1, the thermoelectric ratio can be written as a sum of terms:

$$G = [\ G_o + B\ T^2 + [C/T]\ \exp(-\theta^*/T) + G_x\ ](L_o/L) \quad (3.5)$$

where $G_x$ would be an additional term possibly due to dislocations or the size effect. Figure 3.14 and Figure 3.15 show the results of measurements of G on samples Kh8 and Kh9. The turn up in these plots at ~3.5K is due to the exponential term. For T<1.0K, the exponential term is negligible, and $L=L_o$ to within 3%, so a plot of G vs $T^2$ as shown in Figure 3.16 should give a straight line assuming $G_x=0$. There is a slight deviation from $T^2$ behavior at low temperatures, which is most noticable in Kh9e.

Except for the low temperature deviation from $T^2$, the data can be fit by the above equation. For these fits, $L/L_o$ was calculated using Equation 1.47. The value for F, the coefficient for the $T^3$ term in the thermal resistivity, was obtained from a fit to the data of Newrock and Maxfield(89).

$$F= (2.4154 \times 10^{-3}) - (.12966 \times 10^{-6})(\ \rho_{300}/\ \rho_{4.2}) \text{ cm/W} \quad (3.6)$$

The resulting ratio $L/L_o$ was compared to the the

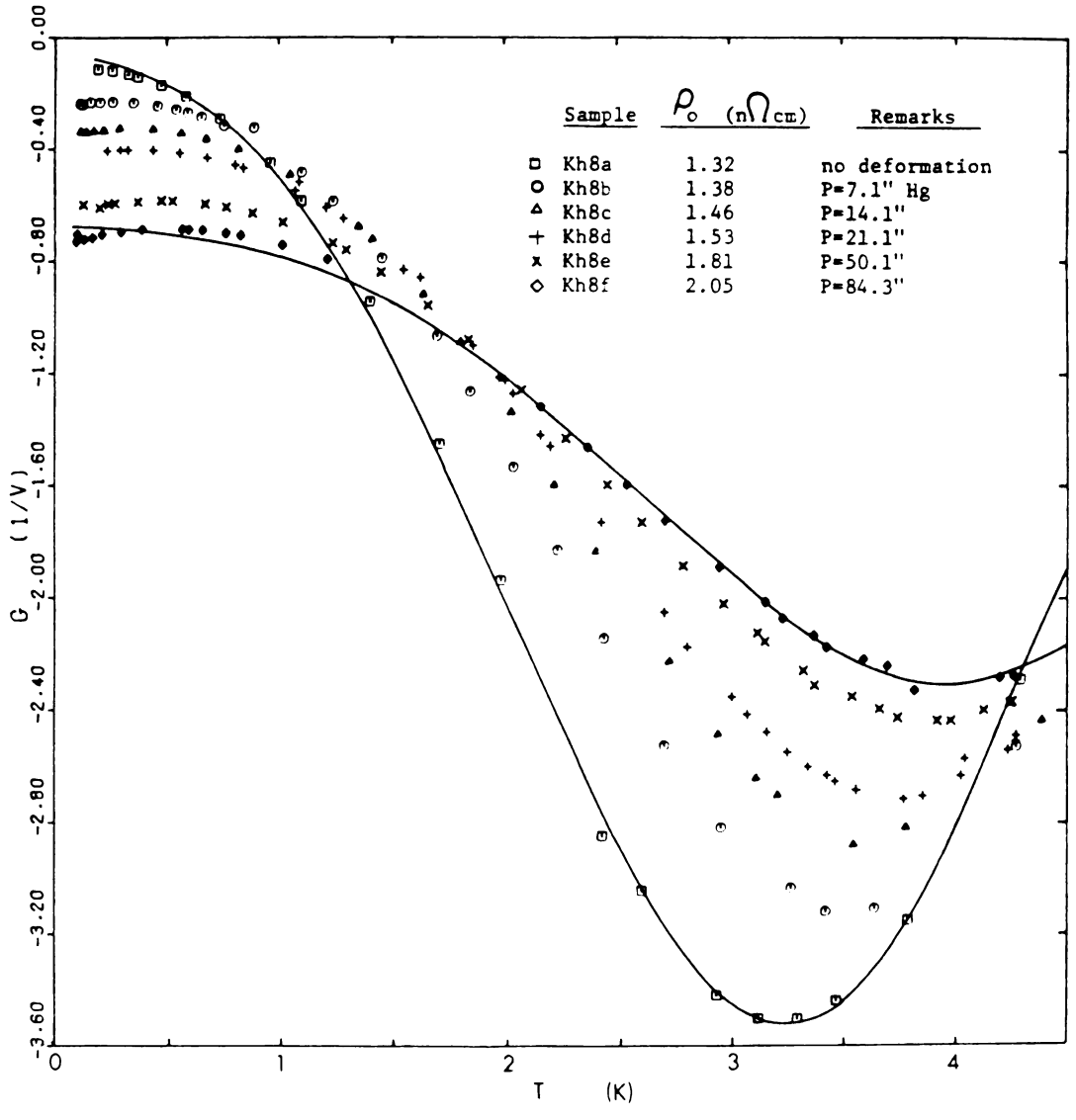


Figure 3.14 The thermoelectric ratio for Kh8.

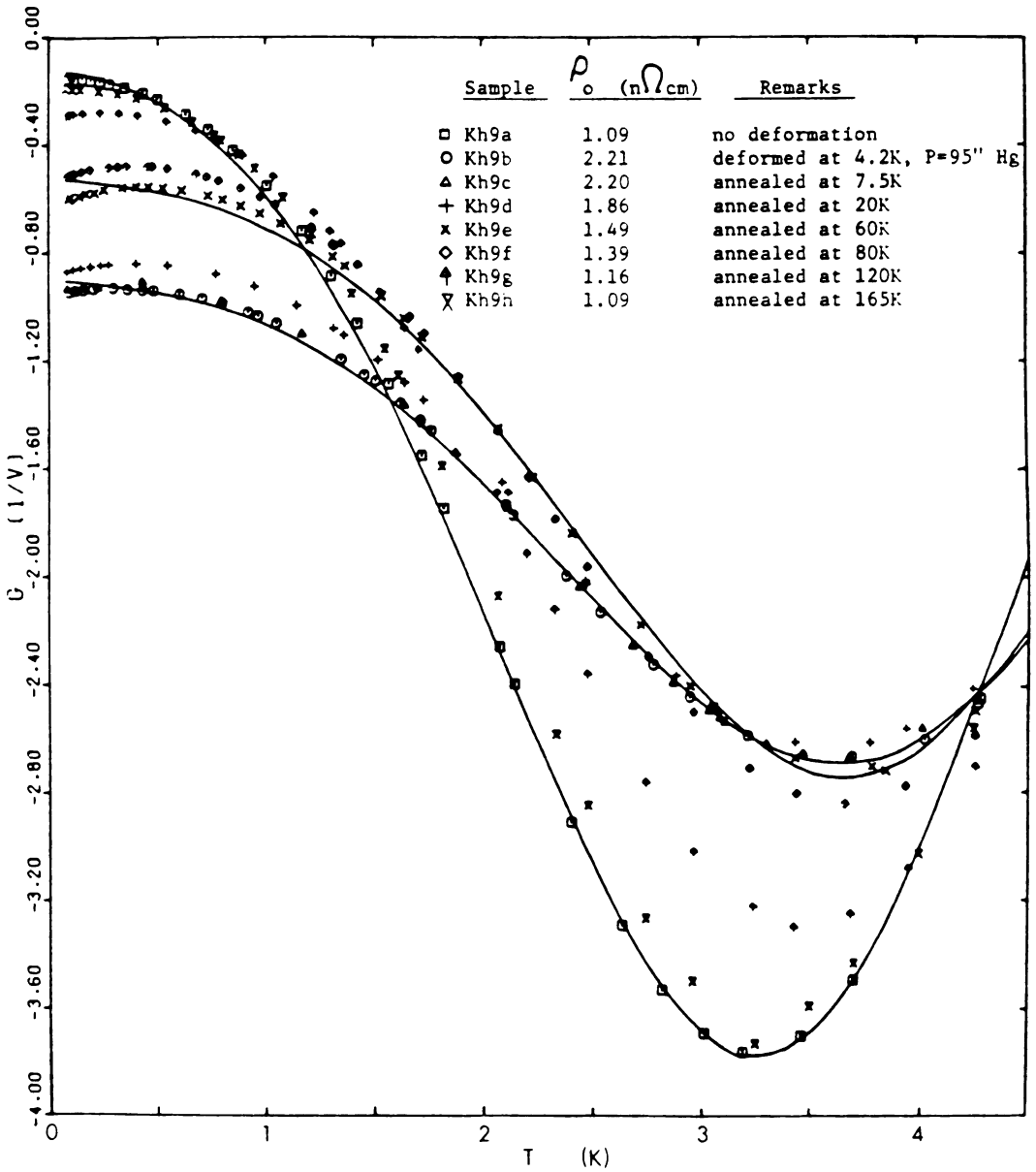


Figure 3.15 The thermoelectric ratio for Kh9.

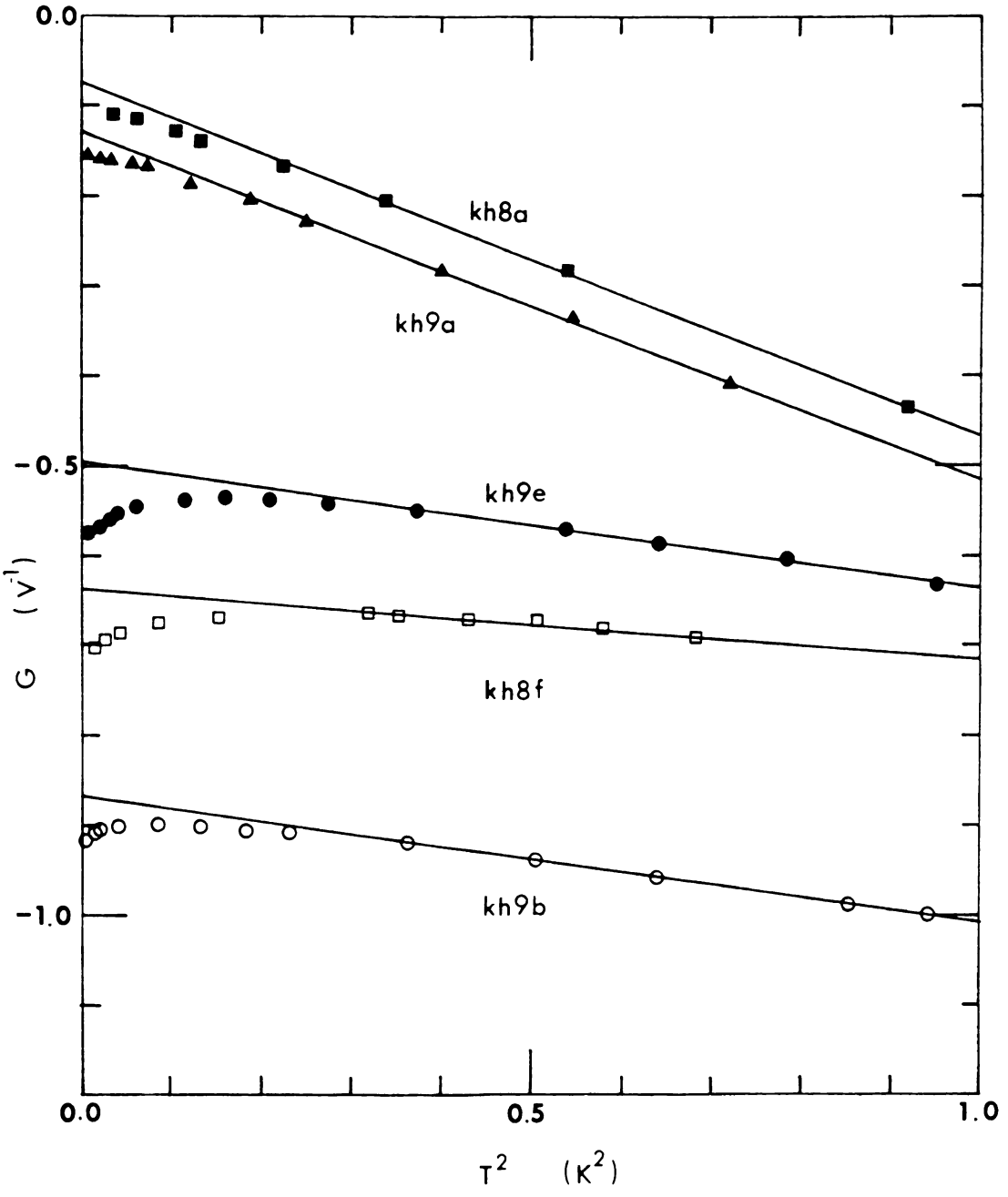


Figure 3.16 G vs $T^2$

experimental measurements performed at MSU, and this ratio agreed with the data to within the experimental scatter of the points, never deviating more than 3% from the data.

Equation 3.5 was fit to the G data of samples Kh8 and Kh9. Some of the curves obtained are shown in Figure 3.14 and Figure 3.15. The resulting coefficients are listed in Table 3.4. For these fits, no account was taken of the low temperature deviation from $T^2(G_x=0)$, so it is not surprising that the fits do poorly near 0.2K for the deformed samples.

First, let us examine the effects of dislocations on $G_o$. Figure 3.17 shows a modified Gorter - Nordheim plot for sample Kh8. Adding more dislocations does increase the magnitude of $G_o$ in proportion to $1/\rho_o$, per the Gorter - Nordheim relation (see Equation 1.31). From sample Kh9 (Figure 3.15), one sees that the point defects, which annealed out at 20K and 60K, make a significant contribution to the diffusion term ($G_o$). Thus the diffusion thermoelectric ratio behaves much as expected.

Next the phonon drag terms will be examined. On looking at the coefficients B and C listed in Table 3.4, one sees that the dislocations added in sample Kh8 suppressed both the normal and umklapp terms. Furthermore, the results for Kh9 show little recovery of either B or C, outside experimental error, until one starts annealing near 80K (Kh9f). Thus one may conclude that dislocations effectively suppress the phonon drag terms, and point defects have a much smaller effect on them.

Table 3.4 The coefficients from fits to the G data.

| sample | $G_o$ (1/V) | B ($1/V/K^2$) | C ($10^3$1/V/K) | $\theta^*$ (K) |
|---|---|---|---|---|
| Kh8a | -.0641 ± .012 | -.419 ± .007 | 1.21 ± .02 | 15.8 ± .10 |
| Kh8b | -.182 ± .010 | -.257 ± .005 | 1.05 ± .03 | 17.6 ± .19 |
| Kh8c | -.287 ± .010 | -.195 ± .004 | .889 ± .031 | 18.1 ± .23 |
| Kh8d | -.336 ± .009 | -.168 ± .003 | .801 ± .023 | 18.3 ± .20 |
| Kh8e | -.539 ± .007 | -.111 ± .003 | .606 ± .030 | 18.9 ± .31 |
| Kh8f | -.656 ± .008 | -.0848± .004 | .512 ± .052 | 19.2 ± .62 |
| Kh9a | -.123 ± .006 | -.409 ± .003 | 1.18 ± .09 | 15.8 ± .06 |
| Kh9b | -.877 ± .006 | -.127 ± .003 | .656 ± .027 | 18.1 ± .25 |
| Kh9c | -.879 ± .007 | -.126 ± .003 | .715 ± .039 | 18.4 ± .30 |
| Kh9d | -.795 ± .008 | -.125 ± .004 | .637 ± .036 | 18.0 ± .35 |
| Kh9e | -.513 ± .009 | -.149 ± .005 | .726 ± .044 | 18.2 ± .36 |
| Kh9f | -.435 ± .008 | -.167 ± .004 | .776 ± .037 | 18.1 ± .29 |
| Kh9g | -.238 ± .010 | -.257 ± .004 | .980 ± .024 | 17.2 ± .16 |
| Kh9h | -.153 ± .009 | -.362 ± .005 | 1.15 ± .02 | 16.2 ± .09 |

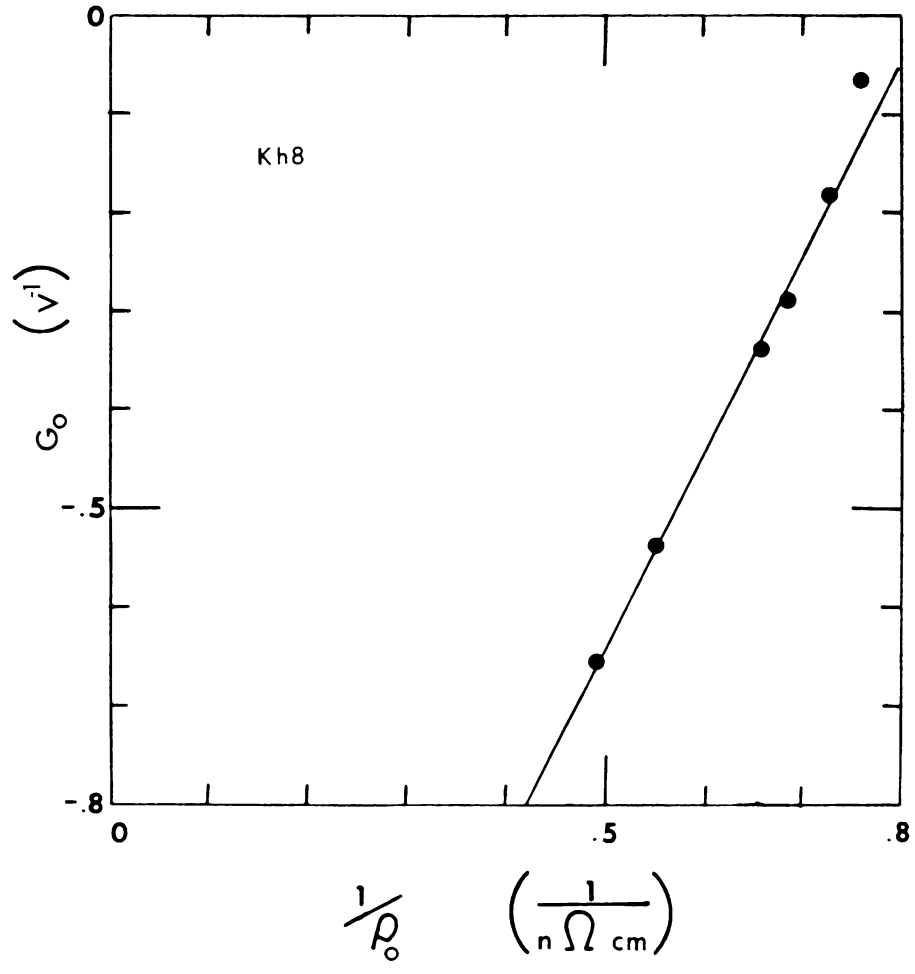


Figure 3.17 Modified Gorter - Nordheim plot

One may ask how the suppression of the phonon drag terms in the thermoelectric ratio relates to the enhanced normal electron - phonon term in the resistivity. In the resistivity case the phonon distibution is pulled into thermal equilibrium through interactions with the dislocations. Thus the rate of momentum loss for the phonons is higher when dislocations are present. Since the phonons are losing momentum more rapidly to the dislocations, the electrons will receive less, so the thermopower due to such interactions will be reduced.

A more detailed examination of the low temperature deviation from $T^2$ behavior is needed. At low temperature,

$$G = G_o + B\,T^2 + G_x \qquad (3.7)$$

$$\frac{dG}{dT} = 2\,B\,T + \frac{dG_x}{dT}$$

Figure 3.18 is a plot of dG/dT vs T. This plot shows roughly a linear behavior, with a non zero intercept. This suggests that $G_x$ may be linear in T. Since the intercept is positive, the coefficient would be positive. The sample Kh9a is undeformed and has an intercept on this graph only a factor of two smaller than the intercept for the heavily deformed samples. The reason the assumed linear term is more noticable for high levels of dislocations is that the $T^2$ term is depressed, and the linear term is larger, permitting easier observation of the linear term. No theories have been discovered which predict a linear term in

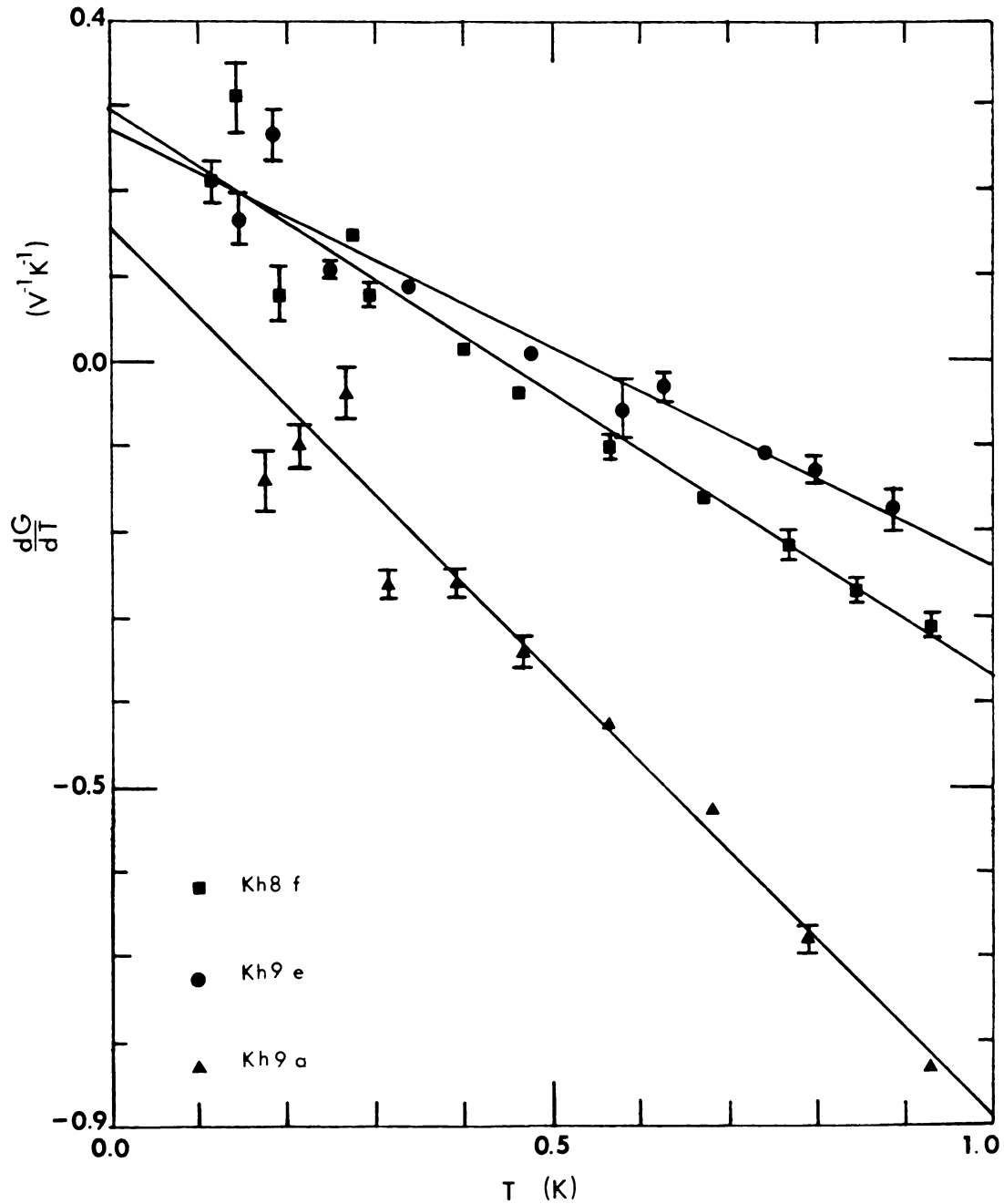


Figure 3.18 dG/dT vs T

G. It is quite possible that this is only the low temperature limit of a more complicated function.

## 3.3 The resistance minimum

The resistivity of samples Kh2e, Kh3, Kh4, and Kh7 shown in Figure 3.19, deviate from any previous published results for potassium. All of these samples show a resistance minimum near 0.2K. Many possible sources for this minimum were examined.

The final conclusion was that a contaminant was entering the potassium from the contact material. The resistance minimum was seen when we used Handiwrap, Parafilm, and polyethylene. All of these are hydrocarbons, whereas, teflon, which does not cause a resistance minimum, is made of a fluorocarbon. It was thought that possibly a hydrogen compound or other impurity from the hydrocarbons was diffusing into the sample. These materials all had been carefully cleaned using high purity alcohol.

The reason for using a material other than teflon was that teflon reacted with the potassium. The teflon reacts with the surface of the potassium sample leaving a layer of carbon. Since none of the hydrocarbons showed signs of reacting with the sample at room temperature, it was felt they might be better to use.

In the end, we simply used teflon as our contact material, even though a black layer was left on the sample,

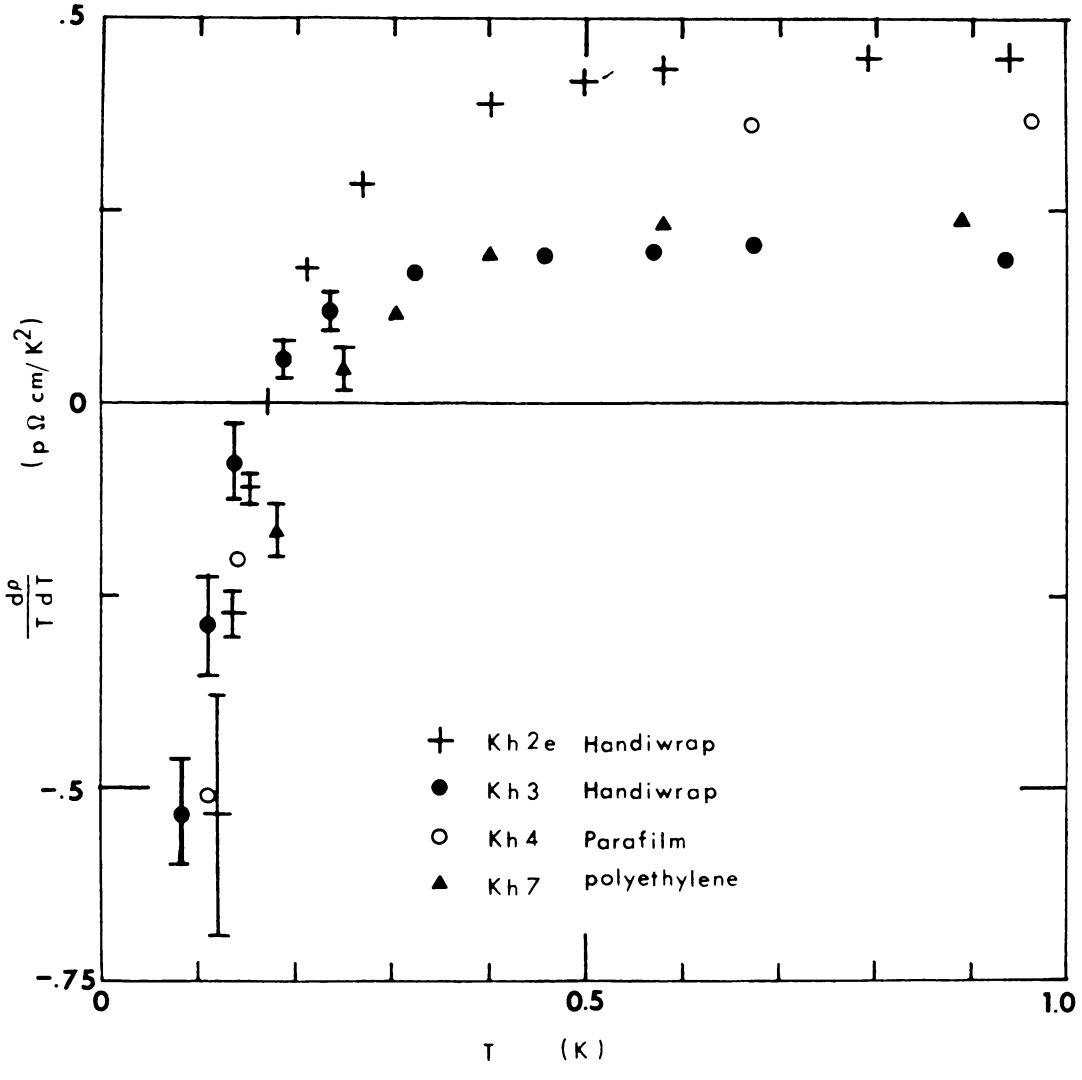


Figure 3.19 (1/T)(dρ/dT) vs T for Kh2e, Kh3, Kh4, and Kh7.

since the low temperature data agreed better with the results of Lee et al.(4) when nothing was in contact with the potassium. An interesting aside, is that many of the previous groups had encapsulated their samples in polyethylene, but they had not gone low enough in temperature to see this effect.

There are several possible theoretical explanations of the results. The most obvious is the Kondo effect(90) for scattering off magnetic impurities. The Kondo effect should produce roughly a -lnT term in $\rho$. Figure 3.20 is a plot which should give a straight line for such a theory. Within the scatter in the data, a straight line is seen. Thus it seems likely a magnetic impurity is entering the sample from the plastics. To date, no attempt has been made to identify the impurity.

It is of some interest to see the effect on G of the mechanism which caused the resistance minimum. Figure 3.21 shows this data. The solid curves on this graph are drawn to guide the reader. No measurement of G was made on sample Kh7. The non-reproducibility of the curves is surprising. If this were a Kondo system one would expect an anomolous value for G, but not this large a variation among samples. In both Kh2e and Kh3, the phonon drag terms appear to be supressed, but not for Kh4. Only sample Kh3 shows a local minimum in G near 1.2K.

Additional measurements are needed to identify the source of the resistance minimum, and the cause of the

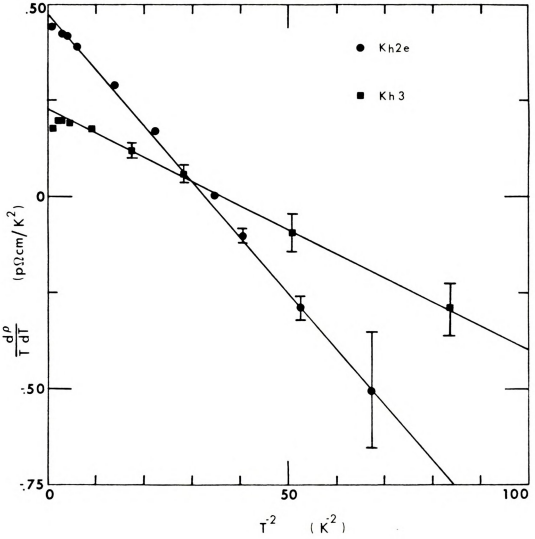


Figure 3.20 (1/T)(d$\rho$/dT) vs $T^{-2}$, a Kondo system?

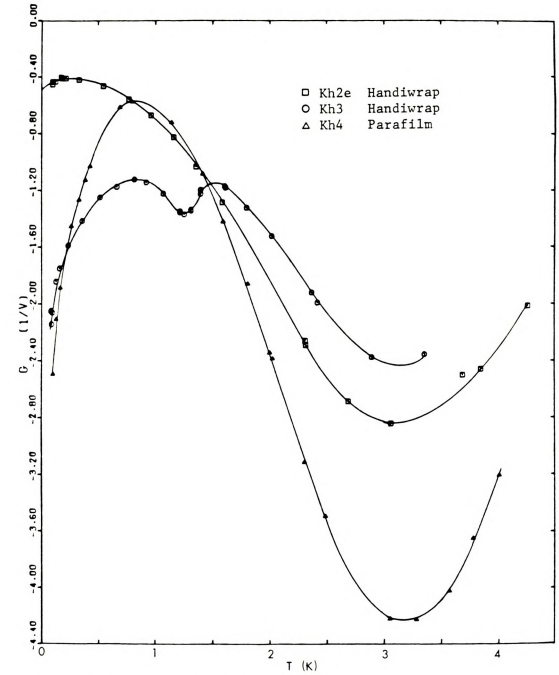


Figure 3.21 G vs T, for the resistance minimum samples.

variation in G.

# CHAPTER 4

## Conclusions

This study has been an investigation of the effects of plastic deformation on the electrical resistivity and thermoelectric ratio of potassium from 70mK to 4.2K. Plastic deformation does have a significant effect on both.

Plastic deformation increased both the residual resistivity and the temperature dependence of resisitivity. The residual resistivity on annealing showed the same general recovery as in the earlier work of Gugan(10).

Deformation enhanced the electron - phonon term from 4.2K to below 1K by causing a $DT^5$ term to appear in $\rho$ near 1K, possibly due to the quenching of phonon drag. The coefficients obtained for D, were always less than its theoretical maximum value computed by Ekin and Maxfield, for completely quenched phonon drag.

Furthermore, a new term was seen ( $\rho_{e\text{-}dis}$), which dominated the temperature dependent resistivity in deformed samples below 1K. This new term was interpreted as being

caused by dislocations, in that it disappears when dislocations are annealed from the sample. This new term can be fit reasonably well with a model of Gantmakher and Kulesko(44) for scattering of electrons off localized phonon modes associated with the dislocation. Although the fits to the data are quite good, it is difficult to understand why the dislocations are dominated by a single vibration frequency, as assumed in the fit.

The effects of dislocations on the electron - electron term in the resistivity predicted by Kaveh and Wiser cannot be easily tested, since $\rho_{e\text{-}dis}$ obscures the $AT^2$ term. Until $\rho_{e\text{-}dis}$ is more fully understood, it will remain difficult to identify any variation in the electron - electron term caused by dislocations.

Plastic deformation of potassium also has a large effect on the thermoelectric ratio. Both the normal and umklapp phonon drag terms are suppressed by dislocations and are effected relatively little by point defects. In addition, the magnitude of the diffusion term is increased by both point defects and dislocations with the systematic addition of dislocations giving agreement with the Gorter - Nordheim relation.

Finally, a resistance minimum near 0.2K was seen for potassium in contact with various plastics. The added term to the resistivity followed a $-\ln(T)$ behavior, consistent with a Kondo system. The thermoelectric ratio for these samples was variable and followed no clear pattern.

# LIST OF REFERENCES

LIST OF REFERENCES

1) I.M. Templeton, J. Phys.F: Metal Physics, 12, L121 (1982).

2) A.W. Overhauser, Adv. in Phys., 27, 343 (1978).

3) Kaveh and Wiser,J. Phys. F: Metal Physics, 10, L37 (1980).

4) C.W.Lee, M.L. Haerle, V. Heinen, J. Bass, W.P. Pratt,Jr., J.A. Rowlands, and P.A. Schroeder, Phys. Rev. B, 25, 1411 (1982).

5) A.C. Anderson and S.C. Smith, J. Phys. Chem. Solids, 34, 111 (1973).

6) L.R. Motowidlo, P.D. Goldman, and J.M. Galligan, Phil. Mag. B, 46, 539 (1982).

7) R.A. Brown, Can. J. of Phys., 60, 766 (1982).

8) Z.S. Basinski, J.S. Dugdale, and A. Howie, Philos. Mag., 8, 1989 (1963).

9) R.A. Brown, Can. J. of Phys., 60, 766 (1982).

10) W.S.C. Gurney and D. Gugan, Phil. Mag., 24, 857 (1971).

11) F. Block, Z. Phys., 59, 208 (1930).

12) D. Gugan, Proc. R. Soc. Lond. A., 325, 223 (1971).

13) J.W. Ekin and B.W. Maxfield, Phys. Rev. B, 4, 4215 (1972).

14) H. van Kempen, J.H.J.M. Ribot, and P. Wyder, J. Phys. F: Metal Physics, 11, 597 (1981).

15) V.G. Orlov, Sov. Phys. Solid State, 16, 2175 (1975).

16) K. Frobose, Z. Physick B, 26, 19 (1977).

17) M. Kaveh and N. Wiser, Phys. Rev. B, 9, 4053 (1974).

18) M. Kaveh, C.R. Leavens, and N. Wiser, J. Phys. F: Metal

Phys., 9, 71 (1979).

19) R.Taylor, C.R. Leavens, M.S. Duesbery, and M.J. Laubitz, J. De Physique, C 6, 1058 (1978).

20) M. Danino, M. Kaveh, and N. Wiser, J. Phy. F: Metal Physics, 11, 2563 (1981).

21) D. Gugan, J. Phys. F: Metal Physics, 12, L173 (1982).

22) Z.S. Basinski, J.S. Dugdale, and A. Howie, Philos. Mag., 8, 1989 (1963).

23) Hans-Lennard Engquist, Phys. Rev. B, 25, 2175 (1982).

24) M. Danino, M. Kaveh, and N. Wiser, J. Phys. F: Metal Physics, 12, L259 (1982).

25) W.E. Lawrence and J.W. Wilkins, Phys. Rev. B, 7, 2317 (1973).

26) A.H. MacDonald, R. Taylor, and D.J.W. Geldart, Phys. Rev. B, 23, 2718 (1981).

27) H. van Kempen, J.H.J.M. Ribot, and P. Wyder, J. Phys. F: Metal Physics, 11, 597 (1981).

28) Levy, M. Sinvani, and A.J. Greenfield, Phys. Rev. Let., 43, 1822 (1979).

29) J.A. Rowlands, C. Durvury, and S.B. Woods, Phys. Rev. Let., 40, 1201 (1978).

30) C.W.Lee, M.L. Haerle, V. Heinen, J. Bass, W.P. Pratt,Jr., J.A. Rowlands, and P.A. Schroeder, Phys. Rev. B, 25, 1411 (1982).

31) J.A. Rowlands, C. Durvury, and S.B. Woods, Phys. Rev. Let., 40, 1201 (1978).

32) The current work is being carried on by, Yu, M.L. Haerle, J. Bass, W.P. Pratt,Jr., and P.A. Schroeder.

33) H. van Kempen, J.H.J.M. Ribot, and P. Wyder, J. Phys. F: Metal Physics, B. 11, 597 (1981).

34) M. Danino, M. Kaveh, and N. Wiser, J. Phys. F: Metal Physics, 11, L107 (1981).

35) D. Gugan, J. Phys. F: Metal Physics, 12, L173 (1982).

36) J.M. Ziman, Electons and Phonons, Oxford University Press, London, 1960.

37) M. Kavey and N. Wiser, J. Phys. F: Metal Physics, 11, 419 (1981).

38) M. Kaveh and N. Wiser, J. Phys. F: Metal Physics, 12, 935 (1982).

39) R.J.M. van Vucht, G.F.A. van Walle, H. van Kempen, and P. Wyder, J. Phys. F: Metal Physics, 12, L217 (1982).

40) M.L. Boriack and A.W. Overhauser, Phys. Rev. B, 18, 6454 (1978).

41) M.F. Bishop and A.W. Overhauser, Phys. Rev. B, 23, 3638 (1981).

42) R.A. Brown, Can. J. of Phys., 60, 766 (1982).

43) V.F. Gantmakher and G.I. Kulesko, Sov. Phys. JETP, 40, 1158 (1975).

44) P. Fulda and I. Peschel, Adv. in Phys., 21, 1 (1972).

45) S.G. O'Hara and A.C. Anderson, Phys. Rev. B, 10, 574 (1974).

46) S.G. O'Hara and A.C. Anderson, Phys. Rev. B, 9, 3730 (1974).

47) V.F. Gantmakher and G.I. Kulesko, Sov. Phys. JETP, 40, 1158 (1975).

48) J.M. Ziman, Electons and Phonons, Oxford University Press, London, 1960.

49) A.M. Guénault and D.K.C. MacDonald, Proc. R. Soc., A 264, 41 (1961).

50) A.M. Guénault and D.K.C. MacDonald, Proc. R. Soc., A 274, 154 (1963).

51) D. Gugan, J. Phys. F: Metal Physics, 12, L173 (1982).

52) A.M. Guénault and D.K.C. MacDonald, Proc. R. Soc., A 274, 154 (1963).

53) P. Fulda and I. Peschel, Adv. in Phys., 21, 1 (1972).

54) A.M. Guénault and D.K.C. MacDonald, Proc. R. Soc., A 274, 154 (1963).

55) J.M. Ziman, Phil. Mag., 4, 371 (1959).

56) M. Bailyn, Phil. Mag., 5, 1059 (1960).

57) R.S. Newrock and B.W. Maxfield, Phys. Rev. B, 7, 1283 (1973).

58) S.H.E. Corporation, 4174 Sorrento Valley Blvd., San Diego, California.

59) Metal Bellows Corporation, 1075 Providence Highway, Sharon, Mass. Part number PN61150-2.

60) Molecular sieve pellets 13X from Linde Corporation, a division of Union Carbide Corporation.

61) Stayclean flux is from J W Harris Co., Inc., 10930 Deerfield Rd., Cinti., Ohio.

62) Vacuum Atmospheres Company, 4652 W. Rosecrane Ave., Hawthorne, California. Dr. Solin permitted us the use of his glove box.

63) Callery Chemical Company, a division of Mine Safty Appliances Company, Callery, Pennsylvania.

64) D. Gugan and J.S. Dugdale, Proc. Roy. Soc. Lond., A 270, 186 (1962).

65) Imperial Metal Industries, P.O. Box 216, Witton Birmingham, B6 7BA, England.

66) Stycast 1266 is from Emerson and Cuming, Inc., Canton, Massachusetts.

67) D. Edmunds, W.P. Pratt, Jr., and J.A. Rowlands, Rev. Sci. Inst., 51, 1516 (1980).

68) Lake Shore Cryotronics, Inc., 64 E. Walnut St., Westerville, OH.

69) Stycast 2850 GT. From Emerson and Cuming, Inc., Canton, Massachusetts.

70) Vespel is a product of Du Pont Company.

71) Dale Electronics, Inc., Box 609, Columbus, Nebr. Part number RS1/4-4K ohms.

72) Airco Speer Electronics, Bradford, PA.

73) J.L. Imes, Ph.D. Thesis, Michigan State University, 1974.

74) G.L. Neiheisel, Ph.D. Thesis, Michigan State University, 1975.

75) National Bureau of Standards, Washington, D.C..

76) D. Edmunds, W.P. Pratt, Jr., and J.A. Rowlands, Rev. Sci. Inst., 51, 1516 (1980).

77) C.W.Lee, M.L. Haerle, V. Heinen, J. Bass, W.P. Pratt,Jr., J.A. Rowlands, and P.A. Schroeder, Phys. Rev. B, 25, 1411 (1982).

78) H. van Kempen, J.H.J.M. Ribot, and P. Wyder, J. Phys. F: Metal Physics, 11, 597 (1981).

79) J.A. Rowlands, C. Durvury, and S.B. Woods, Phys. Rev. Let., 40, 1201 (1978).

80) C.W.Lee, M.L. Haerle, V. Heinen, J. Bass, W.P. Pratt,Jr., J.A. Rowlands, and P.A. Schroeder, Phys. Rev. B, 25, 1411 (1982).

81) W.S.C. Gurney and D. Gugan, Phil. Mag., 24, 857 (1971).

82) M. Danino, M. Kaveh, and N. Wiser, J. Phy. F: Metal Physics, 11, 2563 (1981).

83) Z.S. Basinski, J.S. Dugdale, and A. Howie, Philos. Mag., 8, 1989 (1963).

84) Hans-Lennard Engquist, Phys. Rev. B, 25, 2175 (1982).

85) M. Danino, M. Kaveh, and N. Wiser, J. Phys. F: Metal Physics, 12, L259 (1982).

86) R.J.M. van Vucht, G.F.A. van Walle, H. van Kempen, and P. Wyder, J. Phys. F: Metal Physics, 12, L217 (1982).

87) C.W. Lee, W.P. Pratt, Jr., J.A. Rowlands, and P.A. Schroeder, Phys. Rev. Let., 45, 1708 (1980).

88) J.W. Ekin and B.W. Maxfield, Phys. Rev. B, 4, 4215 (1972).

89) R.S. Newrock and B.W. Maxfield, Phys. Rev. B, 7, 1283 (1973).

90) J. Kondo, Prog. of Theor. Phys., 32, 37 (1964).